The Role of Activity in Regulating the Properties of Brainstem Auditory Neurons

Katarina E. Leão
MSc (Göteborgs Universitet, Sweden)

Thesis submitted for the degree of Doctor of Philosophy of
The Australian National University

The John Curtin School of Medical Research
The Australian National University
Canberra

April 2008

Statement

All research presented in this thesis is original, and was carried out by myself under the supervision of Prof. Bruce Walmsley.

The results of this PhD thesis have contributed to the publication of the following journal article:

> **Leao K.E.,** Leao R.N., Sun H., Fyffe R.E.W. and Walmsley B., Hyperpolarization-activated currents are differentially expressed in brainstem auditory nuclei. *The Journal of Physiology* (2006)

All electrophysiological studies presented in this article were performed by myself, except for a few LSO cell recordings during simulation of the low-threshold potassium current in dynamic clamp experiments[1]. Immunohistochemistry results presented in this article were performed fully by R. Fyffe's group.

I have also co-authored the following publications by providing immunohistochemical data concerning the sodium/potassium exchanger (1), provided electrophysiological recordings of I_A in MNTB cells (2) and data on AVCN bushy cell firing properties and I_h in normal and deaf mice (3). *Please note maiden name Svahn.*

1. Leao R.N., Naves M.M., **Leao K.E.** and Walmsley B., Altered sodium currents in auditory neurons of congenitally deaf mice. *European Journal of Neuroscience* (2006)

2. Leao R.N., Sun H., **Svahn K.**, Berntson A., Youssoufian M., Paolini A.G., Fyffe R.E.W. and Walmsley B., Tonotopic maps in the auditory brainstem of juvenile mice are disrupted in congenitally deafness. *The Journal of Physiology* (2006)

3. Leao R.N., **Svahn K.**, Berntson A., Walmsley B., Hyperpolarization-activated (I_h) currents in auditory brainstem neurons of normal and congenitally deaf mice, *European Journal of Neuroscience* (2005)

---

[1] Performed by RN Leao

The work described in this thesis was presented at several scientific meetings. The following abstracts were published in conjunction with these presentations:

2007 **Leao KE**, Leao RN & Walmsley B. "Dynamic expression of potassium channels after acoustic stimulation improves high-frequency synaptic transmission". The 7th IBRO World Congress of Neuroscience. Melbourne, Australia. July 12-17, 2007.

2006 **Leao KE**, Leao RN, Sun H, Berntson AK, Fyffe R & Walmsley B. "On the role of Ih in SOC nuclei: differential physiology, distribution and function." The 5th Forum of European Neuroscience, Vienna, Austria. July 8-12, 2006.

2006 **Svahn K**, Leao RN, Sun H, Paolini A, Berntson A, Fyffe RE & Walmsley B. "Hyperpolarization-activated cation currents in three auditory brainstem nuclei". The 39th Winter Conference on Brain Research, Steamboat Springs, Colorado, USA. January 21-28, 2006.

2005 **Svahn KE**, Leao RN, Berntson AK, Sun H, Fyffe R & Walmsley B. "Hyperpolarization-activated cation currents in three auditory brainstem nuclei". The 35th annual meeting of the Society for Neuroscience, Washington DC, USA. November 12-16, 2005.

2005 **Svahn KE**, Leao RN, Berntson AK, Sun H, Fyffe R & Walmsley B. "Hyperpolarization-activated cation currents (Ih) in three different auditory nuclei". The 25th annual meeting of the Australian Neuroscience Society, Perth Australia. January 30 – February 2, 2005.

Katarina E. Leão

Katarina E. Leão

Acknowledgments

I would like to thank Professor Bruce Walmsley for being a great supervisor. He has provided a fantastic research environment and guided me calmly through my PhD, allowing me to mature into a successful researcher. He has also ensured all the lab members had many great social events together, creating the splendid atmosphere we have always felt in the Walmsley lab. I am also very grateful to my husband and college Richardson Leão for all the pushing and encouragement during my PhD. I would also like to thank Dr. Amy Eichner for the help and advice, mostly during my first year. Thanks to Monique Youssoufian for being a great office-mate and friend. Also many thanks to Marcell Naves and Kiri Couchman for having fun in the lab with us, and thanks to Christian Stricker for being my advisor, and Caryl Hill for being my very honest mentor. A big thanks to the whole Neuroscience division of JCSMR for creating great memories for life, specifically: Garry, Hiroe, Lucy, Kaori, Johannes, Maarten, Bjorn, Greg, JB, Ivana, Olfat, Nori, Allison, Selma, Zan-Min, Manuel, Clarke, Anna, Marion and Jean-Dider. I am also very grateful to have been collaborating with Robert Fyffe and his lab.

I wish to give a special thank you to my aunt Ann-Kristin Norbäck with family here in Canberra for giving me a sense of family-connections and helping me with everything practical. A big thanks to my family in Sweden (mamma, pappa, Jocke, Bea, mormor, morfar, farmor, Svea) – tack för att ni accepterat att jag bott på andra sidan jorden i så många år. Thanks to my Brazilian family for taking me in as a daughter (eu amo cada um muitissimo). I must also give a huge thanks to my Canberra friends: Cath, Antti, Raul, Paula, Antonella, Angelica & Luciano, and all the girlfriends and boyfriends, turned in to wives and husbands, of neuroscience people.

Finally, I dedicate this thesis to Richardson; with you everything has found its meaning in my life.

Abstract

The aim of the studies in this thesis was to investigate the role of activity in regulating the properties of brainstem auditory neurons. The membrane properties of three different types of brainstem auditory neurons: bushy cells of the anteroventral cochlear nucleus (AVCN), principal cells of the medial nucleus of the trapezoid body (MNTB) and principal cells of the lateral superior olive (LSO) were studied in detail. Neurons from these three nuclei form connections that are crucial for the detection of interaural level differences of sounds arriving at the two ears of mammals. In order to study how membrane properties may be regulated by neural activity an animal model of lack of cochlear activity (the congenitally deaf, *dn/dn*, mouse) was used. In addition, the role of increased neural activity after acoustic stimulation was investigating in normal hearing mice.

The initial chapters of this thesis are dedicated to the investigation of the hyperpolarization-activated cation current (I_h) in AVCN bushy cells and principal neurons of the MNTB and LSO of mice. Patch-clamp recordings have shown that these three auditory neurons express significantly different amplitudes of I_h with LSO cells exhibiting the largest I_h and MNTB neurons the smallest. Kinetically, I_h is faster in LSO neurons and more active at rest compared to AVCN and MNTB cells. I_h half-activation voltages were ~10 mV more hyperpolarized for AVCN and MNTB cells compared to LSO neurons. Using immunohistochemistry, the expression of two different hyperpolarization-activated cyclic nucleotide-gated (HCN) channel subunits, the HCN1 and HCN4 (known to generate a fast and a slow activating I_h, respectively) was studied. HCN1 immunoreactivity was strong in AVCN and LSO neurons in contrast to MNTB cells that had light or very weak expression. HCN4 subunits were intensively labeled in membranes

Abstract

The aim of the studies in this thesis was to investigate the role of activity in regulating the properties of brainstem auditory neurons. The membrane properties of three different types of brainstem auditory neurons: bushy cells of the anteroventral cochlear nucleus (AVCN), principal cells of the medial nucleus of the trapezoid body (MNTB) and principal cells of the lateral superior olive (LSO) were studied in detail. Neurons from these three nuclei form connections that are crucial for the detection of interaural level differences of sounds arriving at the two ears of mammals. In order to study how membrane properties may be regulated by neural activity an animal model of lack of cochlear activity (the congenitally deaf, *dn/dn*, mouse) was used. In addition, the role of increased neural activity after acoustic stimulation was investigating in normal hearing mice.

The initial chapters of this thesis are dedicated to the investigation of the hyperpolarization-activated cation current (I_h) in AVCN bushy cells and principal neurons of the MNTB and LSO of mice. Patch-clamp recordings have shown that these three auditory neurons express significantly different amplitudes of I_h with LSO cells exhibiting the largest I_h and MNTB neurons the smallest. Kinetically, I_h is faster in LSO neurons and more active at rest compared to AVCN and MNTB cells. I_h half-activation voltages were -10 mV more hyperpolarized for AVCN and MNTB cells compared to LSO neurons. Using immunohistochemistry, the expression of two different hyperpolarization-activated cyclic nucleotide-gated (HCN) channel subunits, the HCN1 and HCN4 (known to generate a fast and a slow activating I_h, respectively) was studied. HCN1 immunoreactivity was strong in AVCN and LSO neurons in contrast to MNTB cells that had little or very weak expression. HCN4 subunits were intensively labeled in membranes

of AVCN and MNTB cells but weakly labeled in LSO neurons, in agreement with voltage-clamp recordings showing a large, fast activating I_h in LSO cells, a slow activating I_h in MNTB cells and a more intermediate amplitude and kinetics I_h in AVCN bushy cells. Dynamic clamp experiments in which native I_h was blocked and then reinserted (simulated I_h with altered properties that simulate fast or slow/large or small I_h) show that the native I_h for each cell type influences the resting membrane potential and can delay the generation of action potentials in response to injected current. Fast I_h increases rebound depolarizations following hyperpolarizations in all cell types, and increases the likelihood of rebound action potentials (particularly in multiple-firing LSO neurons).

Another issue investigated by this thesis was the changes of membrane properties of AVCN bushy cells following congenital deafness. Previous studies have found several differences in membrane properties of principal cells of the MNTB of *dn/dn* (deaf) mice compared to CBA (normal) mice (e.g. increased excitability due to a reduction in the low-threshold potassium current). No difference in excitability or response to hyperpolarization was found in recordings of bushy cells of deaf mice when compared to normal mice. Comparing the outward potassium current after voltage steps from –70 mV to 0 mV showed no difference in average steady-state current amplitude. Outward K^+ tail currents had an average half-activation voltage that was shifted to slightly (about 4 mV) more depolarized potentials in bushy neurons of deaf mice. Pervious studies have found endbulbs of Held, the auditory nerve forming large synapses onto AVCN bushy neurons, to have a number of alterations in response to development without spontaneous afferent activity, while the calyx of Held (bushy cell axon forming a large synapse onto MNTB cells) appears to develop normally in deaf mice. Hence, lack of spontaneous activity during development does not seem to affect AVCN bushy cells in the same manner as it affects MNTB principal cells.

Finally, in order to assess the influence of acoustic activity on auditory brainstem neurons, normal hearing mice were presented with loud (but not damaging) sound from

a high-frequency loudspeaker for one hour. c-Fos immunohistochemistry was used to confirm that auditory cells had been exposed to increased neural activity. Using broadband sound (chirps of 4-12 kHz at 75 dB), a large proportion of activated neurons in the lateral region of the MNTB (low frequency region) could be detected. Previous studies have shown that neurons of the MNTB medial region, responding to high-frequency sound input, normally exhibit larger high-threshold potassium currents than lateral neurons (currents that produce rapid repolarization of action potentials, giving the MNTB neurons the ability to respond to high frequency firing). Here, sound stimulated (lateral) cells displayed a significantly shorter delay in firing action potentials, in response to current injections (150 pA, 200 ms) compared to control (lateral) cells. The after-hyperpolarization magnitude upon the repolarization of action potentials was also found to be significantly larger of sound stimulated lateral neurons compared to control lateral cells. Medial neurons, representing control and internal control conditions did not display any differences in action potential firing.

The expression of potassium channels following broadband presentation was investigated using immunohistochemistry with primary antibodies against Kv1.1, Kv1.2 and Kv3.1b channels. Previous studies have shown a gradient in the expression of potassium channels in normal mice, where Kv1.1 immunoreactivity was found to be strongest in the lateral region of the MNTB, in contrast to Kv3.1 labeling which was the strongest in medial MNTB neurons. These results show that one hour of sound stimulation of lateral MNTB neurons did not affect the pattern of Kv1.1 or Kv1.2 immunoreactivity significantly. However, a large increase in Kv3.1b-immunoreactivity was observed in the region of sound stimulated MNTB neurons, seemingly reversing the normal gradient from medial-to-lateral to lateral-to-medial protein expression. This result was further confirmed with electrophysiological recordings, where lateral cells of sound stimulated animals expressed significantly larger outward potassium current in

response to positive voltage steps. This voltage range may activate intermediate and primarily high-threshold potassium currents. Furthermore, using a Kv1 channel blocker (dendrotoxin-I), the Kv1-mediated current was found to be significantly smaller in lateral cells of sound stimulated animals compared to control lateral cells. Less low-threshold potassium current magnitude may produce a shorter delay of action potentials, as was seen in current-clamp recordings of stimulated neurons. These alterations following brief acoustic stimulation may allow MNTB principal neurons to fire at higher frequencies.

The results reported in this thesis provide insight to how specific membrane properties determine different computational features of neurons of the same auditory network, essential for detecting interaural sound level differences. These results furthermore demonstrate that brainstem auditory neurons are distinctly affected by development without spontaneous activity from the cochlea. This thesis finally highlights that brief increased neural activity can rapidly alter the membrane properties of brainstem auditory neurons.

The results of all these studies provide valuable insights into the important issue of the role of activity in regulating the membrane properties of neurons in the intact central nervous system.

Table of Contents

List of Abbreviations

ACSF	Artificial CerebroSpinal Fluid
AHP	AfterHyperPolarization
AMPA	α-Amino-3-hydroxy-5-Methylisoxazole-4-Propionic Acid
AP	Action Potential
ACSF	Artificial CerebroSpinal Fluid
AVCN	Anteroventral Cochlear Nucleus
BCNG	Brain Cyclic Nucleotide Gated
cAMP	Cyclic Adenosine MonoPhosphate
CBA	control mouse strain to *dn/dn* mice
CN	Cochlear Nucleus
D-AP5	D(-)-2-Amino-5-Phosphonopentanoic acid
DCN	Dorsal Cochlear Nucleus
DTX	Dendrotoxin
EPSP	Excitatory Post-Synaptic Potential
GABA	Gamma AminoButyric Acid
GBC	Globular Bushy Cell
HAC	Hyperpolarization Activated cation Channel
HCN	Hyperpolarization-activated Cyclic Nucleotide-gated channel
I_h	Hyperpolarization-activated cation current
IHC	Inner Hair Cell
I_{LT}	Low-threshold potassium current
I_{HT}	High-threshold potassium current
ILD	Interaural Level Difference
IPSP	Inhibitory Post-Synaptic Potential

Kv	Voltage-gated K^+ channel
LSO	Lateral Superior Olive
Map2a/b	Microtubule-associated protein 2a/b
MF	Multiple Firing
MSO	Medial Superior Olive
MNTB	Medial Nucleus of the Trapezoid Body
NMDA	N-Methyl-D-Aspartic acid
OHC	Outer Hair Cell
P#	Postnatal day #
PBS	Phosphate Buffered Saline
PSP	Post-Synaptic Potential
PVCN	Posteroventral Cochlear Nucleus
Rin	Input Resistance
SBC	Spherical Bushy Cell
SF	Single Firing
SOC	Superior Olivary Complex
TEA	Tetraethylammonium
$V_{1/2}$	Half-activation Voltage
VGluT1	Vesicular Glutamate Transporter 1
Vm	Membrane potential
Vrest	Resting membrane potential
Tmc1	Transmembrane cochlear-expressed gene 1
TTX	Tetrodotoxin

List of Figures

List of Tables

Chapter 1. General Introduction

Ion channels determine the fundamental manner in which neurons compute input/output functions. Understanding the mechanisms that regulate ion channel function and expression is therefore one of the most important subjects in neuroscience. Neuronal activity is known to be one of the major determinants of ion channel and cell membrane properties. However, most of the studies that address the role of activity in regulating ion channel expression arise from artificial systems (e.g. neuron cultures) or from systems in which neuronal activity has been suppressed or abnormally increased. The study of ion channel regulation by normal sensory inputs in the intact nervous system is an area of neuroscience that needs to be explored further.

It is generally assumed that neural activity (spontaneous or evoked) is imperative for the development of neurons and the refinement of networks. The auditory nervous system, in particular, requires extreme refinement and neurons that are especially well tuned to the processing of temporal coding and frequency information. The auditory system also contains some of the fastest connections in the brain, and networks in the auditory brainstem form a neural circuit that can detect binaural differences in the order of microseconds. Since the input to this system has a well-defined source, the cochlea, fundamental questions such as 'how does activity regulate a neural system?' can be addressed by presenting sounds to the cochlea or by modifying it. Moreover, the auditory system is elegantly topographically organized into frequency maps providing the means for very specific experiments (e.g. does activity affect the auditory system development evenly or in a frequency dependent manner?)

The work presented in this thesis focuses on the role of cochlear activity on the regulation of membrane properties of brainstem auditory neurons.

Hearing

The auditory system requires a substantial amount of metabolic energy (Klein *et al.*, 1986). The brain is the major energy consumer in the body and the auditory system has the highest rates of blood flow and metabolic activity when compared to other brain areas (Ball *et al.*, 2007).

In order to convey acoustic information to the brain, sound has to be transformed into neural coding. Complex sound waves from our environment are transduced into electrical neural impulses by the cochlea in the inner ear. Waves are converted into codes carrying information regarding their arrival time, frequencies and amplitude, and this information can alert us to dangers in our environment and allows us to understand speech and enjoy music. Sound-information travels through distinct pathways in the brain, entering the brain at the level of the brainstem and continues through the midbrain to ultimately reach the auditory cortex, where this information can be perceived as hearing.

Hearing is one of our most finely tuned senses. It deals with a variety of complex tasks, such as, sound localization. When sound waves enter the mammalian ear canal they cause the tympanic membrane to vibrate, which is connected to the three smallest bones in the body: the hammer, the anvil and the stirrup of the middle ear (figure 1.1 A). There, the sound is converted into mechanical movement, amplified many times, that

causes the oval window of the cochlea to vibrate and set the liquid inside the cochlea in motion. The cochlear duct is a coiled tube filled with endolymph that has an ionic composition similar to cytoplasm (high in K^+). It is surrounded by an additional fluid space filled with perilymph, which is an extracellular-like fluid (high in Na^+) that fills the scala vestibuli and scala tympani (figure 1.1 B). Inside the cochlear duct, on the basilar membrane, sits the organ of Corti, containing the sensory cells that generate the electrical signal that is conveyed to the auditory nerve.

Hair Cells

The sensory cells of the cochlea are called hair cells because of the sensory epithelium, the stereocilia, which gives the hair cells their distinct morphological appearance. There are two types of hair cells, inner and outer hair cells (figure 1.1 C). While inner hair cells (IHC) act as the true sensory cells that transmit impulses to the auditory nerve, outer hair cells (OHC) modify cochlear performance by increasing selectivity or sensitivity (Raphael & Altschuler, 2003). The stereocilia sit on the apical ridge of pear shaped hair cells and they are connected to each other with a tip link. Each IHC has between 20 and 50 stereocilia (with more stereocilia on the IHCs closer to the basal end of the cochlea) organized into two main rows (Raphael & Altschuler, 2003). Hair cells do not generate action potentials, instead they rely on graded potentials to modulate transmitter release continuously, providing a mechanism that can transmit information at much higher rates than spiking (Sterling & Matthews, 2005). The movement of hair cell stereocilia in the direction of the taller row opens transduction ion channels, allowing entry of K^+ and Ca^{2+}, generating a transduction current. The transduction current then activates voltage-sensitive Ca^{2+} channels along the IHC lateral wall and base, as well as Ca^{2+}-activated K^+ channels, leading to the release of neurotransmitter (most likely glutamate) at the hair cell base. The movement of the stereocilia in the

opposite direction closes the channels, and stops the release of neurotransmitter. When the stereocilia are in an upright position (resting position) the transduction channels are partially open, producing a small release of neurotransmitter, which generates spontaneous activity in the auditory nerve (Raphael & Altschuler, 2003). Spontaneous activity can also be generated by spontaneous calcium action potentials found in immature inner hair cells, which disappears around the onset of hearing (in mice during the second postnatal week) due to the expression of calcium-activated potassium channels (Beutner & Moser, 2001).

Each inner hair cell serves as the sole input for 10-30 individual afferent neurons (Fuchs *et al.*, 2003) with each spiral ganglion cell connecting a single unbranched dendrite to a solitary synaptic active zone. Synaptic active zones of inner hair cells have an extraordinary large ready releasable pool of vesicles due to the synaptic ribbon, which has approximately 100 synaptic vesicles tethered to its spherical or ellipsoidal body (figure 1.1 D) (Fuchs *et al.*, 2003; Sterling & Matthews, 2005). Ribbon synapses are also found in vertebrate photoreceptors and bipolar cells, in vestibular hair cells and in electrosensory receptors (Sterling & Matthews, 2005).

Frequency Specializations of the Cochlea

Another important feature of the auditory system is that it is arranged tonotopically, with distinct frequency maps that originate from specializations within the cochlear (figure 1.1 E). Similar to the strings of a harp, the collagen fibers of the basilar membrane are stiffer and shorter in the high-frequency region of the cochlea than in the low-frequency region that have longer and more flexible fibers. Moreover, both inner and outer hair cells vary systematically in morphology (cell size and stereocilia length). The stereociliary length is maximal in the apical and minimal in the basal cochlea,

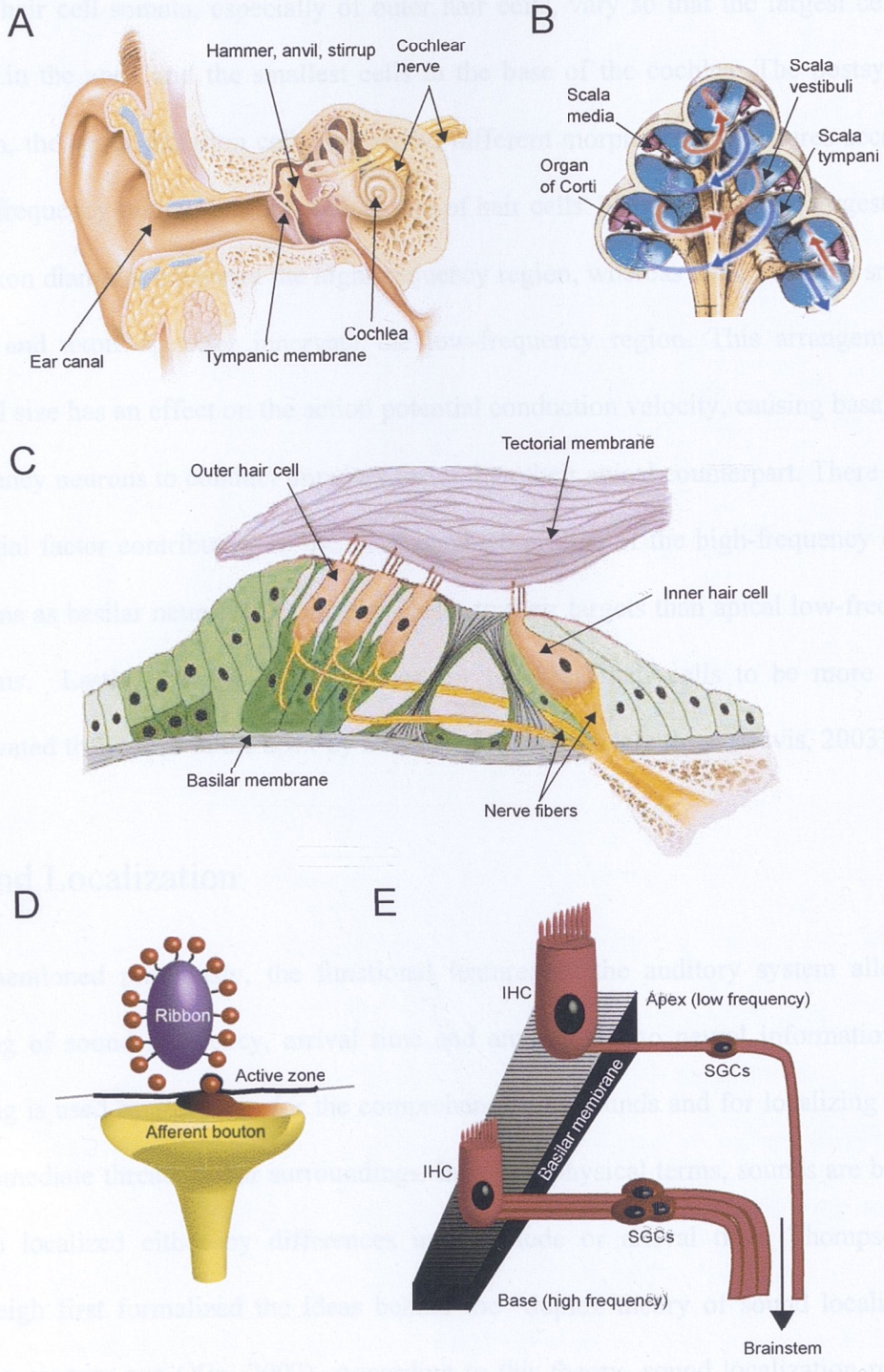

Figure 1.1: Anatomical figure of the ear and the hearing organ. **A**, Schematic figure of the ear, modified from *www.jtc.org/audcorner/images/EarAnatomy.jpg* **B**, figure of the cochlea, depicting the three canals and the organ of Corti. Modified from *www.hoorzaken.nl/images/cochcross.gif* **C**, schematic drawing of the organ of Corti outlining inner and outer hair cells and the tectorial membrane. Modified from *http://ourworld.compuserve.com/homepages/dp5/corti.jpg* **D,** cartoon of a synaptic ribbon and afferent bouton. **E**, schematic drawing of differences of hair cells and spiral ganglion cells along the cochlea, based on a figure of Davis (2003).

while hair cell somata, especially of outer hair cells, vary so that the largest cells are found in the apex and the smallest cells in the base of the cochlea. The postsynaptic neuron, the spiral ganglion cell, also shows different morphological features according to its frequency tuning, but opposite to that of hair cells. Neurons with the largest soma and axon diameter innervate the high-frequency region, whereas those with the smallest soma and axon diameter innervate the low-frequency region. This arrangement in axonal size has an effect on the action potential conduction velocity, causing basal high-frequency neurons to conduct impulses faster than their apical counterpart. There is also a spatial factor contributing to the short conduction time of the high-frequency coding neurons as basilar neurons are situated closer to their targets than apical low-frequency neurons. Lastly, there is also evidence for the basal hair cells to be more highly innervated than those in the apex by a factor of approximately three (Davis, 2003).

Sound Localization

As mentioned previously, the functional features of the auditory system allow the coding of sound frequency, arrival time and amplitude into neural information. This coding is used by the brain for the comprehension of sounds and for localizing sounds of immediate threats in our surroundings. In psychophysical terms, sounds are believed to be localized either by differences in amplitude or arrival time. Thompson and Rayleigh first formalized the ideas behind the "duplex theory of sound localization" over a century ago (Yin, 2002). According to this theory, sound localization relies on two distinct cues, difference in the level and the timing of a sound between the two ears, referred to as interaural level differences (ILD) and interaural time differences (ITD), respectively. ILD is generated primarily at high frequencies (>2-3 kHz in humans), as the wavelength is shorter and the head can act as an effective acoustic shadow giving the sound at the contralateral ear a lower level (figure 1.2 A). Auditory nerve fibers

increase their rate of firing as sound pressure levels of a stimulus increase, with a sigmoidal relationship to dB sound pressure level over a relatively narrow range (20-30 dB) and then saturates at some peak discharge (Yin, 2002). Thereby ILD can be plotted as the rate of firing versus sound level differences at the two ears (figure 1.2 D). Low-frequency sound can instead be detected by the difference in arrival time at the two ears, which critically depends on the size of the head of the animal (figure 1.2 B and E). ILD is important for resolving sound in the horizontal plane, while ITD helps mammals to detect sound in the azimuth (Yin, 2002). If a sound originates from directly in front of the head, following a vertical line of the midsagittal meridian, ILDs and ITDs are minimal yet sound can be distinguished using additional, so called spectral cues. The spectral cues are created by the diffraction and reflection of sound by the external ears, head and shoulders (figure 1.2 C) (Yin, 2002).

The duplex theory, with ILD being the means for high-frequency sound detection and ITD localizing low-frequency sound, only holds for pure tones. ITD can be utilized to detect broadband sounds of high frequency by phase-locking to the acoustic envelope (see figure 1.2 F) even though the frequency components of the broadband sound might be too high to be detected by ITD cues (Yin, 2002).

The computational theory of ITD detection was first proposed by Jeffress in 1948 (Yin, 2002). He proposed that bilateral sounds produce time-locked (phase-locked) excitatory input to the sound localizing system, through differentially distributed delay lines, which are then processed by coincidence detecting neurons. Then, according to Jeffress' model, these neurons would receive gradually delayed inputs that produce a topographic representation of azimuthal space. Anatomical evidence for delay lines is found in birds (Grothe, 2003). Mammalian ITD instead appears to rely on the contribution of inhibitory inputs to the sound localization circuit (Batra *et al.*, 1997).

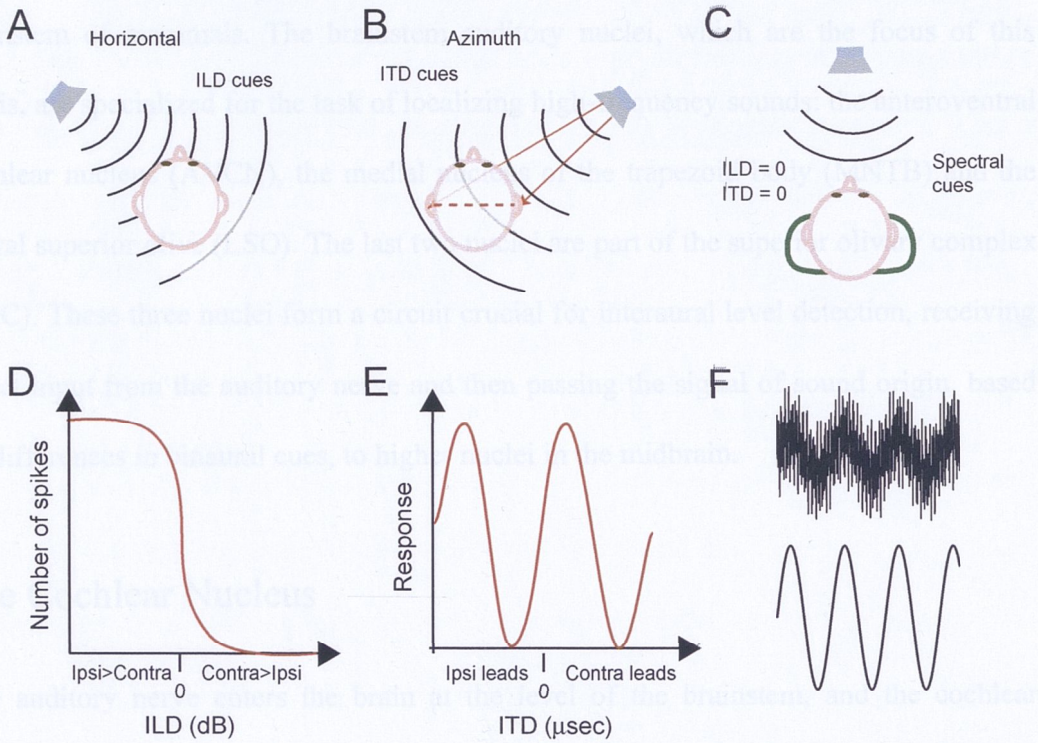

Figure 1.2: The duplex theory of sound localization. **A**, cartoon of interaural level difference (ILD) detection. **B**, cartoon of interaural time difference (ITD) detection. **C**, cartoon of spectral cues for detection of sound right in front of the head. **D**, ILD diagram, based on Yin (2002) **E**, ITD diagram, based on Yin (2002) F, schematic high-frequency sound wave (*top*) and frequency envelope (*bottom*).

Auditory Nuclei in the Brainstem

Binaural cues for sound localization are first computed in distinct nuclei of the brainstem of mammals. The brainstem auditory nuclei, which are the focus of this thesis, are specialized for the task of localizing high-frequency sounds: the anteroventral cochlear nucleus (AVCN), the medial nucleus of the trapezoid body (MNTB) and the lateral superior olive (LSO). The last two nuclei are part of the superior olivary complex (SOC). These three nuclei form a circuit crucial for interaural level detection, receiving direct input from the auditory nerve and then passing the signal of sound origin, based on differences in binaural cues, to higher nuclei in the midbrain.

The Cochlear Nucleus

The auditory nerve enters the brain at the level of the brainstem, and the cochlear nucleus (CN) is the first nucleus in the auditory brainstem to receive input from the cochlear (or auditory) nerve. The CN is subdivided into three major divisions: the anteroventral (AVCN), posteroventral (PVCN), and the dorsal (DCN) cochlear nucleus (Willott, 2001). Each division is topographically organized with regard to incoming auditory nerve fibers. This results in a tonotopic arrangement within each division of the CN in which high-frequency information lies dorsally, middle-frequency coding takes place in intermediate regions, and low-frequency processing takes place in the ventral regions (Oertel, 1999). The ventral division of the cochlear nucleus contains many different intermingled cell types with distinctive morphologies such as bushy, octopus, stellate/multipolar, and small granule cells. Ventral cochlear nucleus neurons are typically classified by their response to current injection as either Type I or Type II

neurons (Manis & Marx, 1991). The Type I cells, referred to as "choppers", fire action potentials at regular intervals independent of the phase of a tone-burst at best frequency and correspond to the morphologically classified stellate cells, with multiple dendrites (usually 3-4) that radiate from the cell body (figure 1.3 A and C) (Willott, 2001). The Type II cell response corresponds to bushy cells that are crucial for sound localization. These cells typically fire one action potential when depolarized by positive current steps (*in vitro)*, while *in vivo* recordings describe the response as 'primary like' as it reflects the input from the auditory nerve (Willott, 2001). The bushy neurons have short primary dendrites with extensive branching, and therefore a "bushy" appearance (figure 1.3 B and D). Bushy cells can be further classified into three types; large and small spherical bushy cells (SBC) that have relatively smooth, round cell bodies found in the anterior AVCN and the globular bushy cells (GBC) that have a more oblong cell body, which are found primarily in the posterior AVCN (Webster, Popper et al., 1992). Bushy cells receive input from the ipsilateral cochlear nerve through large synapses called the end-bulbs of Held. These calyceal type endings engulf the cell body of target and contain numerous release sites apposed to the target neuron (Oertel, 1999). Large SBCs receive a single or several large end-bulb synapses, and then project bilaterally to the medial superior olive (MSO) (figure 1.4). Small SBCs project to the ipsilateral lateral superior olive (LSO). The GBCs receive multiple modified end-bulbs, about 4 in mice (Oertel, 1999), and send their thick axon onto principal cells of the contralateral medial nucleus of the trapezoid body (MNTB) to form another large synapse, the calyx of Held (see figure 1.4).

Bushy cells are optimised for high-frequency firing and can fire in response to every action potential (AP) from the spiral ganglion cell at 400-600 Hz (Popper & Fay, 1992). In response to high-frequency (up to 4000 Hz) input, bushy cells respond by phase-

locking to the sound input, and firing to every second, or third sound cycle for example (Oertel, 1999).

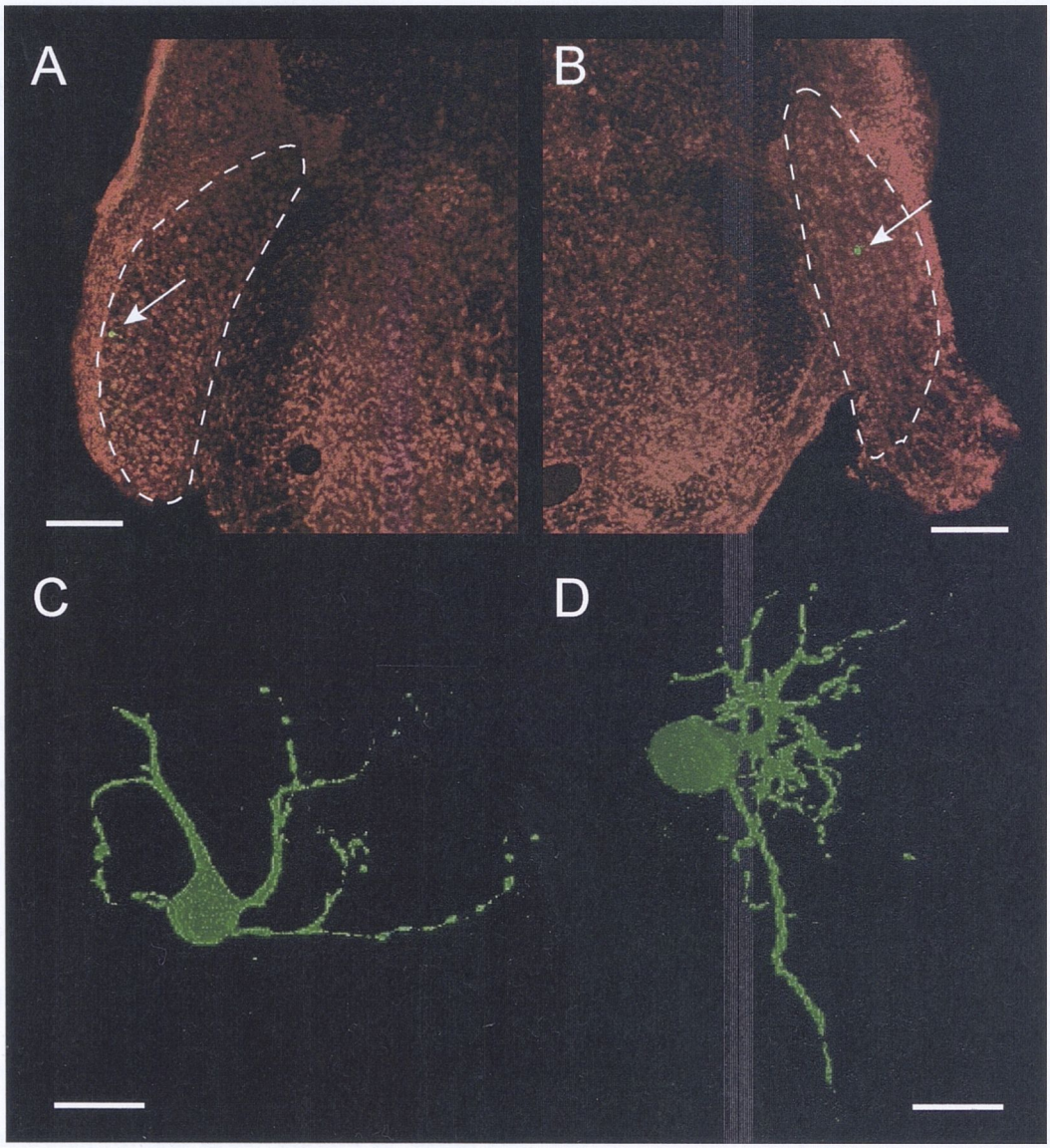

Figure 1.3: Morphology of AVCN bushy cells and stellate cells. **A-B**, confocal images, after staining with deep-red Nissl substance, outlining the AVCN with filled cells in green (arrow). Scale bar 100mm, Ventral - down **C**, filled stellate cell from (A). Scale bar 20mm. **D**, filled bushy cell from (B). Scale bar 20mm.

The Medial Nucleus of the Trapezoid Body

The medial nucleus of the trapezoid body is classically thought to serve as an inhibitory relay nucleus, providing important inhibitory (glycinergic) inputs to neurons of the lateral and the medial superior olive on the same side of the brainstem (figure 1.4). Each principal MNTB neuron provides specifically inhibitory inputs to medial tuft of dendrites of principal cells of the ipsilateral LSO and to somata of principal neurons of the MSO central cell column (Willott, 2001).

The MNTB contains three different cell types; principal cells, stellate cells and elongate cells (Kuwabara & Zook, 1991). The majority of cells in the MNTB are principal cells with a spherical or oval soma with an eccentrically placed nucleus and one or two thick, primary dendrites which end in a spray of secondary branches (Kuwabara & Zook, 1991). MNTB principal cells receive excitatory input arranged so that lateral neurons receive low-frequency and medial neurons high-frequency input (see figure 1.5) (Spangler *et al.*, 1985). Each MNTB neuron is excited through only a single calyx thus mirroring the response from the globular bushy cells in a one-to-one fashion. The calyx of Held conveys excitatory post-synaptic potentials (EPSPs) by activating rapidly desensitising AMPA-type glutamate receptors that lead to rapid and secure generation of single APs in MNTB neurons (Brew & Forsythe, 1995). Similar to AVCN bushy neurons, MNTB cells respond by firing only one or a few action potentials in response to long depolarising current steps (approximately one AP in rat, and one to five APs in mice) (Brew & Forsythe 1995). The temporal code can be correctly preserved across the GBC-MNTB synapse at frequencies as high as 600Hz allowing high synaptic fidelity (Wu & Kelly 1993). However, *in vivo* studies in the gerbil have found MNTB neurons not to respond in a one-to-one fashion, instead they appear to integrate excitatory and inhibitory input (Kopp-Scheinpflug *et al.*, 2003). Non-calyceal inhibitory boutons

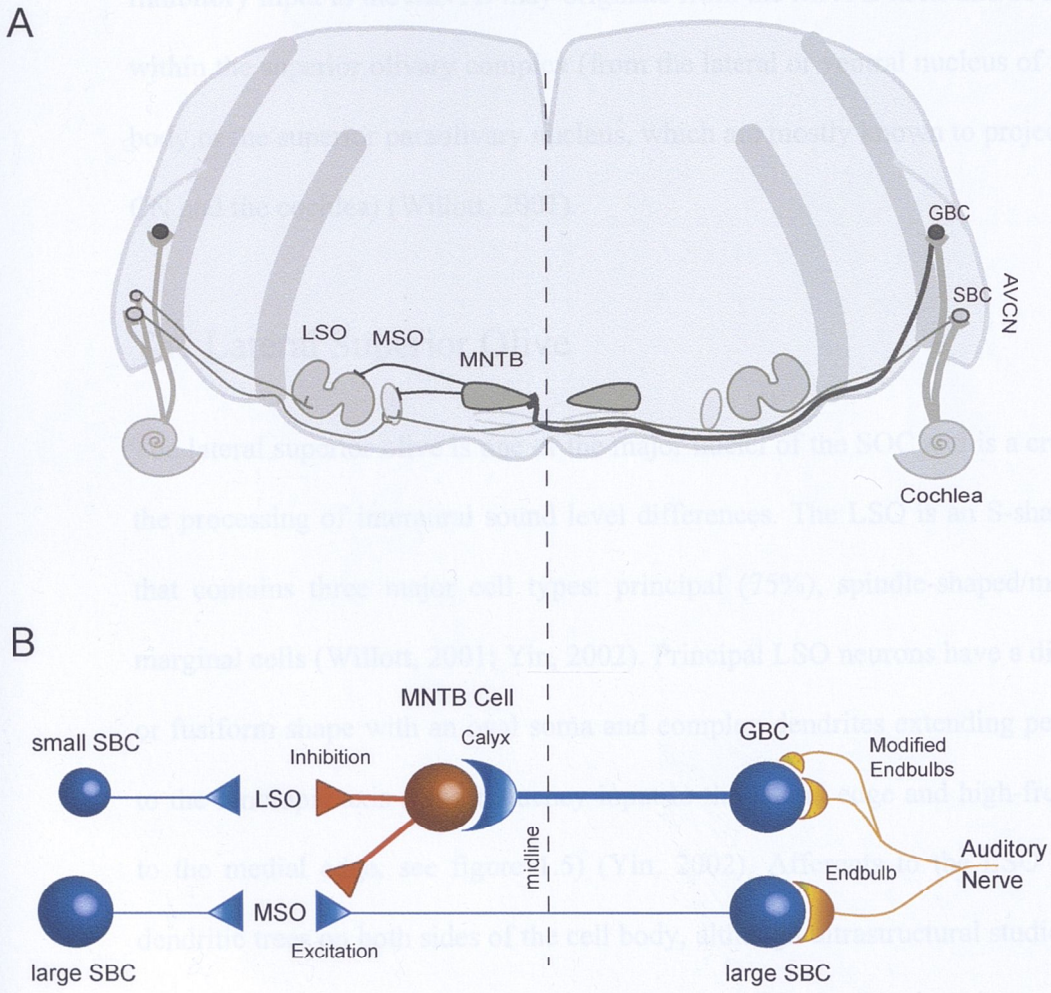

Figure 1.4: Brainstem sound localization circuit. **A**, schematic drawing of a mouse brainstem slice at the level of the AVCN, MNTB, MSO and LSO outlining neuronal connectivity. **B**, simplified drawing of connections in the auditory brainstem that are important for sound localization.

(GABAeric) have been demonstrated on the somata of MNTB neurons (Roberts & Ribak, 1987). MNTB cell bodies also display punctate staining for the glycine receptor clustering protein gephyrin, in immunohistochemical studies (Leao *et al.*, 2004b). Inhibitory input to the MNTB may originate from the MNTB itself and/or nearby nuclei within the superior olivary complex (from the lateral or ventral nucleus of the trapezoid body or the superior paraolivary nucleus, which are mostly known to project back to the CN and the cochlea) (Willott, 2001).

The Lateral Superior Olive

The lateral superior olive is one of the major nuclei of the SOC and is a crucial area for the processing of interaural sound level differences. The LSO is an S-shaped structure that contains three major cell types: principal (75%), spindle-shaped/multipolar and marginal cells (Willott, 2001; Yin, 2002). Principal LSO neurons have a distinct bipolar or fusiform shape with an oval soma and complex dendrites extending perpendicularly to the tonotopic axis (low-frequency input to the lateral edge and high-frequency input to the medial edge, see figure 1.5) (Yin, 2002). Afferents to the LSO innervate the dendritic trees on both sides of the cell body, although ultrastructural studies of the LSO show a segregation of inhibitory input onto the LSO soma and excitatory input on the LSO dendrites (Yin, 2002).

As described earlier, principal LSO neurons are sensitive to the interaural level difference of sound, which is thought to be an important indicator of the horizontal location of the sound source. Excitatory input from the ipsilateral spherical bushy cells is integrated with the inhibitory input from the MNTB and acts as the first stage of binaural interaction (Pollak *et al.*, 2002). The excitation from the ipsilateral ear and the inhibition from the contralateral ear are roughly matched even though the inhibitory signal comes from a pathway with an additional synapse interposed. The axonal

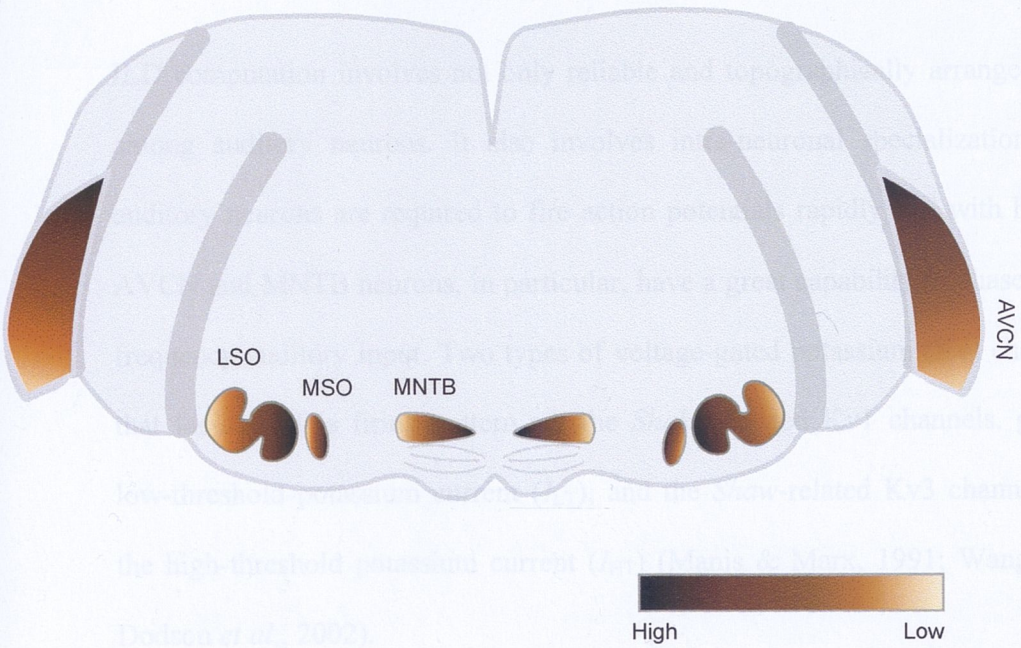

Figure 1.5: Tonotopic gradients in the auditory brainstem. The high (*dark*) and low (*light*) frequency regions are schematically outlined for brainstem auditory nuclei.

diameters of spherical bushy cells are thinner than those of globular bushy cells, giving the SBCs presumably a slower conduction velocity (Oertel, 1999). Moreover, the spatial separation of excitatory input onto the dendrites and inhibitory input onto the cell soma may also help to time-match the input.

Membrane Properties of Brainstem Auditory Neurons

ILD computation involves not only reliable and topographically arranged connections among auditory neurons. It also involves intra-neuronal specializations, as several auditory neurons are required to fire action potentials rapidly and with high accuracy. AVCN and MNTB neurons, in particular, have a great capability to phase-lock to high-frequency auditory input. Two types of voltage-gated potassium (Kv) channel families that facilitate this firing pattern are the *Shaker*-related Kv1 channels, generating the low-threshold potassium current (I_{LT}), and the *Shaw*-related Kv3 channels generating the high-threshold potassium current (I_{HT}) (Manis & Marx, 1991; Wang *et al.*, 1998; Dodson *et al.*, 2002).

Voltage-gated Potassium Channels in Auditory Neurons

The voltage-gated potassium channel (Kv) family contains eight subfamilies (Kv1-Kv6 and Kv8-Kv9) and forms tetramers of α-subunits (Coetzee *et al.*, 1999) surrounding a central aqueous pore for K^+ permeation (figure 1.6 A). Each α-subunit consists of six transmembrane segments (S1-S6) (figure 1.6 B), of which the fourth transmembrane segments (S4) is the voltage sensor domain (Soler-Llavina *et al.*, 2006). A loop between the last two transmembrane segments, S5 and S6, form the ion pore (Soler-Llavina *et al.*, 2006). Kv channels may be formed as homomers or as multimers of closely related principal subunits (for example Kv1.1 and Kv1.2 protein), giving a large diversity of Kv channels. The heteromeric K^+ channels can display properties that are intermediate

between those of two homomeric channels, although certain features may dominate in some cases (Coetzee *et al.*, 1999). Kv channels can be modulated by members of the Kvβ auxiliary subunit family, where up to four cytoplasmic β-subunits can bind to a Kv channel (Coetzee *et al.*, 1999; Sokolowski *et al.*, 2005). The Kvβ subunit genes have been shown to be highly conserved across species and can modulate the rate of inactivation of Kvα subunits (Sokolowski *et al.*, 2005) or lead to a shift in voltage dependency of activation (Coetzee *et al.*, 1999). Auxiliary β-subunits may also act as chaperones during Kv channel biosynthesis and thereby increase protein expression levels at the cell membrane (Coetzee *et al.*, 1999). Kv channels may be further regulated by glycosylation, which is a common posttranslational modification that may affect a protein's folding, stability, trafficking to the cell surface, and/or function (Watanabe 2007). Functionally, potassium channels can set resting potential, keep action potentials short, terminate periods of intense activity, phase the inter-spike interval during repetitive firing, and lower the influence of excitatory inputs (Hille, 2001).

Auditory nuclei express Kv1.1, Kv1.2, Kv3.1 and Kv3.3 mRNA at high levels (Grigg *et al.*, 2000). MNTB, AVCN (SBCs and GBCs) and LSO (single firing) principal neurons express a significant dendrotoxin-sensitive low-threshold potassium conductance (Manis & Marx, 1991; Brew & Forsythe, 1995; Dodson *et al.*, 2002; Barnes-Davies *et al.*, 2004). This low-threshold K^+ current, I_{LT}, produced by Kv1 channels can facilitate fast excitatory post-synaptic potential (EPSP) decay by reducing the membrane time constant (Brew & Forsythe 1995). AVCN bushy cells have a prominent low-threshold K^+ current that is partially active at rest giving the bushy cells a short membrane time constant and low input resistance (Manis & Marx, 1991). MNTB cells also express relatively high densities of Kv1 channels unevenly distributed at somas and neurites (Dodson *et al.*, 2002). These channels are extremely important during calyceal-evoked firing as they decrease the jitter, maintain a one-to-one response to calyceal EPSPs (one

EPSP generates one post-synaptic AP), prevent temporal summation and modulate the resting potential (Dodson *et al.*, 2002; Leao *et al.*, 2005). Principal cells of the LSO are classified according to Kv1 channel density. LSO principal cells respond to prolonged depolarization current injection with single or multiple action potentials (Barnes-Davies *et al.*, 2004). This is due to a difference in expression of DTX-sensitive Kv1 channels, with single-spiking neurons expressing more of these channels (Barnes-Davies *et al.*, 2004).

The Kv3 channel subfamily is highly expressed in fast spiking neurons where action potentials are non-decremental, of short duration and rapidly repolarized, possessing brief afterhyperpolarizations (AHP) and interspike intervals (Rudy & McBain, 2001). Some auditory neurons are examples of fast spiking neurons that are capable of responding to afferent input with action potentials of brief duration and capable of firing at high frequencies. AVCN and MNTB neurons express large densities of Kv3.1 channels (Li *et al.*, 2001). These are though to be responsible for shortening action potentials, allowing the cells to fire at high frequencies and to lock their firing to high-frequency inputs (Manis & Marx, 1991; Wang *et al.*, 1998). On the other hand, LSO neurons have little Kv3.1 channel expression when compared to AVCN and MNTB cells, which may reflect the different functions of LSO neurons compared to AVCN bushy cells and MNTB principal cells.

Hyperpolarization-activated Cyclic Nucleotide-gated Channels

Other potentially important ion channels for auditory neuron function are the hyperpolarization-activated cyclic nucleotide-gated (HCN) channels, which generate the hyperpolarization-activated cation current (I_h). The I_h is an unusual inward ion current that activates when the cell is hyperpolarized. The current was first identified in the central nervous system in rod photoreceptors. Concomitantly, the current was also

described in the sino-atrial node cell and Purkinje fibers of the heart (here termed I_f, for 'funny') where it helps set the pacemaker rhythm (Pape, 1996). I_h is now recognized as a ubiquitous entity within cells of the nervous system. HCN channels generate an inward current of mixed Na^+ and K^+ ions, in response to hyperpolarization, helping to set the resting membrane potential and modulate excitability (Pape, 1996; Chen, 1997; Shaikh & Finlayson, 2003).

There are four genes coding for the family of hyperpolarization-activated cyclic nucleotide-gated channels (HCN1-4) with about 60% identity in amino acid sequence (Moosmang, 1999). These channels have been found in a variety of species such as sea urchin, drosophila and a variety of mammals with expression in neuronal tissue, including sensory organs of the retinal, olfactory and auditory systems (Marx *et al.*, 1999). In mice all four channels are expressed in the brain, although the wide expression of HCN3 channels is at very low levels (Ludwig *et al.*, 1998; Moosmang *et al.*, 1999; Santoro *et al.*, 2000). HCN channels are known by diverse nomenclature depending on their origin and distribution and can also be referred to as *hyperpolarization activated cation channel* (HAC) or *brain cyclic nucleotide gated* (BCNG) amino acid sequence (Marx *et al.*, 1999). The HCN1 channel corresponds to HAC2 (BCNG-1), HCN2 corresponds to HAC1 (BCNG-2), HCN3 corresponds to HAC3 (BCNG-4) and HCN4 corresponds to BCNG-3 (Moosmang *et al.*, 1999).

The structure of this superfamily of voltage-gated cation channels encompasses six transmembrane helixes (S1-S6), an ion-conducting pore (P) region between the fifth and sixth segment and a cyclic-nucleotide binding domain in the C-terminus (Moosmang *et al.*, 1999) (figure 1.6 C).

The amount of I_h that passes through these channels can be (positively) modulated by the binding of cyclic-AMP (cAMP), which in turn can be induced by hormones and

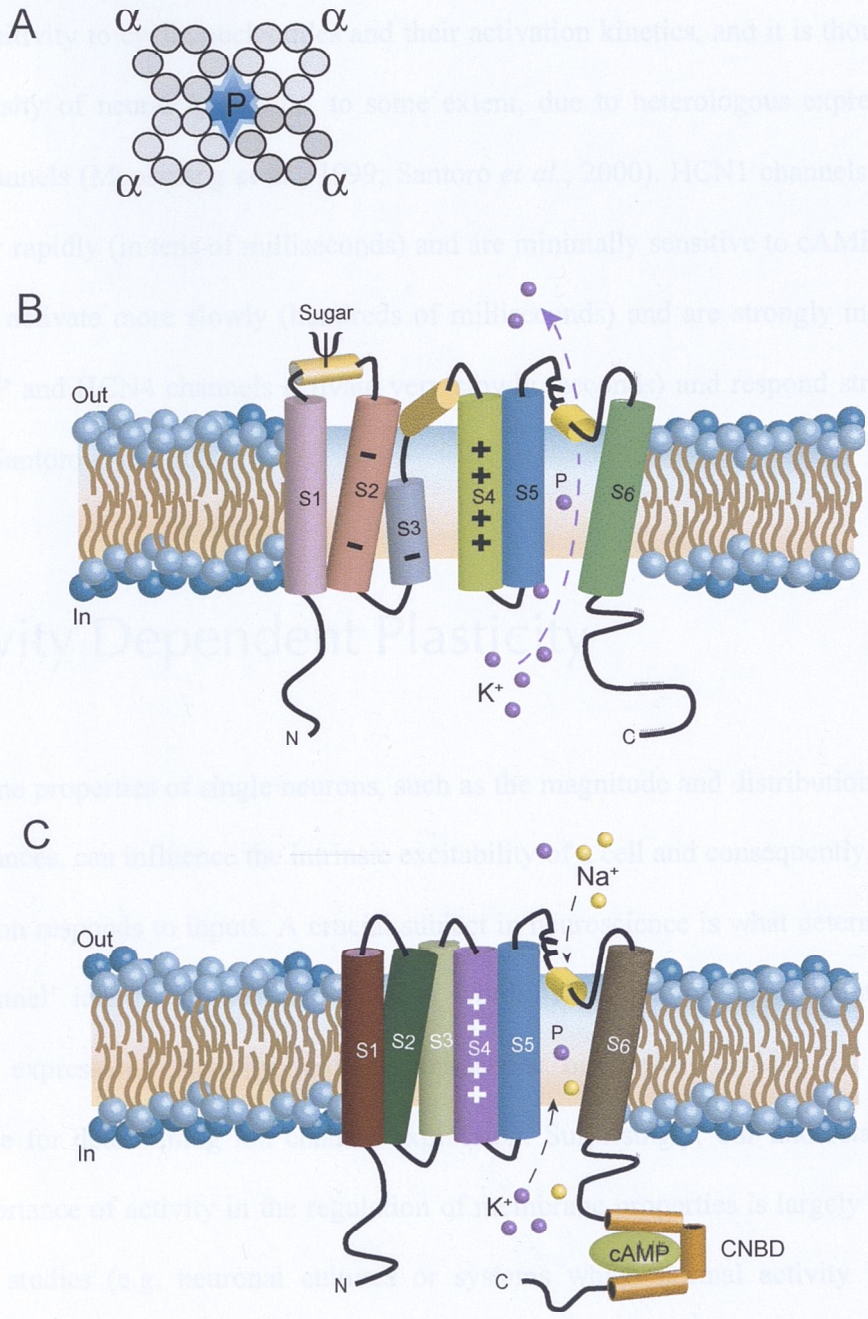

Figure 1.6: Voltage-dependent ion channels. **A**, schematic drawing of four alpha-subunits, with six transmembrane domains each, forming a voltage-dependent channel with an aqueous pore in the centre **B**, schematic drawing of the alpha-subunit of voltage-gated potassium channels, with six transmembrane domains, sitting in a bipolar lipid layer, based on Hille (2001) **C**, schematic drawing of the hyperpolarization-activated cyclic nucleotide-gated channel alpha-subunit, depicting the cyclic nucleotide-binding domain (CNBD) binding to a molecule of cyclic-AMP.

neurotransmitters (Ludwig *et al.*, 1998). The four channel types exhibit differences in their sensitivity to cyclic nucleotides and their activation kinetics, and it is thought that the diversity of neural I_h may be, to some extent, due to heterologous expression of HCN channels (Moosmang *et al.*, 1999; Santoro *et al.*, 2000). HCN1 channels activate relatively rapidly (in tens of milliseconds) and are minimally sensitive to cAMP. HCN2 channels activate more slowly (hundreds of milliseconds) and are strongly modulated by cAMP and HCN4 channels activate very slowly (seconds) and respond strongly to cAMP (Santoro *et al.*, 2000).

Activity Dependent Plasticity

Membrane properties of single neurons, such as the magnitude and distribution of ionic conductances, can influence the intrinsic excitability of a cell and consequently, the way the neuron responds to inputs. A crucial subject in neuroscience is what determines the 'net-channel' identity of neurons, in other words, what are the determinants of ion channel expression? Activity, either spontaneous or sensory-evoked, is a strong candidate for determining ion channel expression. Surprisingly, our understanding of the importance of activity in the regulation of membrane properties is largely based on indirect studies (e.g. neuronal cultures or systems which normal activity has been suppressed) and very few studies have directly examined the role of activity in a normal physiological system. In this context, the auditory system provides a rewarding area of investigation. Inner hair cells trigger both sound evoked and spontaneous action potentials in spiral ganglion neurons, with spontaneous rates as high as 140 action potentials per second in the auditory nerve (Fuchs *et al.*, 2003). When investigating how activity may regulate the properties of synaptic connections and post-synaptic cells, the

auditory system provides several advantages. Genetic models of partial and profound deafness are available (Ryugo *et al.*, 1997; Willott, 2001), alternatively, cochlear ablation or deafferentation are relatively simple procedures (Sie & Rubel, 1992; Francis & Manis, 2000; Illing *et al.*, 2000), thus providing different ways of studying a lack of afferent activity in a physiological system. The opposite scenario, increased activity, can also be studied by presenting an increased acoustic stimulus (Kaltenbach *et al.*, 2005). The sound localization pathway in the auditory brainstem is ideal for studying the role of activity in regulating membrane properties, as it displays a relatively simple circuit and cell morphology within nuclei that are well separated spatially.

Suppression of Activity

Cultures of cortical neurons that were pharmacologically prevented from firing for two days have shown dramatic increase in their intrinsic excitability. Activity-deprived neuron's excitability was mediated by changes in voltage-gated currents: increased sodium currents and decreased persistent potassium currents (Desai *et al.*, 1999). In hippocampal cultures, decreasing the activity of a neuron before synapse formation has been shown to lead to a reduction in synaptic input (Burrone *et al.*, 2002). Auditory nerve activity plays a critical role in maintaining normal synaptic function at the endbulb of Held synapse after the onset of hearing (Wang & Manis, 2005). Auditory nerve activity regulates both presynaptic (release probability) and postsynaptic (receptor composition and kinetics) function at the endbulb synapse after the onset of hearing (Wang & Manis 2005).

The Deafness Mouse

One way to study how a lack of spontaneous activity from the auditory nerve affects the auditory pathways is to utilize animal models for congenital deafness. A very prominent

deafness model is the *deafness* mouse. It suffers from profound asymptomatic hearing loss from birth with degeneration of hair cells soon after birth (Marcotti *et al.*, 2006). The deafness is caused by a spontaneous mutation on the deafness locus (*dn*) which is located on chromosome 19 and this mutation is inherited recessively (Keats *et al.*, 1995) and causes a complete lack of cochlear compound action potential responses (Marcotti *et al.*, 2006). The mutation in the gene Tmc1 (transmembrane cochlear-expressed gene 1) is responsible for the occurrence of deafness. This gene is an ortholog of the TMC1 gene, which when mutated also causes sensorineural hearing loss in humans. The normal Tmc1 protein in mice is specifically expressed in the cochlear hair cells, and can be detected as early as postnatal day 10 (P10) (Kurima *et al.*, 2003). It appears to have a direct and essential role for normal cochlear hair cell physiology but its specific function remains unknown, although the *dn/dn* mutation appears consistent with an ion channel defect since both inner and outer hair cells fail to express the potassium currents that contributes to normal functional maturation of hair cells (Kurima *et al.*, 2003). Moreover, IHC appears to fail to develop normal exocytotic machinery, as they display immature Ca^{2+} currents, suggesting that Tmc1 may also be involved in trafficking of molecules to the plasma membrane or function as an intracellular regulatory signal for differentiation of immature hair cells into fully functional auditory receptors (Marcotti *et al.*, 2006).

The *deafness* mouse has been extensively utilized as an experimental model of lack of activity, due to the absence of functional inner hair cells, causing the lack of spontaneous or acoustically evoked activity during development of the auditory nervous system. Lack of spontaneous APs, in spiral ganglion cells of the auditory nerve of *deafness* mice, have been confirmed by single unit recordings from the auditory nerve (Leao *et al.*, 2006b). This animal model also has a great advantage compared to models

of cochlear ablation where surgical procedures might not only remove the source of activity, but also trigger cell death (Mostafapour *et al.*, 2000).

No drastic reduction in auditory brainstem neuron number has been reported in the deafness mouse. The *dn/dn* mice preserve central auditory function although they undergo a progressive loss of spiral ganglion cells with age (Steel & Bock, 1984). Hence, studies that only aim to suppress the hair cell output would benefit more from *dn/dn* mice than from cochlear ablation.

Excess of Activity

The effect of increased afferent activity on the development of neurons and synapses has been predominantly studied *in vivo,* (e.g. models of tinnitus) (Salvi *et al.*, 1978; Mahlke & Wallhausser-Franke, 2004; Eggermont, 2005; Imig & Durham, 2005; Kaltenbach *et al.*, 2005; Ma *et al.*, 2006). The correlation between increased activity and membrane properties, of individual neurons in the auditory pathways, has been investigated to a much lesser extent than the effect of lack of activity in shaping membrane properties (Basta & Ernest, 2004).

Tinnitus inducing agents, such as antibiotics and excessive loud noise, have shown a decrease or no change in auditory nerve activity, while there is a general finding of increased spontaneous activity in the auditory cortex (Eggermont, 2005). In the auditory brainstem, the dorsal cochlear nucleus has been intensely studied and suggested as a possible tinnitus generator since it becomes hyperactive, with increased spontaneous activity, following exposure to intense sound (Kaltenbach *et al.*, 2005). Basta & Ernst have showed a noise-related decrease in spontaneous activity in the inferior colliculus, *in vitro* (Basta & Ernest, 2004). On the other hand, the inferior colliculus was shown to have a significant increase in spontaneous rate *in vivo,* in sound-exposed mice (Ma *et al.*, 2006). Imig & Durham (2005) used the 2-deoxyglucose techniques to examine the

effect of noise exposure on metabolic spontaneous rate in rat. These authors concluded that the cochlear nucleus is a major contributor to the spontaneous activity seen in the inferior colliculus (Imig & Durham, 2005). The 2-deoxyglucose technique is mostly used for comparing different patterns of excitation since inhibition does not appear to require as much energy as excitation (Imig & Durham, 2005). The induction of c-Fos and arg3.1 (two activity markers) immunoreactivity after salicylate administration or sound exposure has also been investigated in the auditory system of gerbils as evidence for tinnitus related plasticity (Mahlke & Wallhausser-Franke, 2004). Here c-Fos immunoreactivity was present in the VCN after sound stimulation but not following the injection of salicylate. The degeneration of synaptic endings, in the cochlear nucleus of chinchilla, was investigated using electron microscopy several weeks after loud acoustic stimulation by Kim et al. (2004). These authors have shown that degeneration occur in both putative excitatory and inhibitory synaptic endings after noise injury (Kim *et al.*, 2004).

Morphology studies are important for the assessment of the role of decreased or increased activity to the development of neurons and synapses. However, they do not reveal whether neuronal function is altered (by different ion channel expression and distribution). This thesis is dedicated to the assessment of the effect of normal sound activity on the shaping of membrane properties. Studies will be presented showing how different nuclei in the same pathway display different HCN populations in order to match the nucleus-specific computational function, and how normal hearing can rapidly modulate the expression of ion channels in the auditory system.

Chapter 2. General Methods

Methods specific to each experimental project are described in detail in the respective chapter.

Brainstem Slice Preparation

Normal (CBA strain, 12-14 or 16-23 days postnatal) and congenitally deaf (*dn/dn* with CBA background, 12-14 days postnatal) mice were decapitated without anesthetics according to the Australian National University Animal Ethics Committee protocol. The forebrain and cerebellum were removed and placed in ice-cold standard artificial cerebrospinal fluid (ACSF) (in mM: 130 NaCl, 3 KCl, 5 $MgCl_2$, 1 $CaCl_2$ 1.25 NaH_2PO_4, 26.2 $NaHCO_3$, 10 glucose, 218 sucrose equilibrated with 95% O_2, 5% CO_2). The cerebellum/brainstem block was fixed to the stage of an oscillating tissue slicer (Integraslice 7550 PSDS, Campden Instruments, UK), submerged in ice-cold ACSF and transverse slices (180-200mm) were made at the level of the ventral cochlear nucleus, the medial nucleus of the trapezoid body and the lateral superior olive. Brainstem slices were then transferred to a chamber (slice beaker) containing normal ACSF (in mM: 130 NaCl, 3 KCl, 1.3 Mg_2SO_4, 2 $CaCl_2$, 1.25 NaH_2PO_4, 26.2 $NaHCO_3$, 10 glucose, equilibrated with 95% O_2, 5% CO_2) and incubated for one hour at 35 °C and subsequently held at room temperature (22-24 °C) or at physiological temperature (35-37 °C) for electrophysiological recording. All solutions were constantly bubbled with 95% O_2, 5% CO_2.

Electrophysiology

For whole-cell current- and voltage-clamp recordings one brainstem slice was transferred to a recording chamber of standard design and fixed to the glass bottom of the chamber with a nylon grid on a platinum frame. The slice chamber was constantly perfused with ACSF with a speed of 2 ml/min. Neurons in the AVCN, MNTB or LSO were visualized using an Olympus microscope fitted with a x5 objective or a x60 water-immersion objective combined with infrared video microscopy. Patch pipettes were made from borosilicate glass capillaries (Vitrex, MODULOHMA/S, Denmark) using a patch-pipette puller (Narashige PP-83, Japan). The electrode resistance was typically 3-5 MΩ. The intracellular solution for current-clamp and voltage-clamp recordings were either $KMeSO_4$ (in mM): 130 $KMeSO_4$, 9.5 KCl, 3.0 $MgCl_2$, 10 TES, 3 Mg-ATP, 0.3 GTP-tris and 0.2 EGTA) or K-gluconate (in mM: 122.5 potassium gluconate, 17.5 KCl, 9 NaCl, 1 $MgCl_2$, 10 Hepes, 3 Mg-ATP, 0.3 GTP-tris and 0.2 EGTA). The pH was adjusted to 7.2 (for room temperature recordings) or 7.3 (physiological temperature recordings) using KOH. In order to set up the whole-cell configuration a small negative pressure was applied to the patch pipette when in proximity of a visualized target neuron and then left until a high-resistance seal (>1 GΩ) was formed between the recording electrode and the ground electrode. As the cell starts to seal (increase in seal resistance) the holding voltage was switched to –60 mV. To break into the whole-cell mode strong negative pressure pulses were applied to rupture the membrane. For electrophysiology experiments only cells with stable resting membrane potential and appropriate series resistance were used. The access resistance was routinely compensated by >80% and the liquid junction potential was usually between 4-5 mV. Pharmacological compounds were added to the perfusate in order to modulate ionic currents (Table 2.1). Current and voltage steps were applied and the corresponding

neuronal responses recorded using an Axopatch 200B amplifier (Molecular Devices, Sunnyvale, CA, USA). Electrical signals were low-pass filtered at 5 or 10 kHz, digitized at 10 or 20 kHz, respectively, using Axograph (Axon, USA) and data was analyzed with Matlab SV13 (Matworks, USA) software. Cells were also routinely filled with a fluorescent dye (Alexa^{488}, Chemicon) to obtain information on the morphology and location of the neurons recorded from.

Table 2.1: List of Pharmacological Ion Channel Blockers

Compound	*Antagonist*	*Company*
D-AP5	NMDA receptors	Tocris
Bicuculline	GABA receptors	Tocris
CNQX	AMPA/Kainate receptors	Tocris
Dendrotoxin-I (DTX)	Kv1 channels	Alomone
Strychnine	Glycine receptors	Sigma
Tetra-Ethyl-Ammonium (TEA)	Kv-channels	Sigma
Tetrodotoxin (TTX)	Voltage-dependent Na^+ channels	Alomone
ZD7288	HCN-channels	Tocris

Dynamic Clamp

The dynamic-clamp protocol, developed by Sharp *et al.* (Sharp *et al.*, 1993), allows "insertion" of simulated membrane conductances in, and/or simulated synapses between biological neurons. I used the dynamic-clamp method in order to model ionic conductances (I_h and I_{LT} specifically, see Chapter 4). Currents were simulated using a second computer (PC, data acquisition card: PCI-DAS6025 Measurement Computing/Scitech, or PCI-DAS6062 National Instruments) running real-time Linux (Linux-based Real Time Application Interface) and custom-made software (Leao *et al.*, 2005) that monitors voltage and generates currents at 40 kHz.

Sound Stimulation

Experiments were carried out in accordance with the Australian National University Animal Ethics Committee. Awake and freely moving CBA mice (16-23 day old) were presented with broadband noise (4-12 kHz) for one hour from a high-frequency loudspeaker (Scan-speak R2904/700000 tweeter, Model: 25735 59 044, City South Electrics) placed on top of a standard plastic cage, which contained a plastic divider ensuring that mice (1-3 per experiment) were located directly underneath the speaker (area dimensions 12 x 12 cm). The cage was further placed in a soundproofed chamber. Animals were given a period of 15-30 min prior to sound presentation for acclimatization in the new environment. Sound pressure levels were of non-harmful sound pressure levels of 75 dB (maximum 75 dB measured 20 cm directly underneath the speaker, equivalent of the level at the floor of the cage).

Sound Generator

Acoustic stimuli were synthesized using Labview software (National Instruments) programmed by Dr. R.N. Leão. Broadband sound was delivered as chirps of 275 ms duration, ranging from the lowest to the highest frequency within the chosen spectrum, with 12.5 ms ramps in 200 ms intervals. Pure tones were also presented to the animals in a few experiments. The pure tone frequencies (1, 4, 16 and 30 kHz) stimuli consisted of tone pulses of 100 ms duration with a ramp duration of 5 ms and 100 ms intervals between tone pulses.

Sound Calibration

A sound level meter (Type 2230, Brüel & Kjær) was used to calibrate the sound pressure level, and a free-field microphone (Type 4939, Brüel & Kjær) was used to assure the correct frequencies were emitted.

Immunohistochemistry

Animals were either immediately sacrificed, and the brainstem removed as described for electrophysiology experiments, or animals were anaesthetized (Avertin 0.4-0.6 mg/g body weight) before transcardial perfusion with cold normal saline followed by 15-20 mL of fixative (4% paraformaldehyde in 0.1 M phosphate buffer; pH 7.4). The brainstem was dissected and placed in 4% paraformaldehyde for post-fixation for 2-6 hours or over night, and for frozen sectioning thereafter placed in phosphate-buffered saline (PBS) with 30% sucrose until dehydrated. Transverse sections (60-100 µm) were cut on a vibratome (D.S.K Microslicer, Ted Pella Inc., CA, USA) for free-floating incubation. Thin frozen transverse sections were obtained at the level of the SOC on a

cryostat (Leica CM 1850). Free-floating or frozen sections were blocked with antibody blocking solution (AB-solution: 5% Normal Donkey serum in PBS with 0.3% Triton-X-100) for 30-60 minutes and subsequently incubated with primary antibodies diluted to the appropriate concentration with antibody blocking solution (Table 2.2). Sections were washed thoroughly with PBS three times and drained before application of species-appropriate Alexa-conjugated secondary antibodies diluted in AB-solution (Table 2.3) and incubation at room temperature for one hour. Washed (PBS 3 x 10 minutes) and drained sections were cover-slipped with Vectashield mounting medium (Vector Laboratories, CA) by placing a small amount of Vectashield onto a cover-glass, and then placing the cover-glass, with the drop mounting medium facing down, on top of the section and sealing it to the glass slide with nail polish around the edges.

Several experiments included that slices were further processed with Nissl stain before mounted with Vectashield. Drained sections were then incubated for exactly 20 min in PBS with 0.1% Triton-X100 and the appropriate fluorescent Nissl substance (Table 2.4) while shielded from light using aluminum foil. Sections were next washed in PBS for 1-2 hours at 4°C and protected from light. The sections stained with antibody and Nissl stain were mounted with Vectashield as described above.

Fluorescent images were collected using a laser scanning confocal microscope (Ziess LSM) fitted with 10x (Plan-NEOFLUAR 10x/0.30), 20x (Plan-APOCHROMAT 20x/0.7) or 40x oil immersion (Plan-NEOFLUAR 40x/1.30 oil) objectives at 1024 x 1024 pixel resolution.

Table 2.2: Primary Antibodies

Antigen	*Host*	*Company*	*Concentration*
c-Fos	*Rabbit*	*Santa Cruz Biotechnology*	*1:500*
HCN1	*Rabbit*	*Alomone labs*	*1:200*
HCN4	*Rabbit*	*Alomone labs*	*1:200*
Kv1.1	*Rabbit*	*Alomone labs*	*1:100*
Kv1.2	*Rabbit*	*Alomone labs*	*1:100*
Kv3.1b	*Rabbit*	*Alomone labs*	*1:500*
Map2a/b	*Mouse*	*Chemicon international*	*1:200*
VGluT1	*Guinea Pig*	*Chemicon International*	*1:1000*

Table 2.3: Alexa-conjugated Secondary Antibodies

Antigen	*Host*	*Excitation Wavelength*	*Emission Wavelength*
Guinea Pig	*Goat*	*495 nm*	*519 nm*
Mouse	*Donkey*	*495 nm*	*519 nm*
Rabbit	*Donkey*	*555 nm*	*565 nm*

Manufacturer: Molecular Probes

Table 2.4: Fluorescent Nissl Stain

Nissl substance	*Excitation Wavelength*	*Emission Wavelength*
Green fluorescent Nissl stain	*500 nm*	*525 nm*
Red fluorescent Nissl stain	*530 nm*	*615 nm*
Deep-red fluorescent Nissl stain	*640 nm*	*660 nm*

Manufacturer: Molecular Probes

Chapter 3. Hyperpolarization-activated Currents in Three Auditory Brainstem Nuclei

Introduction

Auditory brainstem neurons process and compare binaural signals that are fundamental for sound localization. The superior olivary complex is the first area within the auditory pathway where encoding of interaural time and level disparities take place. The pathway that first processes interaural level difference cues is comprised of the anteroventral cochlear nucleus, the medial nucleus of the trapezoid body and the lateral superior olive. Principal cells of the LSO receive ipsilateral excitation from AVCN spherical bushy cells and are inhibited by MNTB principal cells that relay excitatory input from globular bushy cells of the contralateral AVCN (Oertel, 1999).

Since neurons at different levels of the circuit are required to process signals differently (e.g. AVCN and MNTB phase lock to unilateral inputs while LSO neurons integrate bilateral excitation/inhibition), their membrane properties are likely to be diverse. Two important potassium currents that enable high-frequency firing and preserve single action potential firing are the high- and low-threshold potassium current, respectively. The high-threshold potassium current produces rapid repolarization of the membrane potential upon action potentials, is fast deactivating, and generates large

afterhyperpolarizations that facilitate sodium channel recovery from inactivation and Kv3 channel deactivation (Manis & Marx, 1991; Brew & Forsythe, 1995). The low-threshold potassium current, displayed especially by single firing LSO neurons (Barnes-Davies *et al.*, 2004), as well as by AVCN and MNTB cells, opposes slow depolarizations (for example from NMDA receptor mediated) and preserves single AP firing during high-frequency firing, counteracts small depolarizations and restores the membrane potential below threshold after single AP responses (Manis & Marx, 1991; Brew & Forsythe, 1995). An additional, and potentially important, voltage dependent channel type expressed in these auditory brainstem neurons is the hyperpolarization-activated cyclic nucleotide-gated channel family, which generates the hyperpolarization-activated cation current, I_h (Chen, 1997; Bal & Oertel, 2000; Cuttle *et al.*, 2001; Koch & Grothe, 2003; Santoro & Baram, 2003; Shaikh & Finlayson, 2003; Barnes-Davies *et al.*, 2004). I_h is a mixed inward Na^+/K^+ current that helps set the resting membrane potential and modulates cell excitability (Pape, 1996; Chen, 1997; Shaikh & Finlayson, 2003). Four HCN channel isoforms (HCN1-4) have been cloned (Santoro *et al.*, 1997; Ludwig *et al.*, 1998). These channel isoforms vary in their kinetics and modulation by cyclic-AMP (cAMP), which can alter the voltage sensitivity of HCN channels (Pape, 1996; Santoro *et al.*, 2000). It has been shown that AVCN, MNTB and LSO cells express I_h (Banks *et al.*, 1993; Cuttle *et al.*, 2001; Barnes-Davies *et al.*, 2004; Koch *et al.*, 2004; Leao *et al.*, 2005). This study investigates and compares I_h characteristics between these auditory nuclei, to examine in detail the contribution to the membrane properties of these cells.

Methods

Electrophysiology

Mice (CBA strain) at age 12-14 days postnatal were euthanized according to the Australian National University Animal Ethics Committee. Details about slice preparation and electrophysiology can be found in the previous chapter (General Methods). In summary: following decapitation the brain was dissected in ice-cold standard artificial cerebral spinal fluid (ACSF) (in mM: 130 NaCl, 3 KCl, 5 $MgCl_2$, 1 $CaCl_2$ 1.25 NaH_2PO_4, 26.2 $NaHCO_3$, 10 glucose, 218 sucrose equilibrated with 95% O_2, 5% CO_2). Transverse slices (180-200mm) were made of the ventral cochlear nucleus (VCN), the medial nucleus of the trapezoid body (MNTB) and the lateral superior olive (LSO) using an oscillating tissue slicer. Slices were incubated in normal ACSF (in mM: 130 NaCl, 3 KCl, 1.3 Mg_2SO_4, 2 $CaCl_2$, 1.25 NaH_2PO_4, 26.2 $NaHCO_3$, 10 glucose, equilibrated with 95% O_2, 5% CO_2) at 35 °C for one hour and subsequently held at room temperature (22-24 °C) or at physiological temperature (35-37 °C), using a heater (TC-324B Temperature Controller, Warner instrument corporation), for electrophysiological recording.

Patch electrodes (3-5 MΩ) were pulled from borosilicate glass capillaries using a Narashige electrode puller. The intracellular solution for these experiments was based on potassium methasulphate (in mM): 130 $KMeSO_4$, 9.5 KCl, 3 $MgCl_2$, 10 TES, 3 Mg-ATP, 0.3 GTP-tris and 0.2 EGTA). Whole-cell patch-clamp recordings were made from visualized AVCN bushy cells, MNTB principal cells and LSO principal cells. Bushy cells in the AVCN were identified by their appearance under the microscope and onset-firing pattern in response to depolarizing current injections, and confirmed morphologically using a fluorescent dye in the internal solution (Alexa 488, Molecular

Probes). LSO cells were recognized on their low input resistance (approximately around 70 MΩ). MNTB cell recordings were primarily obtained from neurons located in the intermediate or central region of the MNTB as a previous study have demonstrated a gradient of ionic currents, including I_h, in the MNTB (Leao *et al.*, 2006b). In several experiments, 20 μM ZD7288 (Tocris Cookson Inc., UK) was added to the bath solution in order to block I_h (for 10-20 min before the recordings). Alexa-488 was added to the internal solution in order to determine spatial position of cells.

Immunohistochemistry

Mice (P12-14) were decapitated and the brainstem was immediately removed (as described for electrophysiology experiments) and placed in fixative (4% paraformaldehyde) for 1-2 hours. Transverse sections (100 μm thick) of the brainstem were obtained using an oscillating tissue slicer (Integraslice). Free-floating thick brainstem slices were then incubated overnight in one of the following primary antibodies: anti-HCN1 or anti-HCN4 (Alamone Labs, rabbit, 1:100) followed by incubation (1 hour) in appropriate secondary antibodies (Molecular Probes, 1:1000). Sections were mounted on glass slides and cover-slipped with mounting medium (Vectashield, Vector labs).

Glutamatergic synaptic terminals were visualized with anti-VGluT1 (Chemicon, Guinea Pig, 1:1000), and dendrites and cell somas were visualized with anti-Map2a/b (Chemicon, Mouse, 1:200).

Thick slices from electrophysiology experiments containing cells filled with Alexa^{488} fluorescent dye, after electrophysiological recordings, were fixed in fresh fixative (2-4 hours). Sections were then stained with Fluorescent Nissl stain (Red or Deep-red) for 20 minutes as described in General Methods before mounting on glass slides using Vectashield mounting medium. For the cover-slide to not damage the morphology of

the brainstem slice, due to compression, several small dots of silicone rubber (Dow Corning corporation, USA) were placed in the corners of the glass slide to separate it from the cover slip.

Confocal Microscopy

Fluorescent images of 100 μm thick sections stained with HCN antibodies were collected using a laser scanning confocal microscope (Zeiss LSM) with a 10x (Plan-NEOFLUAR 10x/0.30), 20x (Plan-APOCHROMAT 20x/0.7) or 40x oil immersion (Plan-NEOFLUAR 40x/1.30 oil) objectives (Zeiss), at 1024 x 1024 pixels resolution. Fluorescent images of filled neurons were obtained with the 10x or 20x objective were obtained of the AVCN, MNTB or LSO nuclei and the location of fluorescent neurons was recorded. Stacks of high-magnification thin confocal images (between 20-70, image depth 0.5 μm) were obtained with the 40x oil-immersion lens and subsequently computer processed (LSM software) to generate 3D images of the recorded cell.

Results

Whole-cell patch-clamp recordings were obtained from visualized neurons in three different brainstem auditory nuclei: the AVCN, the MNTB and the LSO, in mice brainstem slices (CBA mice, age 12-14 days post-natal). Firing properties were recorded in current-clamp mode and typical response patterns for each studied cell type, together with 3D cell morphology, can be seen in figure 3.1. Passive membrane properties of cells were measured before and after block of the hyperpolarization-activated channels with ZD7288, and the average values before and after drug application are shown in Table 3.1.

Table 3.1. Passive Membrane Properties of Auditory Neurons Before and After ZD7288

	AVCN	*MNTB*	*LSO*
Resting potential (mV)	*-57.1 ± 0.8*	*-62.6 ± 0.8*	*-56.5 ± 0.6*
+ ZD7288	*-59.6 ± 2.9*	*-63.2 ± 0.7*	*-66.1 ± 3.3*
Input Resistance (MΩ)	*120.8 ± 6.3*	*228.2 ± 14.0*	*70.1 ± 5.3*
+ZD7288	*170.6 ± 15.6*	*257.2 ± 18.5*	*111.4 ± 13.0*
Capacitance (pF)	*22.3 ± 1.1*	*24.1 ± 1.1*	*22.2 ± 1.2*
Control (*n*)	*23*	*7*	*30*
+ZD7288 (*n*)	*9*	*7*	*6*

Neurons in the AVCN, MNTB and LSO Differ in I_h Expression

Activation of I_h was examined after hyperpolarizing the cell by applying negative voltage steps (-60 to -132 mV, 8 mV increments) for 500 ms. Current traces were recorded before and after bath application of 20 μM ZD7288 (figure 3.2 A). Both the amplitude and kinetics of I_h were quite variable in the AVCN, as emphasized by the inset in figure 3.2 A, which shows a second example trace with slower kinetics. Longer voltage steps (1 or 3s) did not significantly increase I_h amplitudes (figure 3.2 B) and these longer voltage steps were not used routinely because they caused electrophysiological recording instability (see right AVCN trace figure 3.2 B).

The ZD7288-sensitive current amplitudes activated by negative voltage steps (from -60 to -132 mV) were 1.05 ± 0.13 nA in AVCN cells (n=7), 0.28 ± 0.07 nA in MNTB cells

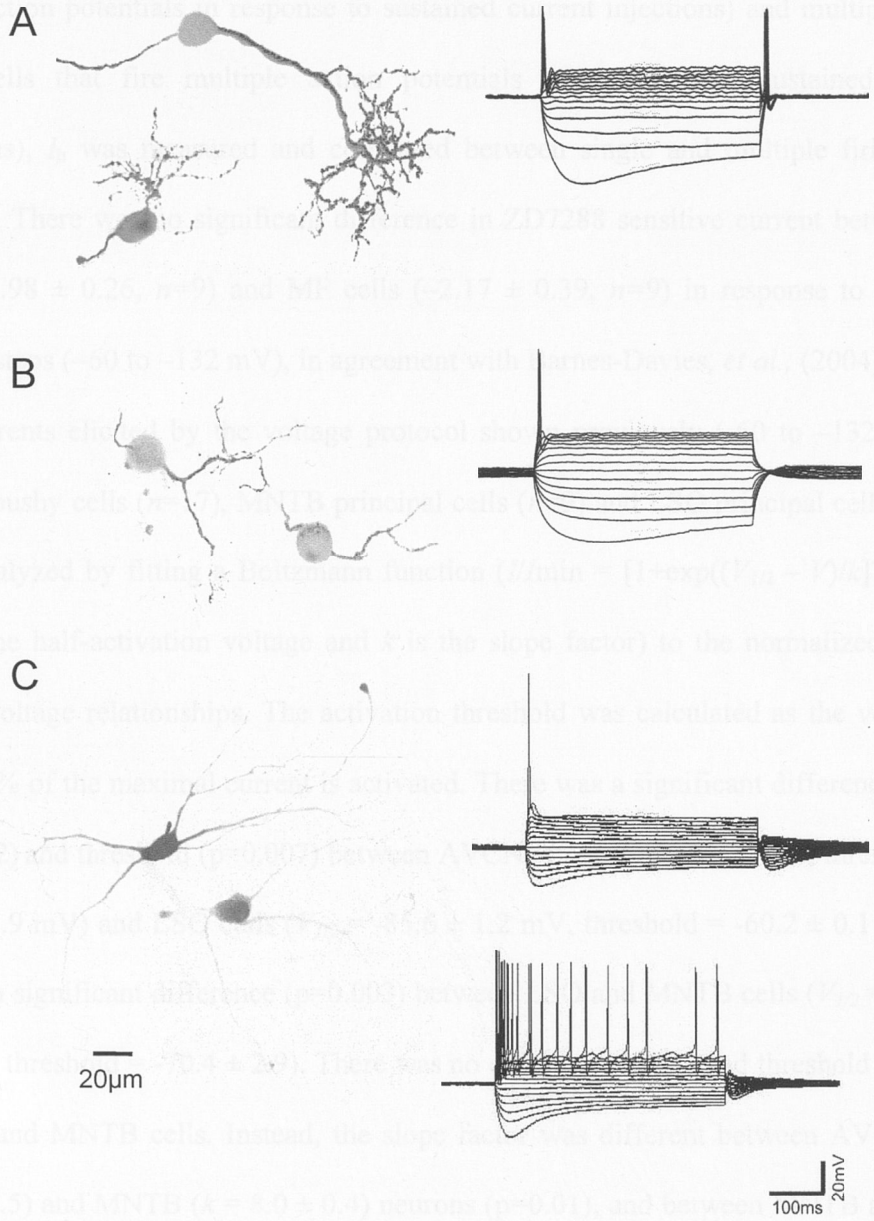

Figure 3.1: Morphology and firing patterns of brainstem auditory neurons. **A**, two examples of filled AVCN bushy cells and a typical example of membrane responses to current steps (-300 to +400 pA, 200ms duration). **B**, examples of filled MNTB principal neurons and voltage responses as in (A). **C**, examples of filled LSO neurons and membrane responses of a single firing LSO principal neuron (*top*) and a multiple firing principal cell (*bottom*).

(n=12) and 2.06 ± 0.20 nA for LSO cells (n=21), and were significantly different (p<0.01, *ANOVA*). Since LSO principal cells can be single firing (SF, cells that fire single action potentials in response to sustained current injections) and multiple firing (MF, cells that fire multiple action potentials in response to sustained current injections), I_h was measured and compared between single and multiple firing LSO neurons. There was no significant difference in ZD7288 sensitive current between SF cells (-1.98 ± 0.26, n=9) and MF cells (–2.17 ± 0.39, n=9) in response to negative voltage steps (–60 to –132 mV), in agreement with Barnes-Davies, *et al.,* (2004).

Tail currents elicited by the voltage protocol shown previously (-60 to –132 mV) in AVCN bushy cells (n=17), MNTB principal cells (n=9) and LSO principal cells (n=17) were analyzed by fitting a Boltzmann function (I/Imin = $[1+\exp((V_{1/2} - V)/k]^{-1}$, where $V_{1/2}$ is the half-activation voltage and k is the slope factor) to the normalized current versus voltage relationships. The activation threshold was calculated as the voltage at which 5% of the maximal current is activated. There was a significant difference in $V_{1/2}$ (p=0.002) and threshold (p=0.007) between AVCN ($V_{1/2}$ = -94.0 ± 2.2 mV, threshold = -65.8 ± 1.9 mV) and LSO cells ($V_{1/2}$ = -85.6 ± 1.2 mV, threshold = -60.2 ± 0.1 mV), as well as a significant difference (p=0.003) between LSO and MNTB cells ($V_{1/2}$ = -93.0 ± 2.2 mV, threshold = -70.4 ± 2.9). There was no difference in $V_{1/2}$ and threshold between AVCN and MNTB cells. Instead, the slope factor was different between AVCN (k = 10.3 ± 0.5) and MNTB (k = 8.0 ± 0.4) neurons (p=0.01), and between MNTB and LSO (k = 10.8 ± 0.4) cells (p=0.0001) (figure 3.2 C).

In order to compare I_h at room temperature to a more physiological temperature, patch-clamp recordings were obtained firstly at room temperature and hyperpolarization-activated current measured with the I_h protocol (as above). Next, the recording chamber was heated to around 35-37°C. The electrode sometimes required to be physically lowered or raised to maintain an optimal seal at the higher temperature. Heating the

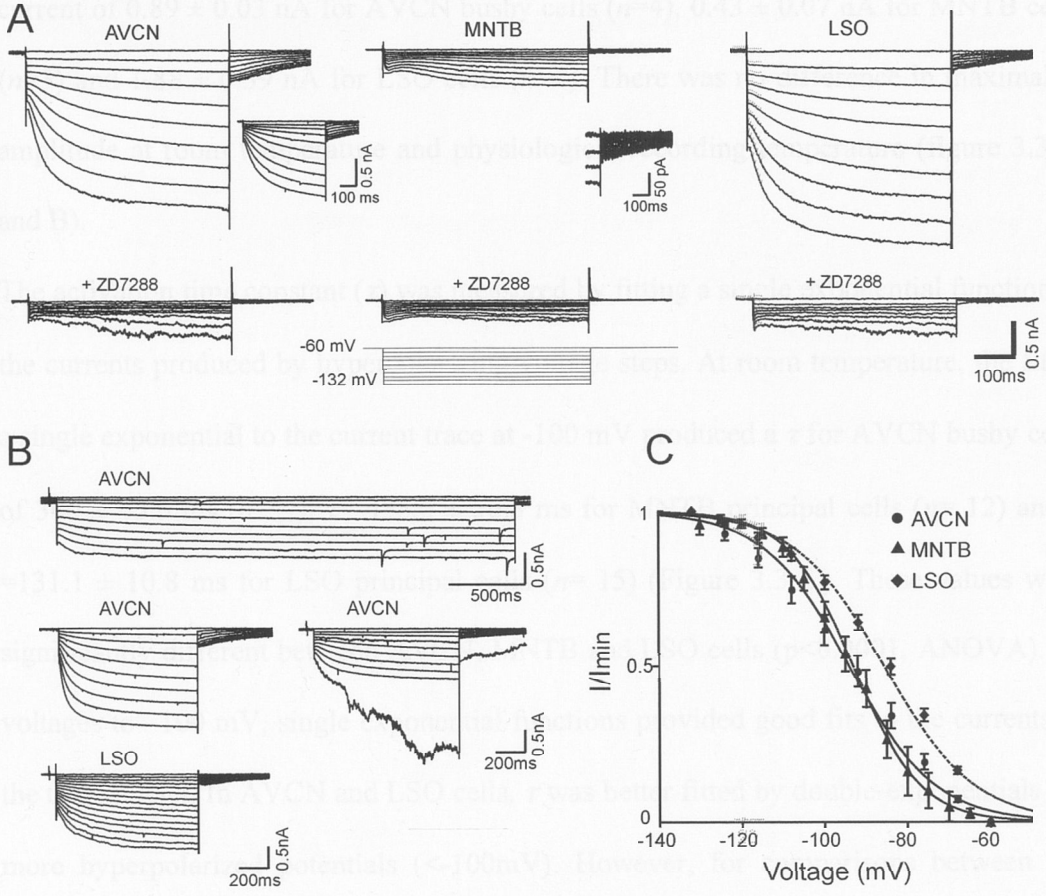

Figure 3.2: Neurons in the AVCN, MNTB and LSO exhibit diverse I_h expression. **A**, upper panel shows example current traces from an AVCN bushy cell, a MNTB principal cell and a LSO principal cell. The cells represent the whole-cell current activated by negative voltage steps (10 steps from -60 to -132 mV in 8 mV increments, during 500 ms, *middle inset*). Lower panel shows current traces from the same cells as above after application of 20 μM ZD7288 (same voltage steps as above) (Scale bars: 0.5nA, 100ms, room temperature). The capacitance artefacts have been subtracted from the beginning of traces. *Inset left:* current trace showing an example with slower kinetics for an AVCN cell (scale bars: 0.5 nA, 100ms). *Inset centre*: tail currents of the MNTB cells on a magnified scale (scale bars: 50pA, 100ms) **B**, examples of longer current responses to voltage steps (-60 to –132 mV) of 3 second (*top*) and 1 second recorded in AVCN and LSO cells. **C**, average AVCN (●, line, n=17), MNTB (▲, line, n=13) and LSO (◆, dashed line, n=17) tail currents fitted to a Boltzmann equation to yield the I_h voltage dependency. Error bars show s.e.m.

slice chamber to physiological temperature (35-37°C) produced a ZD7288-sensitive current of 0.89 ± 0.03 nA for AVCN bushy cells (n=4), 0.43 ± 0.07 nA for MNTB cells (n=3) and 1.88 ± 0.39 nA for LSO cells (n=4). There was no difference in maximal I_h amplitude at room temperature and physiological recording temperature (figure 3.3 A and B).

The activation time constant (τ) was measured by fitting a single exponential function to the currents produced by hyperpolarizing voltage steps. At room temperature, the fit of a single exponential to the current trace at -100 mV produced a τ for AVCN bushy cells of 360 ± 43.5 ms (n= 9), τ =438.6 ± 56.3 ms for MNTB principal cells (n= 12) and τ =131.1 ± 10.8 ms for LSO principal cells (n= 15) (Figure 3.3 C). These values were significantly different between AVCN, MNTB and LSO cells ($p<0.0001$, ANOVA). At voltages to –100 mV, single exponential functions provided good fits to the currents in the three nuclei. In AVCN and LSO cells, τ was better fitted by double-exponentials for more hyperpolarized potentials (<-100mV). However, for comparisons between the three nuclei, data was used in which activation was fitted with single exponentials. Tau values were also significantly different between the nuclei at physiological temperature (p=0.016, ANOVA). Tau decreased to 156.5 ± 26.7 ms for AVCN bushy cells (n=4), 117.2 ± 8.5 ms for MNTB cells (n=3) and 61.2 ± 9.6 ms for LSO cells (n=4) for a single exponential fit, although a double exponential fit was better for LSO traces at physiological temperature at –100mV (τ_{fast} = 22.2 ± 3.7 ms and τ_{slow} = 168.2 ± 38.5 ms). All cells had significantly smaller tau values at 35-37°C compared to room temperature ($p<0.01$ for all – see figure 3.3 C).

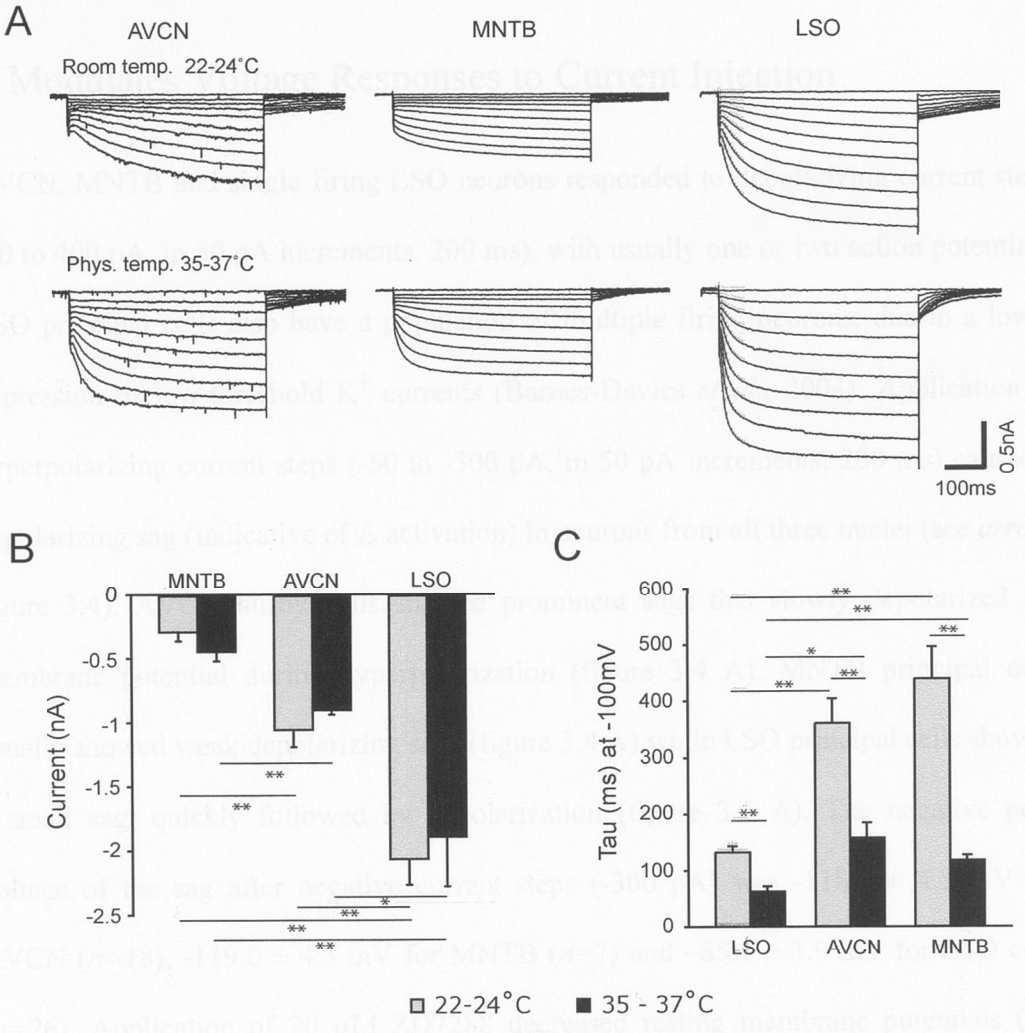

Figure 3.3: Effect of recording temperature on I_h. **A**, upper panel show example current traces from an AVCN bushy cell, a MNTB principal cell and a LSO principal cell recorded in room temperature (22-24°C) after application of negative voltage steps (10 steps from -60 to -132 mV, during 500 ms). Lower panel show current traces from the same cells, using the same voltage steps as above, after the bath temperature was heated to physiological temperature (35-37°C). The capacitance artefacts have been subtracted from the beginning of traces. **B**, summary of ZD7288 sensitive I_h amplitude in room temperature (RT, grey bars) and physiological temperature (PT, black bars) of bushy cells of the AVCN (RT: n=7, PT: n=4) and principal neurons of the MNTB (RT: n=12, PT: n=3) and LSO (RT: n=21, PT: n=4). Error bars represents standard mean of the error (s.e.m.) with p<0.01 (**) or p<0.05 (*).**C**, summary of activation time constants (tau) at -100 mV, when a single exponential function fitted well to all the cells current response in room temperature (RT, grey bars) and physiological temperature (PT, black bars), of bushy cells of the AVCN (RT: n=9, PT: n=4) and principal neurons of the MNTB (RT: n=12, PT: n=3) and the LSO (RT: n=15, PT: n=4). Error bars show s.e.m., p<0.01 (**) or p<0.05 (*).

I_h Modulates Voltage Responses to Current Injection

AVCN, MNTB and single firing LSO neurons responded to depolarizing current steps (50 to 400 pA, in 50 pA increments, 200 ms), with usually one or two action potentials. LSO principal cells also have a population of multiple firing neurons, due to a lower expression of low-threshold K^+ currents (Barnes-Davies *et al.*, 2004). Application of hyperpolarizing current steps (-50 to -300 pA, in 50 pA increments, 200 ms) caused a depolarizing sag (indicative of I_h activation) in neurons from all three nuclei (see *arrow*, figure 3.4). AVCN bushy cells showed prominent sags that slowly depolarized the membrane potential during hyperpolarization (figure 3.4 A). MNTB principal cells usually showed weak depolarizing sags (figure 3.4 A) while LSO principal cells showed a small sag, quickly followed by depolarization (figure 3.4 A). The negative peak voltage of the sag after negative current steps (-300 pA) was -118.3 ± 4.3 mV for AVCN (n=18), -119.0 ± 4.3 mV for MNTB (n=7) and –85.1 ± 3.9 mV for LSO cells (n=26). Application of 20 μM ZD7288 decreased resting membrane potentials (see table 3.1) and abolished depolarizing sags in all cell types (negative peak voltage after ZD7288 in AVCN: -163.6 ± 6.4 mV (n=6), MNTB: -150.1 ± 8.3 mV (n=7) and LSO: -111.3 ± 6.7 mV (n=6)). Post-hyperpolarization action potentials (rebound APs) were also eliminated by ZD7288 (see figure 3.4). However, in some cases when the hyperpolarizing currents caused the membrane voltage to descend below –150 mV (producing very unstable recordings) some multi firing LSO cells generated action potentials upon termination of the negative current step (see figure 3.4 A).

Current-voltage (*I-V*) relationships were also examined for the three cell types (figure 3.4 B) by measuring peak voltages (measured at the most negative voltages) and steady state currents (measured over the last five milliseconds of the current step). All three brainstem neurons showed a flat but linear *I-V* relationship between depolarizing

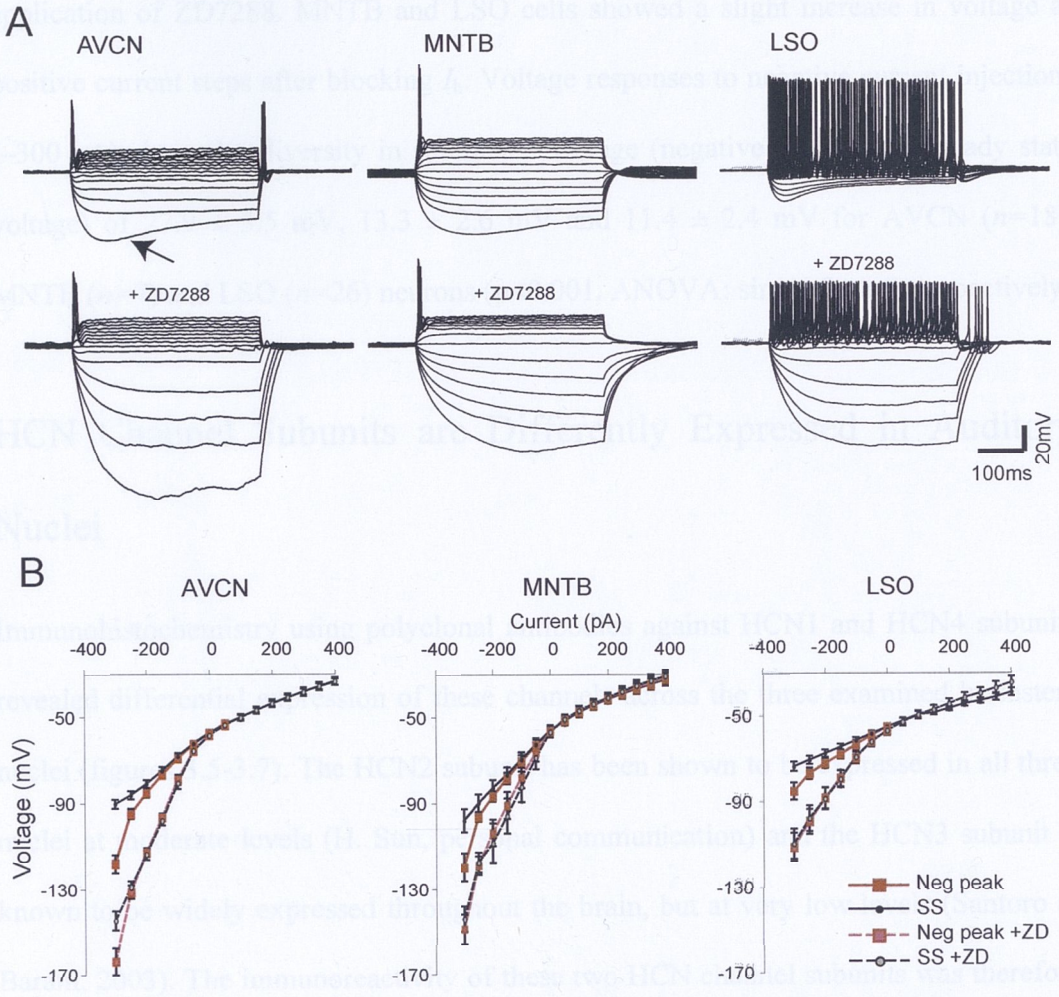

Figure 3.4: Current-voltage responses before and after ZD7288. **A**, example of a voltage response after current protocol (-300 to +400 pA, 200 ms) from an AVCN bushy cell (*left*), an MNTB principal neuron (*middle*) and an multiple firing LSO principal cell (*right*) before (*upper panel*) and after blocking of I_h with ZD7288 (*lower panel*). Scale bars; 100ms and 20mV. **B**, current-voltage relationships of the three neuron types measured at negative peak (Neg peak Ctr, red square) and at the steady state (SS Ctr, ●) of the voltage deflection under normal recording conditions and after application of ZD7288 (Neg peak +ZD pink square, and SS +ZD, ●).

current injections (50 to 400 pA) and steady state voltage, which did not change after application of ZD7288. MNTB and LSO cells showed a slight increase in voltage at positive current steps after blocking I_h. Voltage responses to negative current injections (–300 pA) showed a diversity in subtracted voltage (negative peak minus steady state voltage) of 27.9 ± 3.5 mV, 13.3 ± 2.6 mV and 11.4 ± 2.4 mV for AVCN (n=18), MNTB (n=7) and LSO (n=26) neurons ($p<0.001$, ANOVA: single factor), respectively.

HCN Channel Subunits are Differently Expressed in Auditory Nuclei

Immunohistochemistry using polyclonal antibodies against HCN1 and HCN4 subunits revealed differential expression of these channels across the three examined brainstem nuclei (figures 3.5-3.7). The HCN2 subunit has been shown to be expressed in all three nuclei at moderate levels (H. Sun, personal communication) and the HCN3 subunit is known to be widely expressed throughout the brain, but at very low levels (Santoro & Baram, 2003). The immunoreactivity of these two HCN channel subunits was therefore not compared in this study.

Neuronal cell bodies in the LSO and AVCN exhibited strong membrane expression of HCN1 protein, whereas MNTB neurons expressed HCN1-immunoreactivity at low levels. The HCN4 expression was strongly seen in MNTB and AVCN cells, but only weak expression was seen in the LSO. In the AVCN, membrane labeling of HCN1 channels appeared to be primarily in postsynaptic membranes of bushy cells, including some proximal processes (figure 3.5). Pre-incubation of sections in HCN1 peptides (against the HCN1 binding region of the HCN1 antibodies) abolished all HCN1-immunoreactivity (figure 3.5, *lower panel, middle*). In addition, AVCN cells showed a significant expression of HCN4 in bushy cell surface membranes (figure 3.5). Most of

the HCN1 labeling in the MNTB was co-localized with anti-VGluT1 labeling, which is a marker for glutamatergic presynaptic terminals, thus suggesting a presynaptic localization in calyceal terminals (figure 3.6 *upper panel*). The MNTB exhibits a tonotopic gradient of postsynaptic HCN4 expression in principal neurons (Leao *et al.*, 2006b), with higher HCN4 labeling in medial vs. lateral regions (figure 3.6). Also, there appears to be minimal presynaptic expression of HCN4 in the MNTB (figure 3.6 *lower panel, inset*). HCN1 was highly expressed in LSO principal cells, with very strong somatic and dendritic membrane labeling. The LSO showed weak and more diffuse HCN4 expression (figure 3.7).

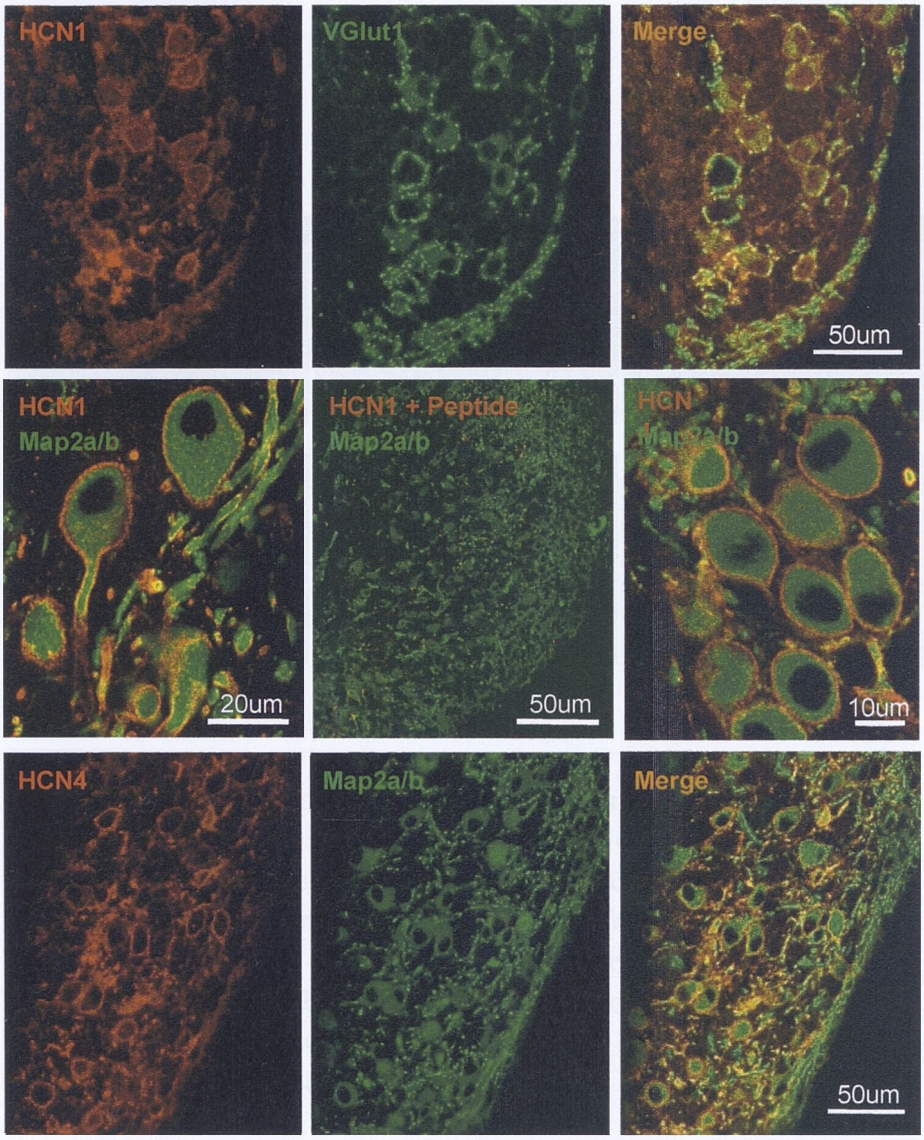

Figure 3.5: Composition of HCN family proteins in the AVCN. Red staining represent anti- HCN1 or HCN4 labelling, green labelling represent either the presynaptic marker VGluT1 or soma and dendritic marker Map2/b (see figure for labels). The HCN1 antibody showed strong membrane labelling of somata and processes in the AVCN. The HCN4 antibody labelled membranes of neurons in the AVCN. Ventral - down.

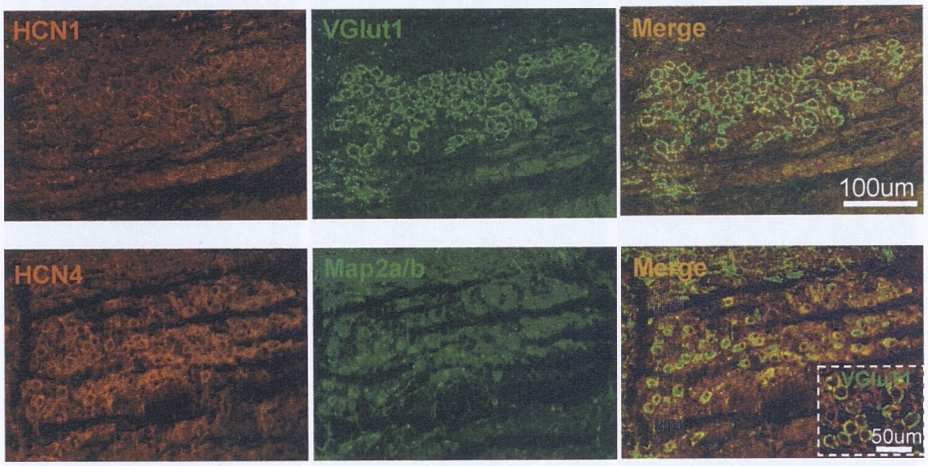

Figure 3.6: Composition of HCN family proteins in the MNTB. Red staining represents anti- HCN1 (*top*) or HCN4 (*bottom*) labelling, green labelling represent either the presynaptic marker VGluT1 or soma and dendritic marker Map2/b (see figure for labels). The HCN1 antibody showed no detectable immunoreactivity compared to background staining. The MNTB expressed some HCN4 labelling that was co-localized with VGluT1, showing a probable presynaptic labelling (*see inset*). Lateral to the left.

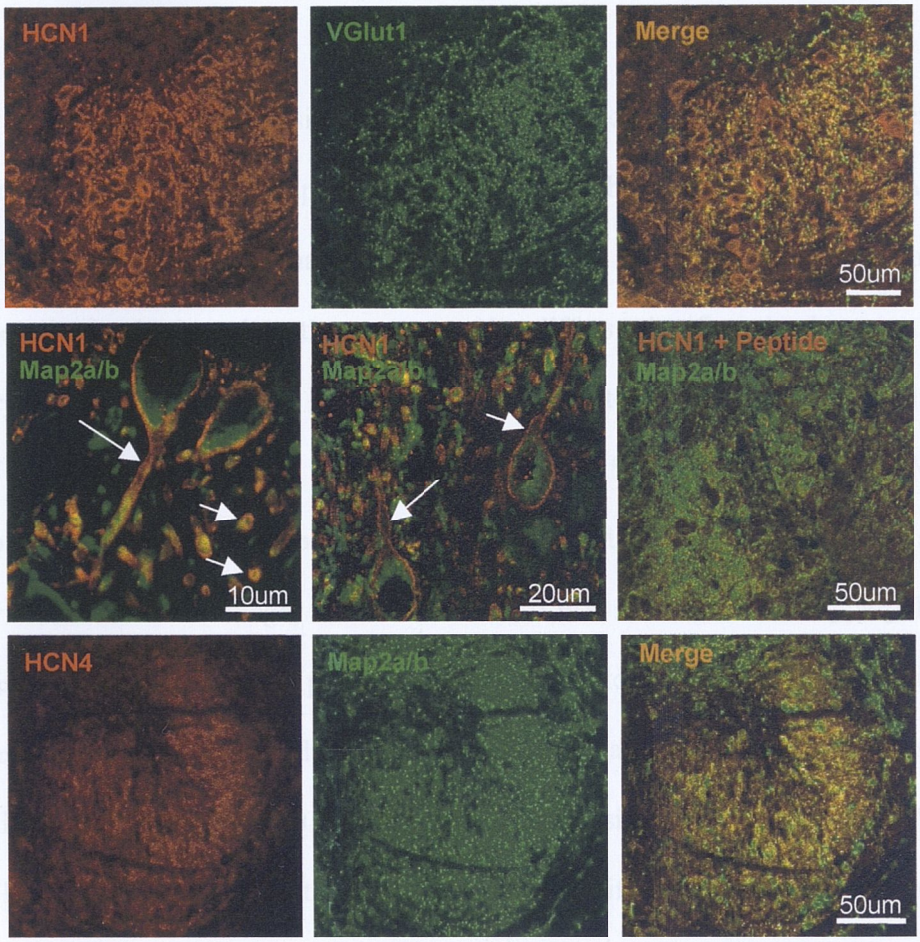

Figure 3.7: Composition of HCN family proteins in the LSO. Red staining represent anti- HCN1 or HCN4 labelling, green labelling represent either the presynaptic marker VGluT1 or soma and dendritic marker Map2/b (see figure for labels). The HCN1 antibody showed strong labelling of LSO neurons somata and dendrites. HCN4 staining was very weak in the LSO. Medial to the left.

Discussion

In this study, using electrophysiology and immunohistochemistry, the differences in I_h properties and HCN channel expression were examined between neurons of the AVCN, MNTB and LSO. In summary, the results show that the expression of the hyperpolarization-activated cation current, I_h, differs significantly between these auditory brainstem nuclei. The magnitude of I_h is greater in LSO principal cells than AVCN bushy cells, which in turn exhibit an I_h significantly larger than in MNTB principal cells. The voltage dependency of I_h shows that AVCN and MNTB cells have similar half-activation voltage, which is about -10 mV shifted towards hyperpolarized potentials compared to LSO principal cells. Activation kinetics of LSO principal neurons were also significantly different to AVCN and the MNTB neurons. The activation time constant of AVCN bushy cells was not significantly different to MNTB cells. The current-voltage relationship demonstrated differences in I_h activation after hyperpolarizing current steps between the three nuclei. Changes in membrane potential and input resistance, after blocking I_h, were greater in LSO cells than in MNTB and AVCN cells, indicating that this current might be more tonically active during rest in LSO neurons.

The immunohistochemistry results displayed considerable variation in HCN subunit expression between the three nuclei: AVCN bushy cells showed robust HCN1 and HCN4 staining, MNTB cells had mostly HCN4 staining and LSO neurons displayed a distinct HCN1 staining. Neurons in the AVCN and LSO also showed a strong membrane expression in both soma and dendrites of HCN1. In the MNTB, HCN1 is also expressed presynaptically in the calyces of Held.

AVCN, MNTB and LSO Cells Express Different Combinations of HCN Subunits

Neurons in the AVCN and SOC express more than one HCN channel type. The HCN subunit composition, examined in the AVCN and the SOC using immunohistochemistry, agrees with the electrophysiology data measured in these nuclei. The slowly activating I_h in AVCN bushy cells is likely to be due to the expression of HCN4 channels, known to have slow kinetics. AVCN cells were also intensely labeled by anti-HCN1 antibodies, suggesting that HCN1 and HCN4 together can account for the substantial I_h expressed by these cells. The observed variability in both amplitude and kinetics of I_h between AVCN neurons may be due to differences in the proportion of HCN1 and HCN4 channels expressed in different neurons (e.g. GBCs and SBCs). MNTB cells appear to mostly express the slowly activating HCN4 channels, which may also be reflected in the wide sag in response to negative current injections. LSO cells strongly express HCN1 channels, in accordance with the fast activating I_h seen in these cells. This is in agreement with studies in rat displaying a strong labeling of HCN1 in the LSO and the AVCN and weak HCN1 staining in the MNTB, which instead exhibited the strongest HCN2 staining of these three nuclei (Koch et al., 2004). Despite the fact that HCN1 is strongly expressed in both AVCN and LSO, I_h is substantially larger and faster in the latter. These differences might be related to heteromerisation of HCN channels. It has been shown elsewhere that I_h channel isoforms can exist as both homomers and heteromers (Moosmang et al., 1999; Santoro et al., 2000). Heteromers of the HCN1/HCN2 have been identified in mouse brain indicating that heteromeric channels exist *in vivo* (Much et al., 2003). Some cells, such as basket and stellate cells of the cerebellum exclusively express HCN1 but not HCN2, suggesting that HCN channels preferentially form homomeric complexes (Moosmang et

al., 1999). Therefore, it is possible that HCN1 homomers are more 'common' in LSO neurons than AVCN bushy cells. Heteromeric HCN1-HCN4 channels have been studied in the rabbit heart, where neither HCN1 channel nor HCN4 channel activation could account for the native current seen in sino-atrial node cells alone, but a heteromeric expression of the two fitted activation kinetics and cAMP sensitivity (Altomare et al., 2003). This expression pattern might be applicable to AVCN bushy cells, accounting for an I_h magnitude that is between that of the largely HCN1 expressing LSO cells and the HCN4 expressing MNTB principal cells. This gradient of I_h magnitude was retained in physiological temperature. I_h kinetics are temperature sensitive, showing significant decreased activation time constants for all cell types at physiological temperature compared to room temperature. The activation constant for LSO cells was about twice as fast at physiological temperatures, compared to MNTB cells that displayed kinetics close to four times as fast.

Modulation of I_h

In addition to different kinetics, there may also be differences in the modulation of I_h. I_h can be regulated by cAMP, which in turn can be modified by neurotransmitters such as dopamine and adrenalin (Shepherd, 1994). However, this modulation is strong in HCN4 subunits and weak for HCN1 subunits. Our results demonstrate that HCN1 channels are the major carriers of I_h in LSO cells but not in the MNTB and AVCN, and therefore, catecholaminergic inputs could tonically alter the resting characteristics of MNTB (see Banks *et al.* 1993) and AVCN neurons but have little effect on LSO cells. Conversely, I_h in LSO neurons can be more 'easily' modulated by neural activity (e.g. APs and IPSPs) than I_h in AVCN and MNTB, as the fast kinetics of HCN1 require less depolarization/hyperpolarization time than other subunits. This means that short bursts

of APs are more likely to deactivate (and for IPSPs bursts, activate) I_h in the LSO than in the MNTB and AVCN.

Previous studies have shown that altered expression of single HCN channel subunits may have significant functional consequences. For example, CA1 pyramidal neurons, from HCN1 knock-outs, showed enhanced performance in learning and memory tasks in mice (Nolan *et al.*, 2004). It was proposed by Santoro and Baram (2003) that neuronal networks may regulate activity by up-regulating either the slow activating channels or the fast acting HCN1 channel. Slow kinetics of I_h has previously been suggested as a mechanism underlying neuronal tuning for sound duration (Casseday 1994, Hooper 2002). A recent study by Proenza and Yellen (Proenza & Yellen, 2006) also focuses on a distinct population of voltage-independent HCN channels. These channels could contribute to the instantaneous currents seen in current traces in response to negative voltage steps, which can accelerate both depolarization and repolarization.

In summary, this study highlights the existence of significant differences in I_h between different auditory brainstem nuclei that are involved in sound localization.

Chapter 4. I_h Regulates the Firing Properties of Auditory Neurons

Introduction

In order to perform complex spatial hearing computations, auditory brainstem neurons are functionally and morphologically specialized. For example, AVCN bushy cells and MNTB principal neurons display one or two simple dendrites and an oval or spherical soma, and both receive giant presynaptic glutamatergic terminals directly onto their somas. They are tuned to high-frequency firing and phase-locking, which is facilitated by strong voltage-dependent potassium channels (Brew & Forsythe, 1995; Popper *et al.*, 2002; Rothman & Manis, 2003). On the other hand, neurons in the lateral superior olive are bipolar with complex dendrites, specialized for synaptic integration and sound envelope coding. In addition to anatomical differences, auditory neurons also show distinct ion channel densities in different subcellular domains. Kv1.2 channels in MNTB cells, for example, are concentrated at initial axonal segments while Kv3.1 channels are mostly localized in cell somas (Wang *et al.*, 1998; Dodson *et al.*, 2002). Variations in ion channel distribution are important for action potential generation and synaptic integration. Subcellular localization of the hyperpolarization-activated cation current (I_h) in particular has been the subject of intense investigation (Berger *et al.* 2003, Desjardins *et al.* 2003, Magee 1999, Migliore *et al.* 2004, Nolan *et al.* 2004, Oviedo and Reyes 2005). I_h localized in dendrites is responsible, for example, for

normalizing excitatory post-synaptic potentials (EPSP) integration along dendritic branches, causing distal and proximal synaptic inputs to have similar integrative properties (Magee 1999).

In the previous chapter differences in I_h and hyperpolarization-activated cyclic nucleotide-gated (HCN) channel expression, of several auditory brainstem nuclei, were presented. Here, cell function/excitability is related to these differences in I_h kinetics and amplitude, in the LSO, AVCN and MNTB, using the dynamic-clamp method.

Methods

Transverse brain slices containing the superior olivary complex (SOC) were obtained from 12-14 day old normal mice (CBA) as described in the General Methods chapter. Electrophysiological recordings using glass pipettes filled with a K^+-methylsulfate internal solution were made as described previously. In all experiments ZD7288 (20μM) was added to the extracellular perfusion solution (ACSF), to block the cells native I_h, before dynamic clamp recordings commenced.

I_h and I_{LT} Simulation

In order to examine the contribution of I_h to the membrane properties of brainstem auditory neurons this current was stimulated using the dynamic clamp method. In order to assess the effect of I_h kinetics on cell function, two kinetically distinct I_h were used, a fast I_h based on the LSO recordings (from Chapter 3, $V_{1/2}$ = -83 mV, k = 10.1 mV) and a slow I_h based on AVCN recordings (from Chapter 3, $V_{1/2}$ = -94 mV, k = 10.4 mV). Simulated I_h also varied in amplitude (a high-amplitude I_h based on the LSO I_h amplitudes and a low-amplitude I_h based on AVCN I_h amplitudes). The dynamic-clamp

method was implemented on a second computer running real-time Linux and custom made software that reads voltage and generates currents at 40 kHz.

In order to add different macroscopic I_h to the neurons, the 'real' I_h was first blocked with 20 μM of ZD7288. Simulated I_h was calculated by $I_h = \bar{g}_h u(V - V_{rev})$ where $\bar{g}_h$ is the maximal hyperpolarization-activated conductance, u is the evolution variable, V is the membrane voltage and V_{rev} is the I_h reversal voltage (for AVCN V_{rev}= -42.8 ± 6.1 mV (n=6), for LSO V_{rev}= -49.6 ± 3.7 mV (n=4)). Evolution variables were obtained by the following equation:

$$\frac{dx}{dt} = \frac{x_\infty - x}{\tau_x}, \; x=u$$

The activation time constant vs. voltage ($\tau_x(V)$) and steady-state conductance vs. voltage (Boltzmann) functions for I_h slow and I_h fast were respectively:

$$\tau_u(V) = \frac{10000}{235.55e^{0.0782(V+23.76)} + 0.33e^{-0.0614(V+23.76)}} + 154.57 \qquad (I_h \text{ Slow})$$

$$u_\infty(V) = \left(1 + e^{0.1022(V+87)}\right)^{-1} \qquad (I_h \text{ Slow})$$

$$\tau_u(V) = \frac{10000}{234.5878e^{0.0648(V+20.049)} + 5.28e^{-0.0369(V+20.049)}} + 37.08 \qquad (I_h \text{ Fast})$$

$$u_\infty(V) = \left(1 + e^{0.144(V+82)}\right)^{-1} \qquad (I_h \text{ Fast})$$

These equations where obtained by fitting the time-constants of I_h and the normalized I_h conductance across various voltages from I_h recordings of AVCN bushy cells (I_h slow) and LSO cells (I_h fast) from Chapter 3. Note that the Boltzmann relations shown refer to steady state conductance, not steady state current. In order to account for the differences

in amplitude found in different nuclei, different amplitudes of $\bar{g}_h$ (15 nS for low amplitude and 30 nS for high amplitude – low amplitudes in MNTB neurons had $\bar{g}_h = 7$ nS) were used. The low-threshold voltage-dependent K^+ currents, I_{LT}, (Leao *et al.*, 2005) have also been simulated using the dynamic clamp in some LSO cells.

Immunohistochemistry

Normal mice (CBA) at P14 and P21 were killed and the brain was dissected, similar to the method used for electrophysiology, and processed for immunohistochemistry as described in General Methods. In summary, following decapitation the brainstem and cerebellum was immediately free dissected and placed in 4% paraformaldehyde for two hours. The tissue block was next glued to a stage (Supa Glue, Selleys Chemical company) of an oscillating tissue slicer (Integraslice), submerged in cold PBS and transverse sections (100 μm) were obtained at the level of the AVCN and the LSO. Free-floating sections were incubated 24-72 hours at 4°C in primary antibodies: HCN1 (Alomone Labs, rabbit, 1:100) and Map2a/b (Chemicon, mouse, 1:200), followed by one hour incubation in secondary antibodies: donkey anti-rabbit and donkey anti-mouse (1:1000, Molecular probes). Sections were cover-slipped with Vectashield mounting medium and sealed with nail polish.

Images were collected on a Carl Zeiss confocal microscope using a 40x oil immersion objective, at 1024 x 1024 pixel resolution.

Results

The dynamic-clamp method was used to investigate the effect of having different I_h magnitude and kinetics, by observing the effects of I_h on resting membrane potential,

action potential firing and rebound depolarization amplitude. This method was used to explore what phenotype a typical AVCN I_h (*slow* kinetics with *low* conductance amplitude: slowτ/lowA) would create if inserted into other brainstem neurons with their distinct membrane properties. The appropriate kinetics and amplitude of I_h for LSO principal cells (*fast* kinetics, *high* conductance amplitude: fastτ/highA) was also used to investigate how neurons with normally slow kinetics would respond to these parameters. In addition, only one parameter was altered at a time, including dynamic clamp models of an I_h with slow kinetics, but still high conductance (as a combination of the AVCN *slow* kinetics and the LSO *high* conductance amplitude: slowτ/highA), and the opposite situation with LSO *fast* kinetics and *low* conductance amplitude of I_h as for the AVCN (fastτ/lowA).

I_h characteristics were first altered of AVCN, MNTB and LSO cells in order to assess the effect of I_h amplitude and kinetics on resting membrane potential. In order to assess whether I_h could be simulated by the dynamic clamp, the control conditions were compared before and after application of ZD7288 with the appropriate dynamic clamp simulations (I_h slow τ/lowA for AVCN and MNTB cells and I_h fastτ/highA for LSO cells – with maximal I_h conductance of 15 ± 1, 7 ± 1 and 30 ± 2 nS, for AVCN, MNTB and LSO respectively,). If a similar membrane potential was reached after I_h was blocked pharmacologically and subsequently reintroduced as the simulated I_h, the cell was accepted for further dynamic clamp experiments in which I_h was altered (figure 4.1 A).

Effect of I_h on Resting Membrane Potential and Action Potentials in the AVCN, MNTB and LSO

The resting membrane potential of AVCN bushy cells (n=4) in control conditions, before application of ZD7288, was -58.8 ± 1.7 mV and –65.4 ± 5.0 mV after blocking I_h. Upon reintroduction of an I_h appropriate for AVCN bushy cells (I_h slowτ/lowA) the membrane potential returned to –60.4 ± 0.4 mV. Increasing I_h amplitude (I_h slowτ/highA) caused the cell to depolarize approximately 1 mV (to -57.7 ± 1.7 mV, p=0.04, paired t-test). Adding a fast I_h to the membrane caused further depolarization (to –56.1 ± 1.7 mV for I_h fastτ/lowA and -53.7 ± 1.4 mV for I_h fastτ/highA, p<0.01 for both cases, paired t-test). In MNTB principal neurons (n=4), altering only I_h amplitude (I_h slowτ/highA) caused the cell membrane to depolarize by 3 mV (from -65.3 ± 0.8 mV to -61.7 ± 0.2 mV, p=0.01, paired t-test). Addition of fast I_h also caused a significant change in cell membrane resting potential (to –63.5 ± 0.6 mV, I_h fastτ/lowA, p=0.02, and to -61.4 ± 0.5 mV, I_h fast/high, p<0.01, paired t-test). In single firing LSO neurons (SF, n=5), simulating I_h with different kinetics and amplitude dramatically altered the resting potential of the cells (from -61.3 ± 0.8 mV to -65.7 ± 0.4 mV, -64.6 ± 0.5 mV and –67.1 ± 0.2 mV for I_h slowτ/highA, I_h fastτ/lowA and I_h slowτ/lowA respectively – p<0.01 for all cases, paired t-test). Dynamic-clamp results are summarized in Table 4.1.

Action potential properties (amplitude and half-width) were also differently affected by changes in I_h in different nuclei. Using a 200 pA current step, control AP amplitude in AVCN cells was equal to 62.8 ± 5.3 mV and did not change significantly by altering I_h amplitude (I_h slowτ/highA). Changes in I_h kinetics significantly decreased the AP amplitude (58.7 ± 5.4 mV for I_h fastτ/lowA and 57.5 ± 5.9 mV for I_h fastτ/highA, p=0.01 in both cases, n=4, paired t-test – figure 4.1 B). AP amplitude in MNTB neurons was only affected by differences in I_h amplitude (control: 61.5 ± 4.1 mV; I_h

slowτ/highA: 60.2 ± 3.9 mV; I_h fastτ/highA: 56.2 ± 3.1 mV; p=0.03 and p=0.01 respectively, n=5, paired t-test – figure 4.1 B). In LSO neurons, 'slowing' I_h increased AP amplitude (control: 91.4 ± 5.7 mV; I_h slowτ/highA: 96.5 ± 3.4 mV; I_h slowτ/lowA: 99.8 ± 4.2 mV; p=0.02 and p=0.04 respectively, n=5, paired t-test – figure 4.1 B). Action potential half-width in AVCN bushy cells was also affected by changes in I_h amplitude and kinetics (control: 1.30 ± 0.05 ms; I_h slowτ/highA: 1.13 ± 0.02 ms; I_h fastτ/lowA: 1.18 ± 0.01 ms; I_h fastτ/highA: 1.16 ± 0.02ms; p<0.01, p=0.04, p=0.03, n=4, paired t-test). In MNTB and LSO neurons, AP half-width was not affected by changes in I_h properties.

I_h is known to contribute to AP delay (time between 5% maximum AP amplitude and peak) in MNTB cells (Leao *et al.* 2005a). Action potential delay in MNTB neurons were affected by changes in simulated I_h (control: 3.1 ± 0.1 ms; I_h slowτ/highA: 2.7 ± 0.2 ms, p=0.01; I_h fastτ/lowA: 2.6 ± 0.3 ms, p=0.03; I_h fastτ/highA: 2.5 ± 0.2 ms, p<0.01; n=4, paired t-test – figure 4.1 B). No delay in action potential generation was consistently observed for AVCN and LSO neurons due to alterations of I_h amplitude and kinetics (for 200 pA current steps, figure 4.1 B).

Rebound Depolarizations

Hyperpolarizing current steps elicited rebound depolarizations in all three nuclei (figure 4.1 C). Under control conditions, a -300 pA current step produced an average depolarization of 4.3 ± 0.9 mV in AVCN cells at the end of the step (figure 4.1 C). Increasing the speed of I_h kinetics, with a v-half 10 mV more depolarized, increased the post-step depolarization (I_h fastτ/lowA: 5.4 ± 2.2 mV, p=0.05; I_h fastτ/highA: 7.0 ± 0.8 mV, p<0.01; n=4, paired t-test – figure 4.1 C). These differences were more dramatic in MNTB cells; altering both I_h amplitude and kinetics caused significant increases in

rebound depolarization, and addition of I_h fastτ/highA (figure 4.1 B) triggered post-step APs (control: 3.8 ± 0.5 mV; I_h slowτ/highA: 6.3 ± 0.3 mV, p=0.01; I_h fastτ/lowA: 7.7 ± 0.7 mV, $p \leq 0.01$; n=4, paired t-test – figure 4.1 C). Interestingly, I_h properties did not seem to affect rebound amplitude in LSO cells except when I_h slowτ/lowA was added to the membrane (control: 6.2 ± 0.2 mV versus I_h slowτ/lowA: 6.9 ± 0.2 mV; $p<0.01$, n=5, paired t-test – figure 4.1 C). This larger depolarization was probably due to the decreased resting membrane potential, causing the relative increase in afterhyperpolarization potential. If consideration was taken as to whether the LSO cell was multiple or single firing, changes in I_h properties similarly affected resting membrane potential and AP characteristics in MF and SF LSO cells. However, rebound depolarizations in MF cells were able to trigger APs (see following subsections). The dynamic-clamp results are summarized in Table 4.1.

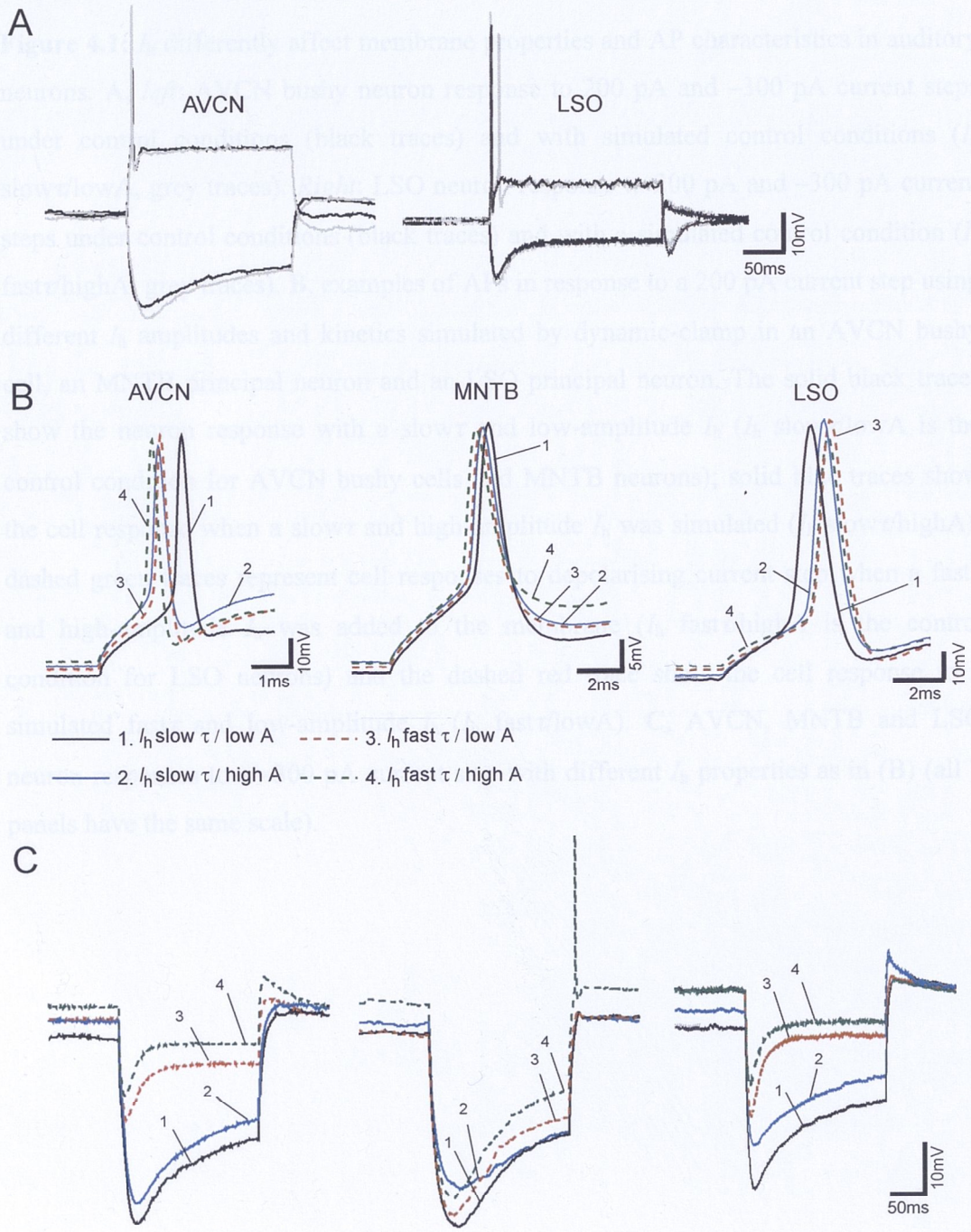
A
AVCN
LSO
10mV
50ms
B
AVCN
MNTB
LSO
1
2
3
4
10mV
1ms
5mV
2ms
10mV
2ms
1. I_h slow τ / low A
2. I_h slow τ / high A
3. I_h fast τ / low A
4. I_h fast τ / high A
C
10mV
50ms

Figure 4.1: I_h differently affect membrane properties and AP characteristics in auditory neurons. **A,** *left*: AVCN bushy neuron response to 200 pA and –300 pA current steps under control conditions (black traces) and with simulated control conditions (I_h slowτ/lowA, grey traces). *Right*: LSO neuron response to 200 pA and –300 pA current steps under control conditions (black traces) and with a simulated control condition (I_h fastτ/highA, grey traces). **B**, examples of APs in response to a 200 pA current step using different I_h amplitudes and kinetics simulated by dynamic-clamp in an AVCN bushy cell, an MNTB principal neuron and an LSO principal neuron. The solid black traces show the neuron response with a slowτ and low-amplitude I_h (I_h slowτ/lowA is the control condition for AVCN bushy cells and MNTB neurons); solid blue traces show the cell response when a slowτ and high-amplitude I_h was simulated (I_h slowτ/highA); dashed green traces represent cell responses to depolarising current step when a fastτ and high-amplitude I_h was added to the membrane (I_h fastτ/highA is the control condition for LSO neurons) and the dashed red trace show the cell response to a simulated fastτ and low-amplitude I_h (I_h fastτ/lowA). **C**, AVCN, MNTB and LSO neuron responses to a –300 pA current step with different I_h properties as in (B) (all 3 panels have the same scale).

Table 4.1 Effects of I_h on Resting Membrane Potential and Action Potentials in the AVCN, MNTB and LSO

Vrest (mV)	*AVCN*	*MNTB*	*LSO*
Slowτ/lowA	***-58.8 ± 1.7***	***-65.3 ± 0.8***	*-67.1 ± 0.2 ‡*
Slowτ/highA	*-57.7 ± 1.7 †*	*-61.7 ± 0.2 †*	*-65.7 ± 0.4 ‡*
Fastτ/lowA	*-56.1 ± 1.7 ‡*	*-63.5 ± 0.6 ‡*	*-64.6 ± 0.5 ‡*
Fastτ/highA	*-53.7 ± 1.4 ‡*	*-61.4 ± 0.5 ‡*	***-61.3 ± 0.8***
AP amplitude (mV)	*AVCN*	*MNTB*	*LSO*
Slowτ/lowA	***62.8 ± 5.3***	***61.5 ± 4.1***	*99.8 ± 4.2 †*
Slowτ/highA	*62.5 ± 5.5*	*60.3 ± 4.0 †*	*96.5 ± 3.4 †*
Fastτ/lowA	*58.7 ± 5.5 †*	*57.8 ± 2.9*	*91.2 ± 3.7*
Fastτ/highA	*57.5 ± 5.9 †*	*56.3 ± 3.1 †*	***91.4 ± 4.4***
AP half-width (ms)	*AVCN*	*MNTB*	*LSO*
Slowτ/lowA	***1.33 ± 0.04***	***1.05 ± 0.09***	*0.70 ± 0.06*
Slowτ/highA	*1.14 ± 0.02 ‡*	*1.20 ± 0.12*	*0.67 ± 0.07*
Fastτ/lowA	*1.17 ± 0.02 †*	*1.21 ± 0.12*	*0.64 ± 0.07*
Fastτ/highA	*1.16 ± 0.01 †*	*1.13 ± 0.10*	***0.59 ± 0.04***
AP delay (ms)	*AVCN*	*MNTB*	*LSO*
Slowτ/lowA	***5.5 ± 0.4***	***3.1 ± 0.1***	*3.1 ± 0.3*
Slowτ/highA	*4.6 ± 0.3*	*2.7 ± 0.2 †*	*3.3 ± 0.5*
Fastτ/lowA	*4.6 ± 0.3*	*2.6 ± 0.3 †*	*3.0 ± 0.1*
Fastτ/highA	*4.5 ± 0.3*	*2.5 ± 0.2 ‡*	***3.4 ± 0.2***
Rebound dep. (mV)	*AVCN*	*MNTB*	*LSO*
Slowτ/lowA	***4.3 ± 0.9***	***3.8 ± 0.5***	*6.9 ± 0.2 ‡*
Slowτ/highA	*5.4 ± 2.2*	*6.3 ± 0.3 †*	*7.0 ± 0.9*
Fastτ/lowA	*5.5 ± 1.3*	*7.7 ± 0.7 ‡*	*6.7 ± 0.2*
Fastτ/highA	*7.0 ± 0.8 ‡*	NA	***6.2 ± 0.2***

Presented as average ± s.e.m, bold numbers represents control conditions

Significant difference from control condition († $p<0.05$, ‡ $p<0.01$, *Students t-test, paired*)

No rebound APs were observed in MNTB cells in a study by Leao *et al.* (2005b), and I_h is unlikely to generate rebound APs in MNTB neurons under normal conditions. Therefore the relationship between I_h properties and rebound depolarization was only further investigated in AVCN bushy cells and LSO principal neurons. In order to

investigate the relationship between the duration of hyperpolarization, rebound depolarization amplitude, I_h properties and rebound firing, current steps (-300pA) of various durations (10 to 110 ms, 5 ms steps – Koch and Grothe, 2003) were injected into AVCN and LSO cells as well as dynamic-clamp I_h. AVCN neurons displayed a linear relationship between current-step duration and rebound depolarization under control conditions. In terms of depolarization amplitude, AVCN bushy cells did not show any difference between I_h control and slowτ/highA for any time step (figure 4.2 A and C). Addition of a fast I_h, however, significantly increased rebound depolarization following steps from 45 ms to 55 ms for I_h fastτ/lowA (n=4, p=0.04 for all points) and after steps from 10 to 70 ms for I_h fastτ/highA (n=4, p<0.01 for all points). Also, under control conditions, the relationship between hyperpolarization step duration and depolarization potential could be well fitted with a linear function (e.g. $y=ax+b$) while logarithmic functions (e.g. $y=a.\log(x)+b$) were more suited to fit this relationship if the I_h amplitude was increased or its kinetics were changed (the goodness of fit was assessed by the magnitude of the residuals – data not shown).

Different I_h properties caused greater changes in the dependency of rebound depolarization on the hyperpolarizing current step duration in SF LSO cells (figure 4.2 B and C). In general, rebound depolarizations were larger under control conditions (p<0.05, when compared with I_h slowτ/lowA and I_h slowτ/highA for all steps, n=5) except when compared to I_h fastτ/lowA (figure 4.2 B and C). In contrast to AVCN neurons, all hyperpolarizing step duration vs. rebound amplitude relationships were better fitted with a logarithmic function. These results show that I_h fastτ/highA produces the largest rebound depolarization in AVCN cells, and fastτ/lowA produce the largest depolarizations in LSO neurons, compared to control conditions.

Rebound APs in response to hyperpolarizing current steps were observed in 29% of AVCN cells (n=21) and in 35% of LSO cells (n=20). Most of the LSO cells that fired

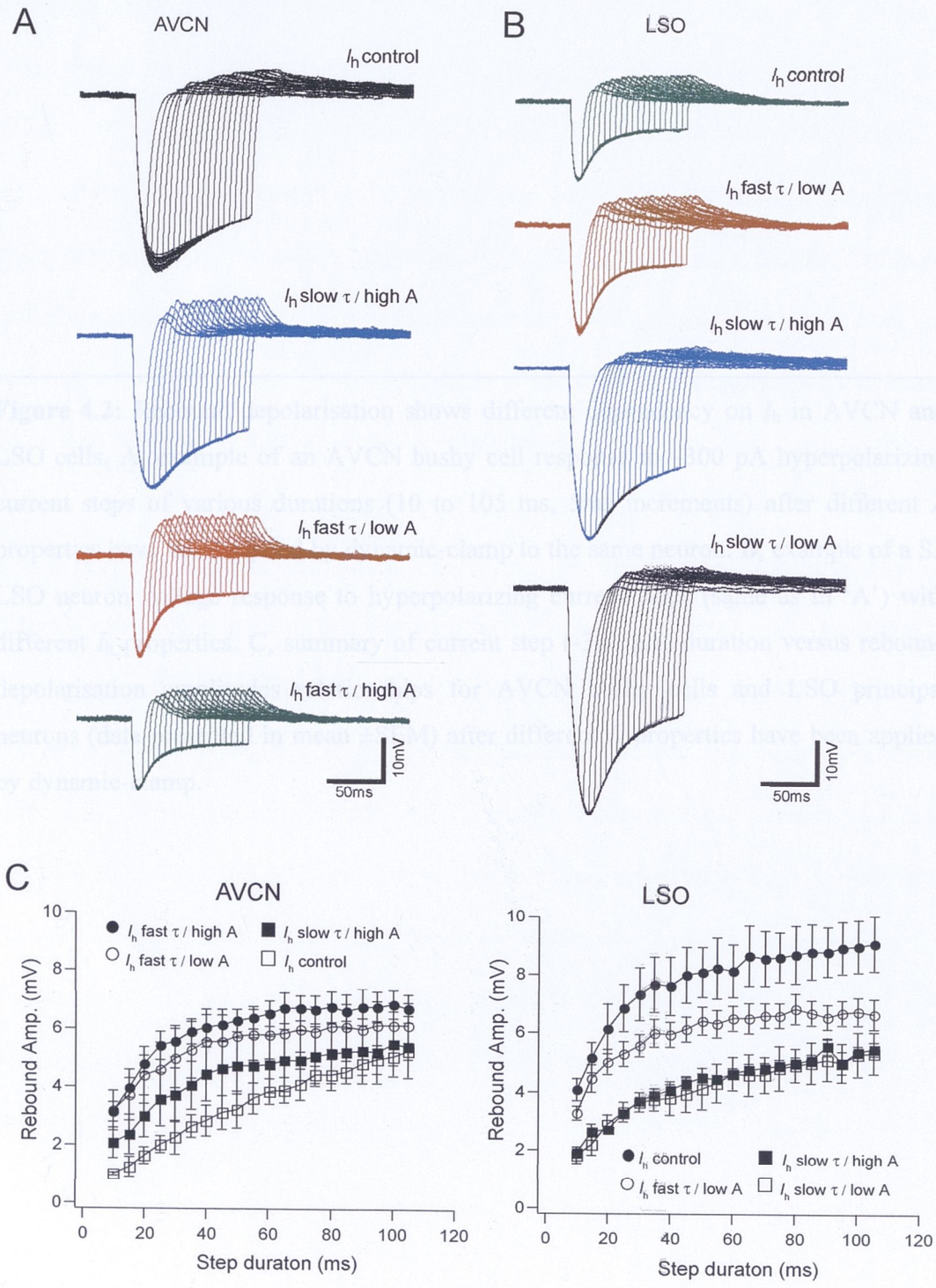
A
AVCN
I_h control
I_h slow τ / high A
I_h fast τ / low A
I_h fast τ / high A
10mV
50ms
B
LSO
I_h control
I_h fast τ / low A
I_h slow τ / high A
I_h slow τ / low A
10mV
50ms
C
AVCN
I_h fast τ / high A
I_h slow τ / high A
I_h fast τ / low A
I_h control
Rebound Amp. (mV)
Step duraton (ms)
LSO
I_h control
I_h slow τ / high A
I_h fast τ / low A
I_h slow τ / low A
Rebound Amp. (mV)
Step duraton (ms)

Figure 4.2: Rebound depolarisation shows different dependency on I_h in AVCN and LSO cells. **A**, example of an AVCN bushy cell response to –300 pA hyperpolarizing current steps of various durations (10 to 105 ms, 5ms increments) after different I_h properties have been applied by dynamic-clamp to the same neuron. **B**, example of a SF LSO neuron voltage response to hyperpolarizing current steps (same as in 'A') with different I_h properties. **C**, summary of current step (-300 pA) duration versus rebound depolarisation amplitudes relationships for AVCN bushy cells and LSO principal neurons (data presented in mean ±SEM) after different I_h properties have been applied by dynamic-clamp.

rebound APs were MF cells (6 of 7 cells vs. 1 of 13 SF cells). Rebound APs were eliminated by the addition of ZD7288 (figure 4.3 A, see LSO MF). Hyperpolarization durations necessary for rebound AP firing were significantly longer in AVCN cells when compared to LSO cells (58 ± 15 ms vs. 26 ± 10 ms, p=0.04, n=10). AVCN bushy cells were invariably SF, therefore, the amount of I_{LT} was measured by applying depolarizing voltage steps. After a voltage step to –40 mV there was a significant difference (p<0.05) in outward current between AVCN bushy cells that fired rebound action potentials (235 ± 16 pA, n=21) compared to AVCN bushy cells that did *not* fire rebound action potentials (340 ± 33 pA, n=21). Non-rebound spiking AVCN bushy cells also showed smaller rebound depolarizations when compared to non-rebound spiking LSO cells (for 55 ms long hyperpolarization: 4 ± 1 mV for AVCN cells vs. 7 ± 1 mV for LSO cells, p=0.01, n=22 – figure 4.3 B). In addition, I_{LT} was artificially injected, using the dynamic-clamp, in four MF LSO cells in order to assess the effect of these currents on rebound spiking. Dynamic-clamp K^+ currents caused MF LSO cells to fire single-spikes in response to depolarizing current steps and abolished rebound APs after -250 pA current steps (figure 4.3 C, *inset*). However, these neurons still fired rebound APs after -300 pA current steps, but the hyperpolarization duration necessary for AP firing increased significantly (from 28 ± 18 ms to 62 ± 17 ms, p=0.04, n=4 – figure 4.3 C). The rebound depolarization magnitude was found to depend jointly on I_h and I_{LT}, as these two currents appear to balance each other (I_h promoting rebound depolarization after hyperpolarizations and I_{LT} impeding rebound depolarizations to cause AP firing).

Dendritic I_h in AVCN and LSO Neurons

Immunohistochemistry was carried out to further examine the subcellular location of HCN1 channels in the AVCN and LSO. AVCN neurons displaying only one dendrite

were identified as likely bushy neurons (figure 4.4 A and C). Neurons from the AVCN and LSO displayed strong punctate membrane staining on both soma and proximal dendrite. The HCN1 membrane staining on AVCN and LSO neurons could be followed along dendritic processes as far as 75 μm (see figure 4.4 D) from the soma. The HCN1 staining was further examined in slices from older mice (P21) to assess whether the HCN1 protein undergoes further development after the ear canal opens. The HCN1 staining patterns did not change in P21 animals when compared to P14. The similar HCN1 expression, in the two different age groups, was supported by voltage-clamp recordings. Figure 4E shows examples of hyperpolarizing currents from an AVCN bushy cell and a LSO neuron from P14 and P21 animals. Current magnitude and kinetics were similar, and the currents were also similarly blocked by application of ZD7288 (figure 4.4 E).

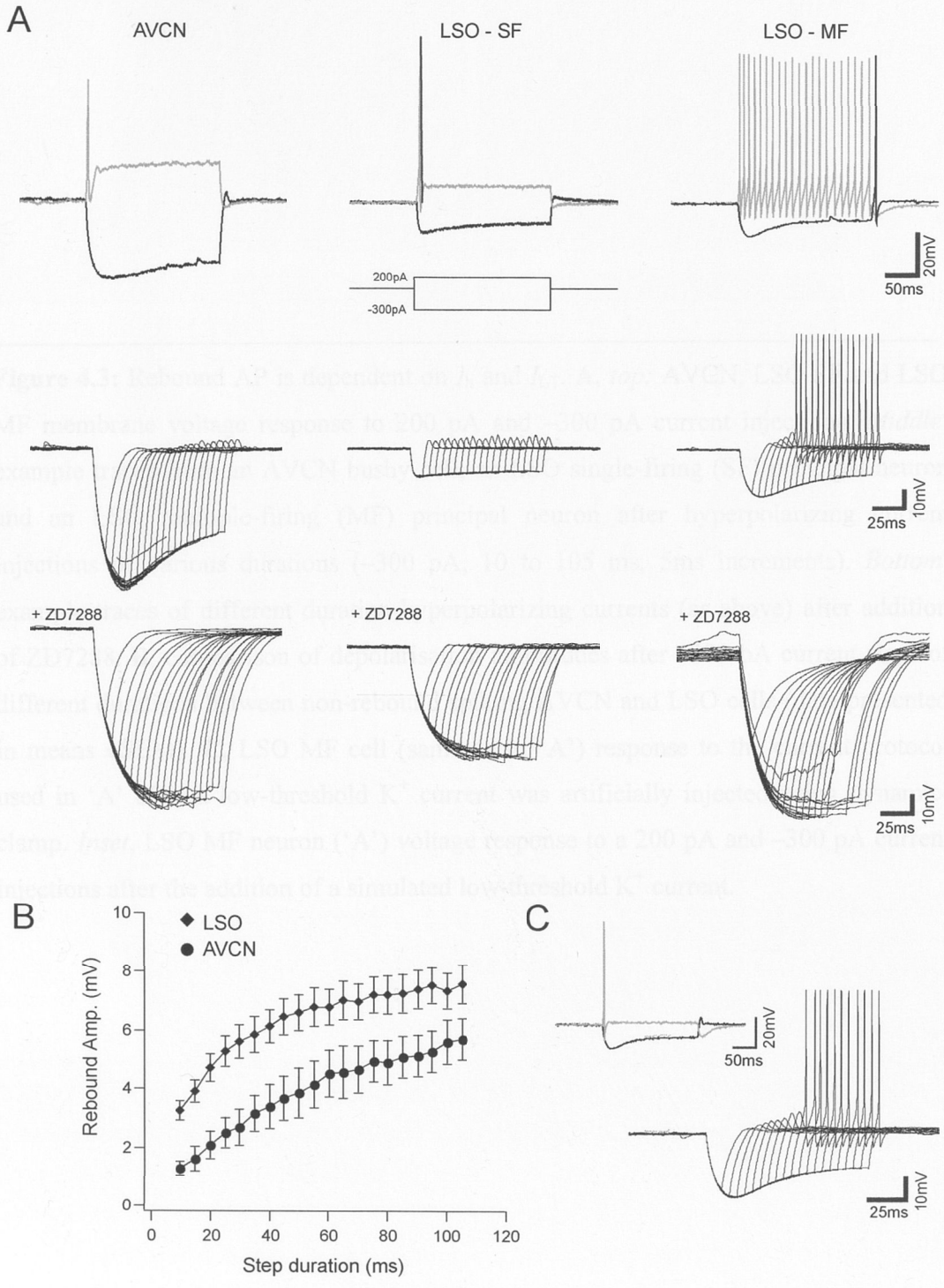
A
AVCN
LSO - SF
LSO - MF
200pA
-300pA
20mV
50ms
25ms
10mV
+ ZD7288
+ ZD7288
+ ZD7288
25ms
10mV
B
LSO
AVCN
Rebound Amp. (mV)
Step duration (ms)
0
2
4
6
8
10
0
20
40
60
80
100
120
C
20mV
50ms
25ms
10mV

Figure 4.3: Rebound AP is dependent on I_h and I_{LT}. **A**, *top:* AVCN, LSO SF and LSO MF membrane voltage response to 200 pA and –300 pA current injections. *Middle*: example traces from an AVCN bushy cell, an LSO single-firing (SF) principal neuron and an LSO multiple-firing (MF) principal neuron after hyperpolarizing current injections of various durations (–300 pA, 10 to 105 ms, 5ms increments). *Bottom*: example traces of different duration hyperpolarizing currents (as above) after addition of ZD7288. **B**, comparison of depolarisation amplitudes after –300 pA current steps of different durations between non-rebound spiking AVCN and LSO cells (data presented in means ±SEM). **C,** LSO MF cell (same as in 'A') response to the current protocol used in 'A' after a low-threshold K^+ current was artificially injected using dynamic-clamp. *Inset*, LSO MF neuron ('A') voltage response to a 200 pA and –300 pA current injections after the addition of a simulated low-threshold K^+ current.

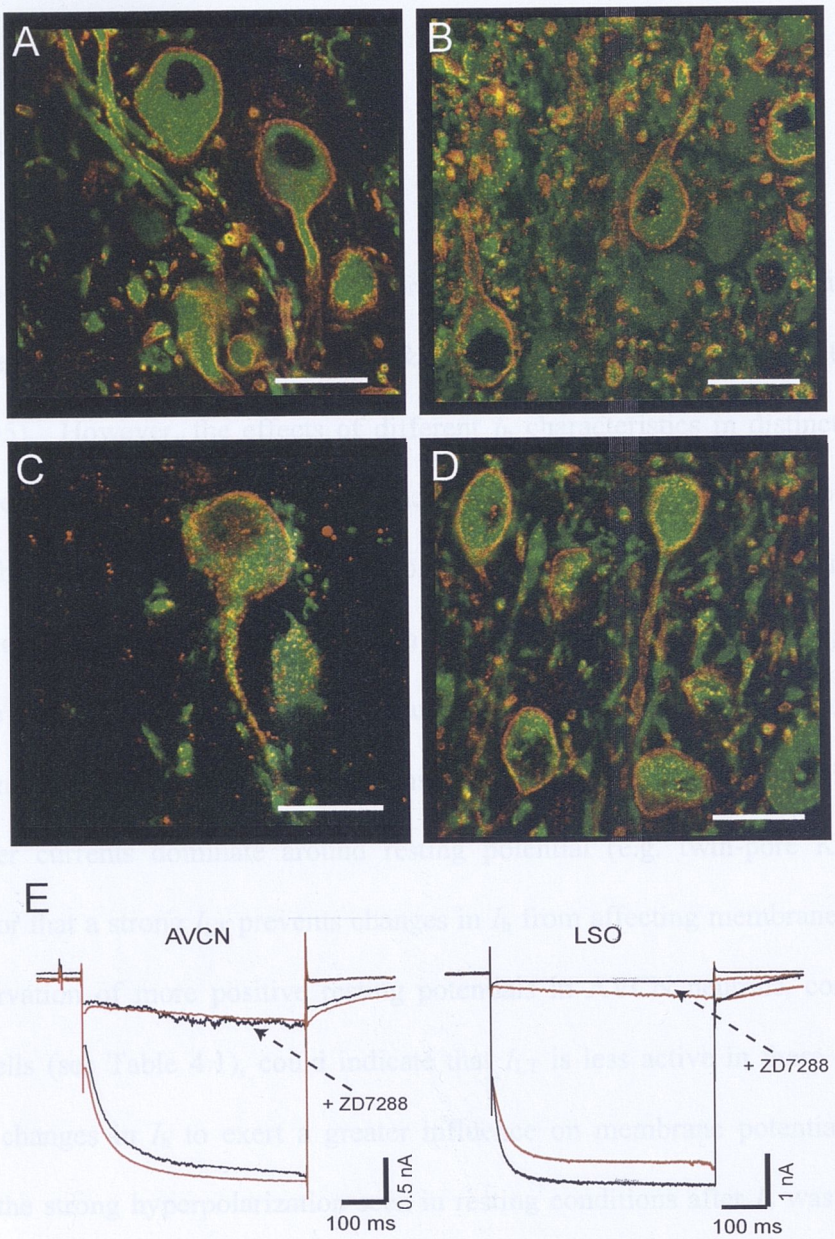

Figure 4.4: Subcellular location of HCN1 **A-D**, example images of HCN1-immunoreactivity (red) and anti-Map2a/b (green) labelling, staining soma and dendrites, from the AVCN (A) and LSO (B) of mice age P14, and AVCN (C) and LSO (D) neurons at high magnification from mice age P21. Scale bar 20mm. **E**, current response to a –132 mV voltage step from a bushy cell (*left*) and a LSO cell (*right*) from a P14 (black) and P21 (red) animal, before and after ZD7288.

Discussion

Several studies have demonstrated the importance of I_h in modulating cell excitability in auditory neurons (Banks *et al.*, 1993; Bal & Oertel, 2000; Koch & Grothe, 2003; Leao *et al.*, 2005). However, the effects of different I_h characteristics in distinct auditory nuclei have not been systematically examined. In this study a dynamic-clamp was used to assess the effect of different types of I_h on cell excitability, by altering I_h amplitudes and kinetics. The results reveal effects on the resting membrane potential, with the membrane potential of AVCN bushy cells and LSO principal neurons more affected by changes in I_h compared to MNTB neurons. This difference suggests that in MNTB cells, other currents dominate around resting potential (e.g. twin-pore K^+ channel currents) or that a strong I_{LT} prevents changes in I_h from affecting membrane potential. The observation of more positive resting potentials in AVCN neurons, compared to MNTB cells (see Table 4.1), could indicate that I_{LT} is less active in these cells, thus allowing changes in I_h to exert a greater influence on membrane potential. In LSO neurons, the strong hyperpolarization seen in resting conditions after I_h was decreased (see table 3.1) shows that I_h is a strong modulator of resting potential in these cells.

In vivo recordings have shown that blocking I_h leads to reduced excitability in the SOC (Shaikh and Finlayson 2003). This effect is probably due to hyperpolarization of the resting membrane potential. Since the changes in membrane potential were greatest in LSO cells, this might indicate that I_h is more tonically active during rest in LSO neurons than in MNTB and AVCN cells. This is also supported by the greater increase in input resistance after blocking I_h in LSO cells when compared to both MNTB and AVCN cells (see Table 3.1).

I_h Affects Rebound Depolarization

Another important aspect of this study was the assessment of the role of I_h in the generation of rebound over-threshold depolarizations. Activation of I_h by hyperpolarization is known to cause rebound APs in a variety of cells, including auditory neurons (Koch & Grothe, 2003; Ma *et al.*, 2003). However, other ionic currents associated with I_h can prevent rebound APs (Ma *et al.*, 2003). Here, the effect of different I_h kinetics and amplitude was studied on rebound firing in AVCN and LSO neurons, but not in the MNTB (because a previous study showed that it is unlikely that MNTB principal cells would fire rebound APs after prolonged activity, Leao *et al.*, 2005b). For both the AVCN and LSO, changing I_h characteristics did not cause rebound spikes in a previously non-rebound spiking neuron. Increasing amplitude or accelerating I_h kinetics altered the time dependency of hyperpolarization on rebound depolarization amplitudes in AVCN cells (from linear to logarithmic). This effect was probably due to larger rebound amplitudes activating low-threshold voltage dependent K^+ channels. Overall, rebound depolarizations were larger in LSO neurons when compared to AVCN cells, and more LSO neurons fired rebound APs compared to AVCN bushy cells. The strong correlation between small I_{LT} and rebound spiking in AVCN cells suggested that this current prevent rebound depolarizations from reaching AP threshold. The same hypothesis is applicable to LSO cells, where multiple firing LSO cells, exhibiting less I_{LT} (Barnes-Davies, 2004), fired rebound APs with a greater frequency than single firing cells. By simulating I_{LT} in LSO cells, using the dynamic clamp, rebound APs could be strongly inhibited, supporting this theory. However, these dynamic clamp experiments failed to abolish rebound APs after application of long hyperpolarization protocols, probably because the activation of 'real' I_{LT} in LSO cells might be faster than the simulated current used in this work (Nayagam *et al.*, 2005). In conclusion, the rebound

depolarization or rebound AP is probably modulated by the balance between I_h and I_{LT} activity.

A physiological implication of rebound spiking has been proposed in models of sound 'duration' detection (Casseday *et al.*, 1994; Hooper *et al.*, 2002). Here, inhibition would produce a temporal frame within which excitation can occur. If inhibitory input arrive first and is sustained for the duration of stimuli, there will be a rebound upon the termination of the input, which itself is insufficient to produce a spike, but if it coincides with a delayed excitation a spike occurs (Casseday *et al.*, 1994).

Regulation of I_h by Catecholamines and Preceding Neural Activity

The effects on resting membrane potential and AP properties caused by adding a fast I_h to AVCN bushy cells and MNTB neurons can emulate the changes of the 'normal' I_h of these cells caused by cAMP. I_h is regulated by cAMP, which is basically regulated by adenylyl cyclase (enzyme converting ATP to cAMP) (Pape, 1996). Stimulation of receptors that are negatively and positively coupled to adenylyl cyclase activity reciprocally shifts the I_h activation curve along the voltage axis, thereby controlling availability of the I_h channel over a wide range of membrane potentials without changing the maximal conductance (Pape, 1996). These effects of cAMP activation have been studied *in vivo* in auditory neurons; for example, SOC neurons increased spontaneous and tone-evoked AP firing after application of a pharmacological agent that elevates intracellular cAMP (Shaikh & Finlayson, 2005). Using the I_h blocker ZD7288 instead reduced excitability of SOC neurons *in vivo* (Shaikh & Finlayson, 2003). MNTB neurons can also be modulated by catecholamines, such as noradrenalin, that cause voltage shifts of kinetics and steady state activation of I_h (Banks *et al.*, 1993).

Cyclic nucleotides have been shown to be able to shift HCN2 and HCN4 channels (the major contributors of I_h in AVCN and MNTB cells – see Chapter 3) voltage dependency around 10 mV towards more depolarized potentials (Accili *et al.*, 2002; Baruscotti *et al.*, 2005). As mentioned earlier, I_h fast kinetics has a $V_{1/2}$ 10 mV more positive than the $V_{1/2}$ from I_h slow kinetics, and, steady-state I_h, helping to set the resting membrane potential, would not be influenced by the faster kinetics of I_h fast, therefore only mimicking the cAMP effect. HCN1 channels, possibly the most important mediators of I_h in LSO neurons, are minimally modulated by cAMP (Santoro *et al.*, 2000), therefore, preceding activity, not cyclic nucleotides, would be the most important determinant of I_h state in these neurons. The subcellular location of HCN1 channels may be of significance, where certain compartments of the dendrite may summate EPSPs differently depending on the activation of HCN1 channels. In layer 5 pyramidal neurons, I_h channel number increases exponentially along the dendrite with distance (Kole *et al.*, 2006). Poolos *et al.,* (2002) have shown that neuronal excitability can be altered by pharmacologically up-regulating HCN channels selectively in the dendrites of hippocampal neurons, which may be important for controlling epileptogenesis (Poolos *et al.*, 2002). Dendritic HCN1 labeling was observed for both AVCN and LSO neurons, in co-staining with the dendritic marker for microtubuli associated protein 2a/b (Map2a/b).

Maturation of I_h in auditory neurons appears to occur earlier than the maturation of 'inhibition'. Anatomical studies suggest that the expression of the "adult" glycine receptor subunit (α1) does not peak until around 3 weeks after birth in rats (Friauf *et al.*, 1997). Conversely, the calyx of Held has its adult type morphology and electrical properties around at hearing onset, at two weeks postnatal age (von Gersdorff & Borst, 2002). Here, no apparent differences in HCN1-immunoreactivity, I_h magnitude or kinetics, of AVCN and LSO neurons at P14 compared to at P21 were observed. This

suggests that the HCN1 expression may be functionally mature already at the onset of hearing.

In summary, this study highlights significant differences in I_h characteristics between different auditory brainstem nuclei, with each cell type expressing a distinct repertoire of I_h and HCN channel subtypes. These results show I_h to be a key modulator of cell excitability.

Chapter 5. Normal AVCN Bushy Cells in Congenitally Deaf Mice

Introduction

Postsynaptic neuronal membrane properties play a crucial role in determining the response of a neuron to synaptic inputs. Different types of neurons express particular complements of voltage-dependent and voltage-independent (leakage) channels, appropriate to their specific physiological roles. It seems likely that the expression of these channels is regulated by neuronal activity, particularly during development when neuronal circuits are being shaped. Several studies of decreased afferent activity, involving models of blindness and hearing loss, have found changes in cellular properties leading to an increased neuronal excitability (Jentsch *et al.*, 2002; Kotak *et al.*, 2005). In congenitally deaf mice, neurons from the medial nucleus of the trapezoid body (MNTB) show increased excitability (Leao *et al.*, 2004a). However, there is a lack of information regarding firing properties of the other auditory nuclei in congenitally deaf mice. This study is focussed on the bushy cells of the anteroventral cochlear nucleus (AVCN), as these cells receive direct powerful excitatory input directly from the auditory nerve.

The congenitally deaf (*dn/dn*) mouse, the deafness mouse (Bock *et al.*, 1982; Keats *et al.*, 1995), is an excellent model for studying the effect of lack of sound activity to the auditory system. Homozygous mice for the *dn* gene suffer from profound asymptomatic

deafness (Kurima *et al.*, 2003) from birth. The deafness mouse has advantages over other models of deafness, such as cochlear ablation and denervation, which destroy the cochlea and the auditory nerve (Walmsley *et al.*, 2006). The *dn/dn* animals have dysfunctional hair cells, display early degeneration of the organ of Corti, and lack spontaneous and acoustically evoked auditory nerve activity (Leao *et al.*, 2006b), although the central connections in the auditory pathway appears functional (Bock *et al.*, 1982).

The auditory brainstem of deafness mice have been intensely studied, particularly the neurons of the MNTB and the large presynaptic terminal the calyx of Held. The principal cells of the MNTB display altered membrane properties after development with lack of spontaneous auditory nerve activity, when compared to its normal development. Neurons of the MNTB have shown an increased excitability due to a reduced low-voltage activated K^+ conductance, display larger hyperpolarization-activated current (I_h) and altered sodium currents (Leao *et al.*, 2004a; Leao *et al.*, 2005; Leao *et al.*, 2006a). The expression of channels is therefore affected differently by the lack of activity. Interestingly, the effect of deafness on the two giant excitatory synaptic terminals, the endbulb and calyx of Held, is also different. While the endbulbs appear to have increased synaptic strength via presynaptic mechanisms, the calyx of Held seems to develop normally in *dn/dn* mice (Oleskevich *et al.*, 2004).

Although, the postsynaptic membrane properties of MNTB neurons have been examined in deaf mice, this information is lacking for AVCN neurons of which the globular bushy cells of the AVCN give rise to the calyces of Held in the MNTB.

Here, the potential role of neuronal activity during development in regulating membrane properties of AVCN bushy cells have been examined in congenitally deaf (*dn/dn*) mice at postnatal age 12-14 days.

Methods

Transverse brainstem slices containing the AVCN were obtained from normal (CBA) and deaf (*dn/dn*) mice age P12-14 as described in the General Methods chapter. Whole-cell patch-clamp recordings were made from visualized neurons located in the AVCN. Current and voltage recordings were made with K^+-methylsulphate as internal solution (as described previously). Bushy neurons were verified histologically after filling the cells with a fluorescent dye (Alexa^{488}, Molecular Probes) and the brain slices were processed as in Chapter 3 for 3D reconstruction using the confocal microscope and appropriate confocal software (LSM, Zeiss). Data was analyzed using student's *t*-test (two samples, equal variances, one sided) and error bars are shown as standard error of the mean (s.e.m).

Results

Whole-cell patch-clamp recordings were obtained from spherical and globular bushy cells in the AVCN of normal (CBA) and deaf (*dn/dn*) mice age P12-14. Cells were confirmed as bushy cells by their low input resistance compared to stellate cells (<150 MΩ, compared to around 300-400MΩ for stellate cells) and their onset firing pattern in response to long depolarising current injections. Bushy cell morphology was also confirmed visually, using a UV-light source (Olympus) that excites the intracellular fluorescent dye (Alexa^{488}), at the end of the recording, and later filled cells were fixed and processed for confocal 3D reconstruction. Bushy cells were not separated into spherical or globular bushy cells, as these subpopulations are primarily confirmed by their projection patterns (Popper *et al.*, 2002).

Passive membrane properties did not differ significantly between normal and deaf mice bushy cells. Resting membrane potential of cells from normal and deaf mice was -56.0 ± 1.2 mV (n=23) and –54.6 ± 1.6 mV respectively (n=11). Input resistance for cells from normal and deaf mice was 129.2 ± 6.5 MΩ and 130.8 ± 10.8 MΩ, respectively. The average whole-cell capacitance was 21.5 ± 1.2 pF and 24.8 ± 2.5 pF for AVCN cells from normal and deaf mice respectively.

A previous study on the deafness mouse reported increased excitability due to a decrease in the low-threshold potassium current (Leao *et al.*, 2004a). Here, no increase in excitability was observed when comparing firing properties of bushy cells from normal and deaf mice (figure 5.1). In response to 200ms long depolarising current-steps, varying from 50pA to 400pA (50pA steps), the max number of action potentials fired was 2.2 ± 0.3 for normal and 2.5 ± 0.6 for deaf mice bushy cells. There was no difference in AP properties (peak amplitude and half width) between normal and deaf bushy cells (data not shown). In response to hyperpolarizing current steps (-50 to –300 pA) bushy neurons displayed variability in the size of the depolarising sag and the presence of rebound action potentials upon the termination of the hyperpolarizing step (figure 5.1). Bushy cells from deaf animals exhibited rebound spikes of a higher frequency than bushy cells from normal mice (73% versus 35%, respectively). Membrane and firing properties are summarized in table 5.1.

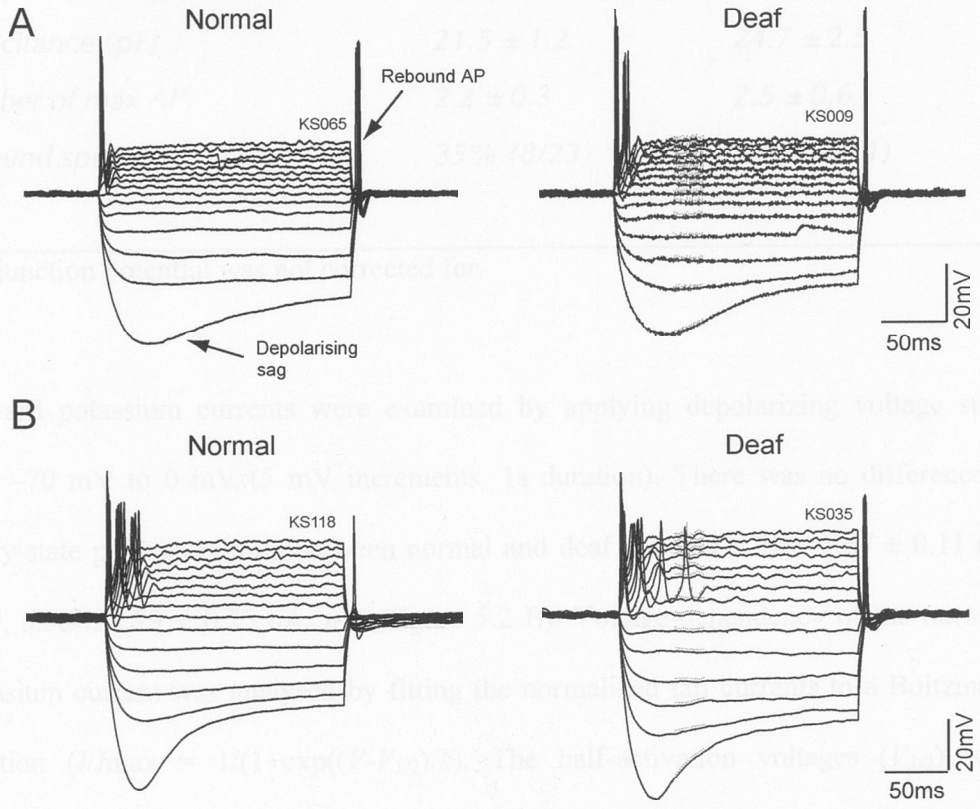

Figure 5.1: Normal voltage responses of AVCN bushy cells from deaf animals. **A**, example of very similar bushy cell response from a normal and a deaf animal to current injections (-300 to +400 pA, 200ms). **B**, another example of similar voltage responses from bushy cells from a normal and a deaf animal. Both neurons display onset response, with one or a few action potentials when depolarized and a sag in response to hyperpolarizing currents that terminates as a rebound spike. Scale bar x=50ms, y=20mV.

Table 5.1: Properties of Bushy Cells from Normal and Deaf Mice

	Normal (n=23)	*Deaf (n=11)*
*Resting membrane potential (mV)**	*-56.0 ± 1.2*	*-54.6 ± 1.6*
Input resistance (MΩ)	*129.2 ± 6.5*	*130.8 ± 10.8*
Capacitance (pF)	*21.5 ± 1.2*	*24.7 ± 2.5*
Number of max AP	*2.2 ± 0.3*	*2.5 ± 0.6*
Rebound spiking	*35% (8/23)*	*73% (8/11)*

*the junction potential was not corrected for.

Outward potassium currents were examined by applying depolarizing voltage steps from –70 mV to 0 mV (5 mV increments, 1s duration). There was no difference in steady-state peak amplitude between normal and deaf animals (CBA: 1.67 ± 0.11 nA, n=19, *dn/dn*: 1.79 ± 0.25 nA, n=8, figure 5.2 B). Voltage-dependency of the outward potassium current was analysed by fitting the normalized tail currents to a Boltzmann equation ($I/I\text{max} = 1/(1+\exp((V-V_{1/2})/k)$). The half-activation voltages ($V_{1/2}$) were different between normal (–42.7 ± 0.9 mV) and deaf (–38.1 ± 2.2 mV) mice (p=0.02), as well as slope factors (k) which were 8.4 ± 0.4 mV for normal and 10.1 ± 0.8 mV for deaf mice respectively (p=0.02, figure 5.2 C). The threshold potential (required to elicit 5% of the total current) was not different between normal (66.6 ± 0.7 mV) and deaf (–66.6 ± 1.9 mV) mice. Bushy cell morphology was also similar in normal and deaf animals (figure 5.2 D).

In order to examine any differences in the hyperpolarization-activated cation current (I_h), which was found to be different in MNTB principal cells of *dn/dn* mice compared to normal, hyperpolarizing voltage steps (-60 to –132 mV, 6mV increments, as in Chapter 3) were applied in voltage-clamp. The membrane responses to negative voltage steps did not differ between normal and deaf mice (figure 5.3 A). Instantaneous and

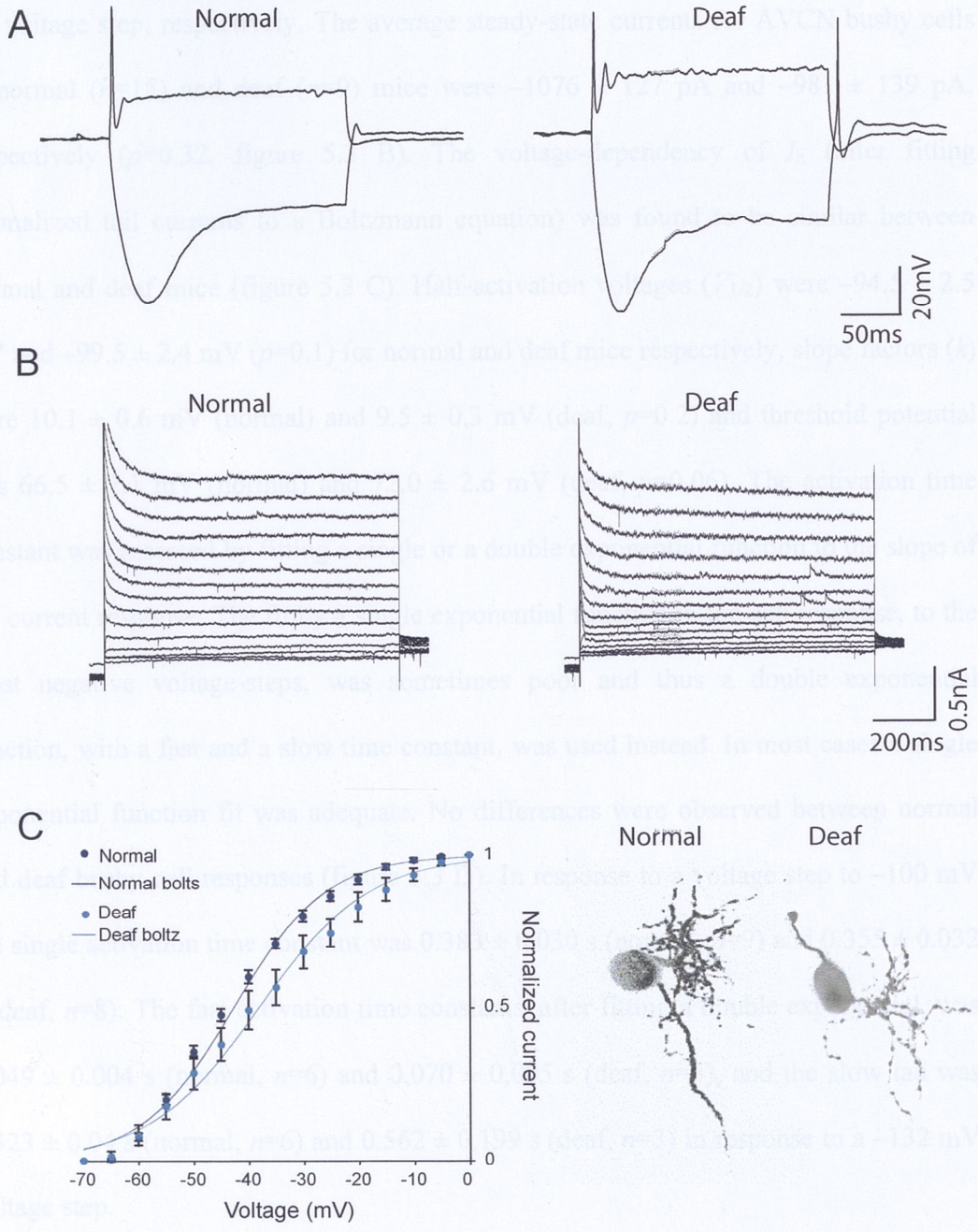

Figure 5.2: Outward K^+ current in bushy cells of normal and deaf mice. **A**, Voltage response to depolarizing (+400 pA) and hyperpolarizing (-300 pA) current steps of bushy cells from a normal and a deaf animal. **B**, current response to voltage steps (-70 to 0 mV, 5 mV increments, 1 s duration) of the same bushy cells as in (A). **C**, normalized tail current magnitude versus test potential fitted to a Boltzmann function (continuous line) for normal (dark blue) bushy cells (n=17) and deaf (light blue) bushy cells (n=8). Error bars are shown as s.e.m. *Right*: example of a filled bushy cell from a normal and a deaf animal.

steady-state currents were measured at 5-10ms and 490-495ms from the beginning of the voltage step, respectively. The average steady-state currents for AVCN bushy cells in normal (n=15) and deaf (n=9) mice were –1076 ± 127 pA and –981 ± 139 pA, respectively (p=0.32, figure 5.3 B). The voltage-dependency of I_h (after fitting normalized tail currents to a Boltzmann equation) was found to be similar between normal and deaf mice (figure 5.3 C). Half-activation voltages ($V_{1/2}$) were –94.5 ± 2.5 mV and –99.5 ± 2.4 mV (p=0.1) for normal and deaf mice respectively, slope factors (k) were 10.1 ± 0.6 mV (normal) and 9.5 ± 0.3 mV (deaf, p=0.2) and threshold potential was 66.5 ± 2.1 mV (normal) and 72.0 ± 2.6 mV (deaf, p=0.06). The activation time constant was assessed by fitting a single or a double exponential function to the slope of the current response. The fit by a single exponential function to the cell response, to the most negative voltage-steps, was sometimes poor and thus a double exponential function, with a fast and a slow time constant, was used instead. In most cases a single exponential function fit was adequate. No differences were observed between normal and deaf bushy cell responses (figure 5.3 D). In response to a voltage step to –100 mV the single activation time constant was 0.383 ± 0.030 s (normal, n=9) and 0.355 ± 0.032 s (deaf, n=8). The fast activation time constants, after fitting a double exponential, was 0.049 ± 0.004 s (normal, n=6) and 0.070 ± 0,005 s (deaf, n=3), and the slow tau was 0.323 ± 0.04 s (normal, n=6) and 0.562 ± 0.199 s (deaf, n=3) in response to a –132 mV voltage step.

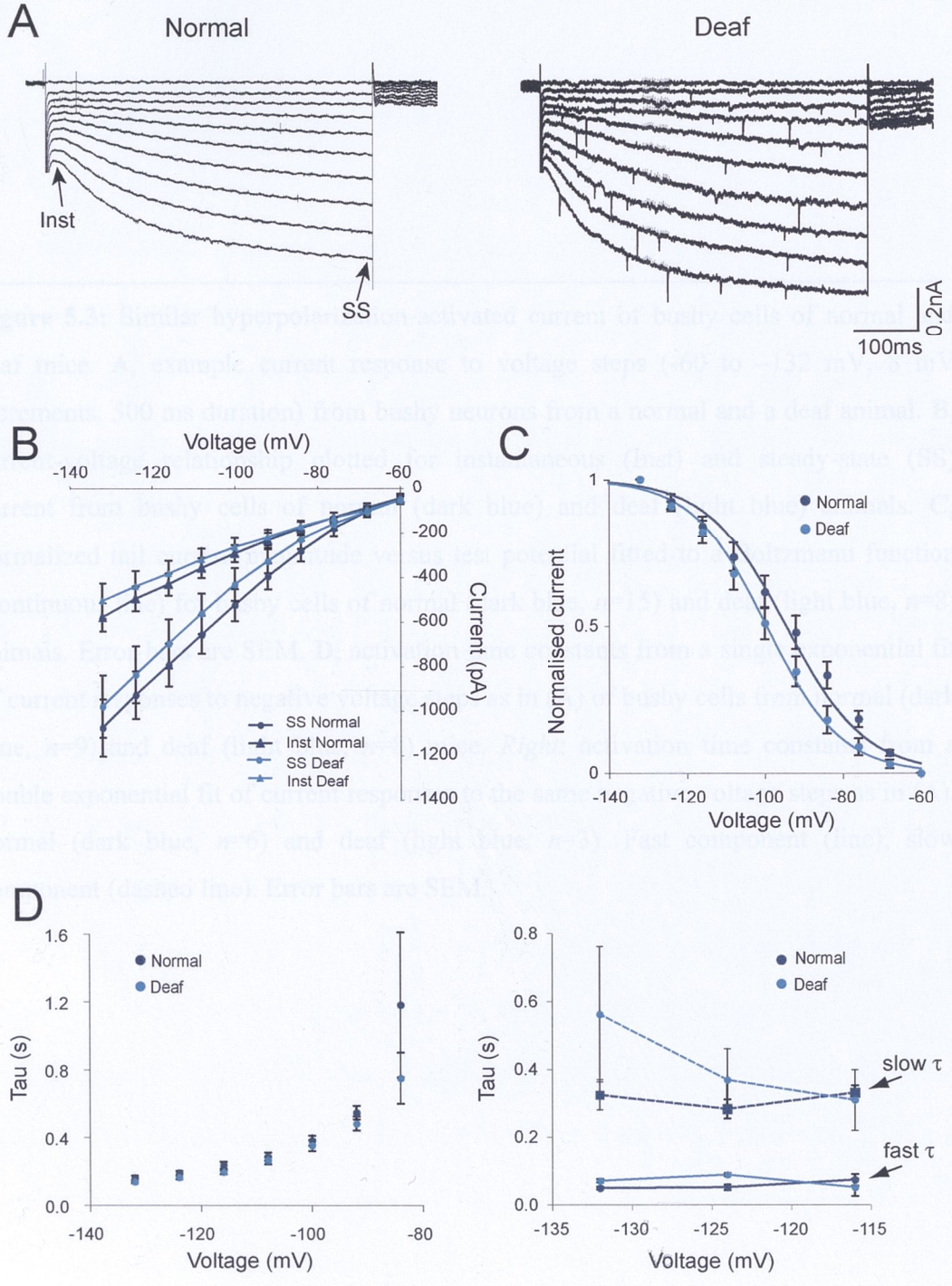
A
Normal
Deaf
Inst
SS
0.2nA
100ms
B
Voltage (mV)
-140
-120
-100
-80
-60
0
-200
-400
-600
-800
-1000
-1200
-1400
Current (pA)
SS Normal
Inst Normal
SS Deaf
Inst Deaf
C
1
0.5
0
Normalised current
Normal
Deaf
-140
-120
-100
-80
-60
Voltage (mV)
D
1.6
1.2
0.8
0.4
0.0
Tau (s)
Normal
Deaf
-140
-120
-100
-80
Voltage (mV)
0.8
0.6
0.4
0.2
0.0
Tau (s)
Normal
Deaf
slow τ
fast τ
-135
-130
-125
-120
-115
Voltage (mV)

Figure 5.3: Similar hyperpolarization-activated current of bushy cells of normal and deaf mice. **A**, example current response to voltage steps (-60 to –132 mV, 8 mV increments, 500 ms duration) from bushy neurons from a normal and a deaf animal. **B**, current-voltage relationship plotted for instantaneous (Inst) and steady-state (SS) current from bushy cells of normal (dark blue) and deaf (light blue) animals. **C**, normalized tail current magnitude versus test potential fitted to a Boltzmann function (continuous line) for bushy cells of normal (dark blue, n=15) and deaf (light blue, n=8) animals. Error bars are SEM. **D**, activation time constants from a single exponential fit of current responses to negative voltage steps as in (A) of bushy cells from normal (dark blue, n=9) and deaf (light blue, n=8) mice. *Right*: activation time constants from a double exponential fit of current responses to the same negative voltage steps as in (A), normal (dark blue, n=6) and deaf (light blue, n=3). Fast component (line), slow component (dashed line). Error bars are SEM.

Discussion

No differences in firing properties were seen in AVCN bushy cells from normal mice compared to deaf mice that have developed without spontaneous activity. Instead, electrophysiological recordings were surprisingly similar to normal conditions, despite some internal variance.

When comparing outward K^+ currents a difference in half-activation voltage was observed, although more experiments are needed to pharmacologically separate the components generating this outward K^+ current. Previous studies have showed that bushy cells of the AVCN expresses several potassium ion channel subunits, including the high-voltage activated, Kv3.1 (Perney & Kaczmarek, 1997) and A-type (rapidly inactivating) K^+ channels Kv3.4, Kv4.2 and 4.3 (Pal *et al.*, 2005). Bushy cells also expresses several Kv1 subunits (1.1, 1.2 and 1.6) (Pal *et al.*, 2005), that generate low-threshold potassium conductances (Rothman & Manis, 2003).

No increase in excitability was seen in AVCN bushy neurons from deaf animals in contrast to MNTB cells from deaf animals. Neither was any difference in hyperpolarization-activated current observed in this study, although bushy cells from deaf mice tended to generate rebound action potentials more often than normal bushy neurons. The rebound spike can be abolished by the specific I_h blocker ZD7288 (see Chapter 3) and is therefore dependent on this current. Rebound action potential have been suggested to be important for coding of sound duration, which could allow neurons to be tuned to specific ranges of duration when firing upon the termination of stimuli (Casseday *et al.*, 1994). I_h and I_{LT} have been shown to counteract each other in generating rebound action potentials (see Chapter 4), where I_{LT} can oppose small

depolarizations generated by the slow inactivating I_h. Here, the increase in rebound spike frequency might be partly due to the shift in half-activation voltage of the I_{LT}, to more positive potentials, allowing I_h to generate a larger afterhyperpolarization amplitude before I_{LT} becomes sufficiently activated to cancel the rebound spike (see Chapter 4).

Interestingly, when comparing development with or without spontaneous cochlear activity, there appear to be differences in robustness of the pre- and postsynaptic properties at different levels of the auditory system. In previous studies of the endbulbs of Held, large synapses onto bushy cells of the AVCN have shown a number of alterations in response to development without spontaneous afferent activity, while the calyx of Held synapse instead appears to function normally. A normal calyx of Held is congruent to the results shown here since the axon of globular bushy cells form this giant synapse. Lack of spontaneous activity during development does not seem to affect post-synaptic bushy neurons in the same manner as it affects MNTB principal neurons. Burrone *et al.,* suggested that global attenuation of synaptic activity increases synaptic function in all neurons, whereas attenuation of activity in an individual developing neuron (such as the AVCN bushy cell) reduces the function of its synapses (Burrone *et al.*, 2002). Hence, the lack of hair cell input effects the auditory brainstem differently as local nuclei may try to compensate for the absence of afferent activity.

Chapter 6. Acoustic Stimulation Alters K^+ Channel Expression in the MNTB

Introduction

The effect of lack of cochlear activity in the auditory brainstem has been intensely studied using genetic models of deafness (Ryugo *et al.*, 1997; Lee *et al.*, 2003; Leao *et al.*, 2004a; Walmsley *et al.*, 2006) or deafferentation such as cochlear removal/ablation (Francis & Manis, 2000; Lu *et al.*, 2004). On the contrary, the effect of increased cochlear activity has only been studied, *in vivo,* in models of tinnitus (Imig & Durham, 2005; Kaltenbach *et al.*, 2005; Ma *et al.*, 2006). There are almost no studies, however, that correlate increased activity and membrane properties of neurons in auditory pathways (Basta & Ernest, 2004). Spontaneous cochlear activity appears to be important for cell survival and network formation (Friauf & Lohmann, 1999; Kim & Kandler, 2003) and sensory-evoked activity is necessary for the generation of auditory maps and the sharpening of frequency tuning curves (Sanes & Constantine-Paton, 1985; Friauf & Lohmann, 1999).

The tonotopic organization of the cochlea leads to the generation of topographic gradients of ion channel expression along the auditory pathway (Li *et al.*, 2001; Davis, 2003; Barnes-Davies *et al.*, 2004; von Hehn *et al.*, 2004; Kaczmarek *et al.*, 2005). The

importance of spontaneous activity in forming and preserving topographic ion channel organization was demonstrated by a study using congenitally deaf mice, which lacks gradients of the low- and high-voltage activated currents, and the hyperpolarization-activated current, I_h (Leao *et al.*, 2006b). The lack of a Kv3.1 expression gradient was also seen in the MNTB due to the lack of sensory activity in hearing impaired mice (von Hehn *et al.*, 2004).

Voltage-gated potassium currents are crucial for shaping the responses of auditory brainstem neurons to acoustic stimuli (Klug & Trussell, 2006). The AVCN and MNTB, for example, display K^+ currents that allow neurons of these nuclei to fire single APs in response to prolonged stimulation and to fire at extremely high frequency (Manis & Marx, 1991; Wang *et al.*, 1998; Hermann *et al.*, 2007). The MNTB and the AVCN show high expression of voltage-gated potassium channels, especially Kv1.1, Kv1.2 and Kv3.1 potassium channels (Grigg *et al.*, 2000). Kv3.1 channels, give rise to the high-threshold voltage activated potassium current, I_{HT}, (Kaczmarek *et al.*, 2005) that is critical for MNTB neurons and AVCN bushy cells to phase-lock action potentials to inputs from the enbulb and calyx of Held, respectively (Manis & Marx, 1991; Wang *et al.*, 1998). Low-threshold voltage activated potassium currents, I_{LT}, generated by Kv1 channels, are instead important for AVCN bushy cells and MNTB principal cells ability to generate single action potentials in response to large depolarisations (Dodson *et al.*, 2002) and may be important for shortening the membrane time constant in LSO principal cells, which together with I_h, may affect synaptic integration (Manis & Marx, 1991; Barnes-Davies *et al.*, 2004).

The cellular localization and topographic expression of ion channels determines the way in which the auditory system process auditory information of different frequencies. Membrane ion channel expression may exhibit plasticity and understanding the

mechanisms that regulate expression is crucial for the study of long- and short-term adaptations in the brain.

In this chapter, acoustic stimulation has been used to demonstrate the effect of activity on the regulation of ion channels in auditory neurons. The study is focused on the protein expression of Kv1.1, Kv1.2 and Kv3.1b channels, outward potassium current produced by these channels, and hyperpolarization-activated currents, in the MNTB of normal hearing mice (CBA strain) after sound stimulation.

Methods

Sound stimulation

CBA mice (P16-P22) were acoustically stimulated as described in General Methods. In brief, freely moving non-anaesthetized mice were presented with sound stimuli from a high-frequency loudspeaker for one hour. A few experiments required sound stimulation only for 10 or 30 min. Pure-tone frequencies were of 1, 4, 16 or 30 kHz, while broadband noise (chirps) was of the frequencies 4-12 kHz, see details in Chapter 2. Sound pressure levels were constrained to 75 dB maximum (except for a few initial experiments where 80-85 dB sound pressure levels were tested). Control animals were handled and housed in the same manner as sound stimulated animals without acoustic stimulus.

Electrophysiology

Following sound stimulation, or silent control conditions, mice were decapitated and the forebrain and cerebellum were removed in ice-cold low-calcium ACSF as described in

the General Methods chapter. In summary, transverse slices (200 μm) containing auditory brainstem nuclei were made using an oscillating tissue slicer and incubated for one hour in normal ACSF at 35°C and subsequently held at room temperature (22-25°C) for electrophysiological recordings. Whole-cell voltage-clamp and current-clamp recordings from visualized MNTB neurons were made using an Axopatch 200B amplifier and Axograph data acquisition and analysis software. The internal solution was based on potassium gluconate: (mM: 122.5 K-Gluconate, 17.5 KCl, 9 NaCl, 1 $MgCl_2$, 10 Hepes, 3 Mg-ATP, 0.3 GTP-tris and 0.2 EGTA). The pH was adjusted to 7.2 using KOH. Current and voltage steps were applied and analysed using Axograph and Matlabb R13 (Mathworks). Potassium currents were elicited by 500 ms voltage steps to test potentials between –70 and +44 mV in 6 mV increments, with 300 ms pre-potential at –80 mV. Firing properties were recorded in current-clamp mode using 200 ms long current steps from –50 pA to +400 pA. The dendrotoxin-sensitive low-threshold potassium current was isolated using 50μM $CdCl_2$, 1μM tetrodotoxin (Alomone), 10μM ZD7288 (Tocris) and 100nM dendrotoxin (Alomone) in 0.1% bovine serum albumin. $Alexa^{488}$ (Molecular Probes) was added to the internal solution in order to determine the position of the cell within the MNTB. Recorded cells were separated into lateral or medial cells.

Immunohistochemistry

Sound stimulated and control animals were anaesthetized (Avertin 0.4-0.6 mg/g body weight) before transcardial perfusion with cold normal saline followed by 15-20 mL of fixative (4% paraformaldehyde in 0.1 M phosphate buffer; pH 7.4). The brainstem was dissected and placed in 4% paraformaldehyde for post-fixation over night, and thereafter placed in PBS with 30% sucrose until dehydrated. Transverse sections (35 μm) were obtained at the level of the AVCN, MNTB and LSO on a cryostat (Leica CM

1850). Frozen sections were blocked with 5% Normal Donkey serum in PBS with 0.3% Triton-X-100 for 30-60 minutes and subsequently incubated over night at room temperature with the appropriate primary antibody: c-Fos (Santa Cruz, rabbit, 1:500), Kv1.1 and Kv1.2 (Alomone, rabbit, 1:100) and Kv3.1b (Alomone, rabbit, 1:500), followed by incubation (1 hr) with species-appropriate Alexa-conjugated secondary antibody (Molecular Probes, 1:1000). Sections were cover-slipped with Vectashield mounting medium (Vector Laboratories, CA) and sealed with nail polish. Guinea pig anti- Vesicular glutamate transporter 1 (VGluT1) was used to outline presynaptic membranes (specifically the large calyx of Held synapse onto MNTB neurons). Blocking peptides for Kv1.1, Kv1.2 and Kv3.1b was used as controls.

Image Capture and Analysis

Fluorescent images were collected using a laser scanning confocal microscope (Ziess LSM) with a 20x objective at 1024 x 1024 pixel resolution. Confocal images (collapsed z-stacks) were thresholded using ImageJ (NIH) and positive c-Fos immunoreactive cells were plotted. Only c-Fos staining found for cells with calyces (labeled with VGluT1) were counted as activated principal cells of the MNTB. For potassium channel immunoreactivity the relative mean optical density (OD) was measured as the average mean pixel value of manually outlined cells (10 cells/region per slice) of the most lateral and medial region of the MNTB (<150 μm from the edge). Background intensity was routinely measured and subtracted from the average mean pixel value per region of each section. The ratio lateral/medial OD was calculated and values below 1 indicates medial predominance of immunoreactivity and values above 1 indicates lateral predominance of immunoreactivity.

Statistical Analysis

Student's *t*-test (two sample, equal variance, one-tail) was used and statistically significant differences are shown as asterisks (* $p<0.05$ or ** $p<0.005$), unless otherwise mentioned in the text. Error bars indicate standard error of the mean (s.e.m).

Results

Normal hearing CBA mice (~P21) were presented with pure tones or broadband (chirp) sound and the animals were subsequently sacrificed for immunohistochemical or electrophysiological experiments. Increased neural activity was assessed using an antibody against the protein product (c-Fos) of the cellular immediate early gene c-*fos* (Sheng & Greenberg, 1990). Auditory brainstem nuclei are tonotopically organized (see figure 1.5), with low frequency input ventrally located in the AVCN and laterally in the MNTB and LSO (and high frequency input to the dorsal AVCN and the medial region of the MNTB and LSO) (Spangler *et al.*, 1985). By exposing animals to pure tone sound stimulation (1, 4, 16 and 30 kHz) the putative low- and high-frequency input regions of the AVCN, MNTB and LSO were assessed. Friauf observed a band of c-Fos positive neurons in the low-frequency region of auditory nuclei of the rat after sound presentation of 1 kHz pure tones (Friauf, 1992). Here, no such c-Fos immunoreactivity could be observed in auditory nuclei of sound stimulated mice following 1 kHz pure tone stimuli. Pure tone presentation of 4 kHz was found to generate c-Fos immunoreactivity at the lateral edge of the MNTB (figure 6.1 A) similar to previous findings in the mouse (Brown & Liu, 1995; Brew & Forsythe, 2005). AVCN neurons exhibited variable staining with c-Fos after pure tone stimulation (4 kHz) predominantly at the ventral or ventral/lateral edge (figure 6.1 A). LSO neurons showed activated

neurons at the lateral edge of the S-shaped nucleus after 4 kHz sound presentation (figure 6.1 A). For the intermediate pure tone frequency (16 kHz) stimulation generated inconsistent c-Fos staining in all three investigated nuclei. Instead, a 30 kHz-pure-tone stimulation reliably generated c-Fos immunoreactivity in a cluster of AVCN neurons at the dorsal border of the nucleus (figure 6.1 B). The MNTB exhibited labeled neurons in the medial region, with a few scattered positively labeled neurons in more intermediate regions (figure 6.1 B). LSO neurons typically showed broader labeling of neurons in the medial region of the nucleus (figure 6.1 B).

In order to generate a larger proportion of activated neurons, allowing for additional electrophysiological studies, animals were presented with broadband sound of 4-12 kHz in the form of chirps of non-harmful levels (max 75 dB) for one hour. Specifically, the MNTB was investigated due to the simple morphology of the nucleus containing mainly a single neuronal type, and previous studies have shown activity dependent preservation of topographic ion channel distribution of the MNTB (von Hehn *et al.*, 2004; Leao *et al.*, 2006b). Here, 4-12 kHz would represent the characteristic frequencies of lateral MNTB neurons (Spangler *et al.*, 1985). Exposing mice to 4-12 kHz broadband noise confirmed, using c-Fos immunohistochemistry, that stimulated/activated neurons were confined to the most lateral region of the MNTB (figure 6.2).

Sound Stimulation Alters Kv3.1b Topographic Distribution

Sound stimulated animals were first examined for potassium channel expression after acoustic stimulation. The lateral to medial distribution of Kv1.1, Kv1.2 and Kv3.1b channels was examined using immunohistochemistry, where the lateral region of the nucleus contains neurons presented with increased neuronal activity. The medial third of the MNTB represent an internal control for sound presented animals, in addition to results from control animals (no sound stimulation). No potassium gradients were

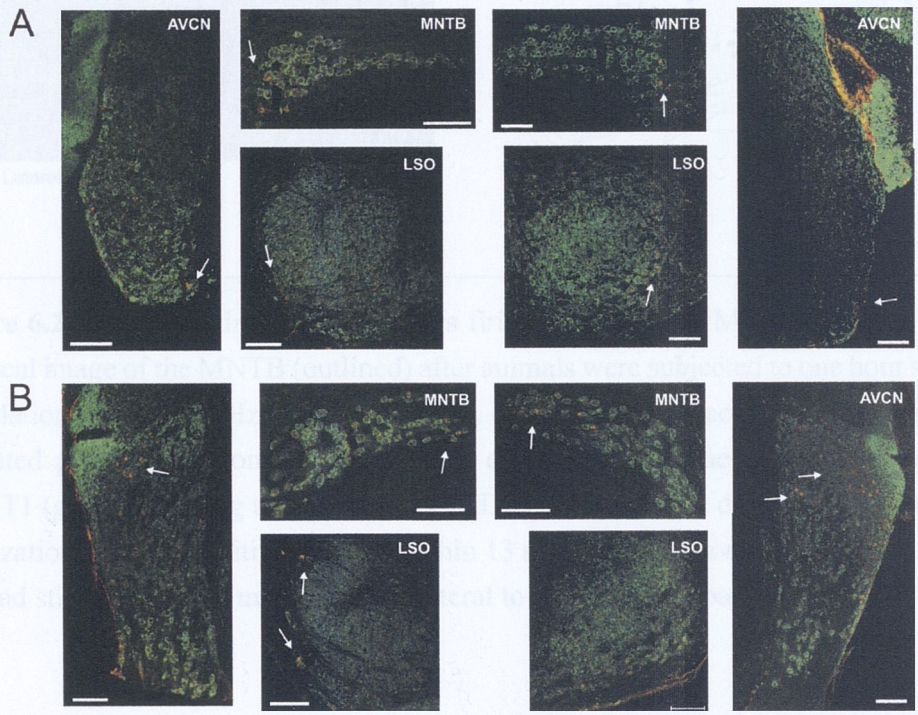

Figure 6.1: Specific c-Fos immunoreactivity after pure tone sound stimulation. **A**, examples of c-Fos immunoreactivity (red) in the AVCN, MNTB and LSO after 4 kHz pure tone stimulation for 1 hour. Slices are co-stained with the presynaptic marker VGluT1 (green). Arrows point to areas of activated neurons. Scale bars 100μm. **B**, examples as above after 30 kHz sound stimulation. Scale bars 100μm.

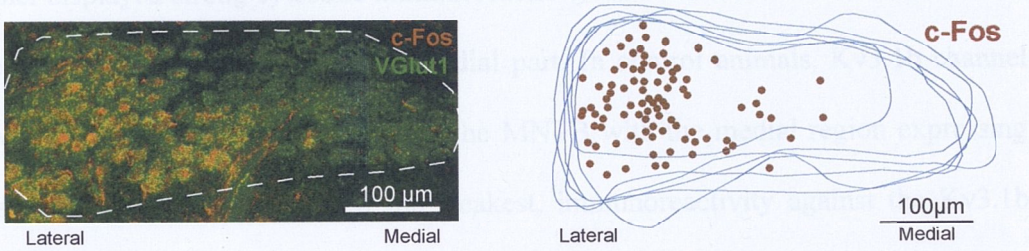

Figure 6.2: Acoustic stimulation modifies firing properties of MNTB neurons. *Left:* confocal image of the MNTB (outlined) after animals were subjected to one hour sound stimulation with 4-12 kHz broadband noise. c-Fos immuno-reactivity (red) indicates activated principal neurons of the MNTB, co-stained with the presynaptic marker VGluT1 (green) labelling the calyces of Held. *Right*: schematic drawing summarizing localization of c-Fos positive neurons within 13 sequential sections of an MNTB from a sound stimulated CBA mouse (P21). Lateral to the left, scale bar 100µm.

observed in the orthogonal axes of the MNTB (dorsal-to-ventral, or rostral-to-caudal), in agreement with previous results in the rat (Brew & Forsythe, 2005). The Kv1.1 and Kv1.2 potassium channels subunits showed no change in topographic expression between control and sound stimulated animals (figure 6.3 A). Both Kv1.1 and Kv1.2 channel displayed strong cytosolic immunoreactivity that was more intense in the lateral edge of the MNTB compared to the medial part. In control animals, Kv3.1b channel showed a typical gradient expression in the MNTB with the medial region expressing the strongest, and the lateral part the weakest, immunoreactivity against the Kv3.1b antibody (figure 6.3 A, *bottom left*). Interestingly, after a brief presentation of the low-frequency chirp stimulus (increasing the neuronal activity of the lateral part of the MNTB) a large increase in Kv3.1b-immunoreactivity was observed, seemingly reversing the gradient from medial-to-lateral to lateral-to-medial protein expression (figure 6.3 A, *bottom right*). The Kv3.1b staining of the chirp stimulated neurons revealed high levels in the cell membrane and moderate levels in the cytosol. The average ratio of lateral/medial optical density for MNTB neurons of stimulated and control animals was not different for the Kv1.1 (control: 1.05 ± 0.07, n=10; stimulated: 1.19 ± 0.08, n=17, p=0.11, Student's t-test, unequal variance) or Kv1.2 subunits (control: 1.32 ± 0.14, n=11; stimulated: 1.24 ± 0.11, n=8, p=0.33 Student's t-test, unequal variance) but significantly different for Kv3.1b channels (control: 0.89 ± 0.04, n=13; stimulated: 1.25 ± 0.08, n=15, p=0.0003) (figure 6.3 B). The time dependency of Kv3.1b protein expression demonstrated no up-regulation in Kv3.1b protein expression after only 10 min sound stimulation, in contrast to one hour chirp stimulation. Animals scarified two hours post-stimulus time (PST) showed Kv3.1b-immunoreactivity with stronger expression in the medial region, and sound stimulating the animals for one hour with a PST of 24 hours brought the Kv3.1b-immunoreactivty back to the normal gradient seen in control animals (Optical density ration after; 10min:

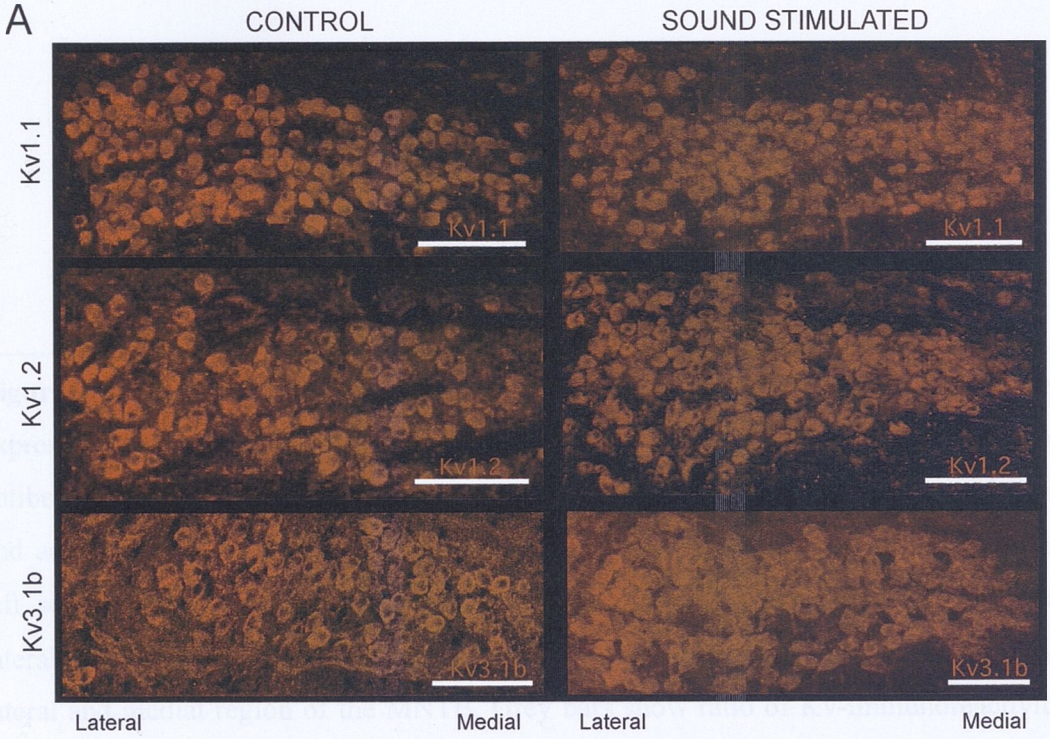
A
CONTROL
SOUND STIMULATED
Kv1.1
Kv1.2
Kv3.1b
Kv1.1
Kv1.2
Kv3.1b
Kv1.1
Kv1.2
Kv3.1b
Lateral
Medial
Lateral
Medial

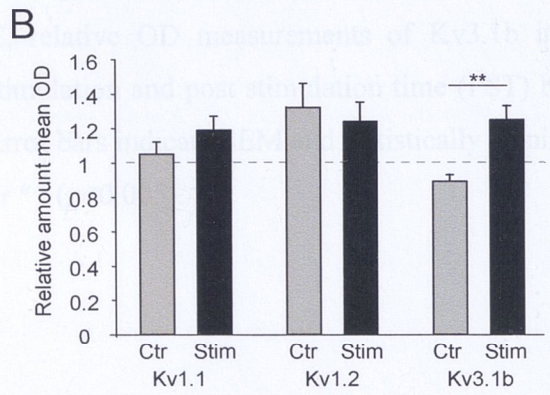
B
Relative amount mean OD
1.6
1.4
1.2
1
0.8
0.6
0.4
0.2
0
**
Ctr
Stim
Kv1.1
Ctr
Stim
Kv1.2
Ctr
Stim
Kv3.1b

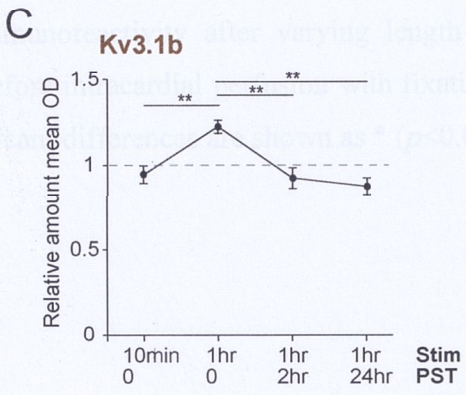
C
Kv3.1b
Relative amount mean OD
1.5
1
0.5
0
**
**
**
10min
0
1hr
0
1hr
2hr
1hr
24hr
Stim
PST

Figure 6.3: Increased neuronal activity can rapidly increase potassium channel expression in the MNTB. **A**, confocal images showing typical immunoreactivity of antibodies against Kv1.1, Kv1.2 and Kv3.1b (red) in MNTB sections from control (*left*) and acoustically stimulated (*right*; 4-12 kHz, 75 dB, 1 hr) CBA mice. Lateral on the left, scale bar 100μm. **B**, bar graph showing relative mean optical density (OD) (ratio of lateral/medial mean OD after background subtraction) of Kv-immunoreactivity from the lateral and medial region of the MNTB. Grey bars show ratio of Kv-immunoreactivity in control conditions and black bars indicate measurements after sound stimulation. Average relative OD lower than 1 indicates predominance of medial immunoreactivity. **C**, relative OD measurements of Kv3.1b immunoreactivity after varying length of stimulation and post stimulation time (PST) before intracardial perfusion with fixative. Error bars indicate SEM and statistically significant differences are shown as * ($p<0.05$) or ** ($p<0.005$).

0.94 ± 0.05, n=6, 1hr: 1.22 ± 0.04, n=4, 1hr + 2hr PST: 0.92 ± 0.06, n=8 and 1hr + 24hrs PST: 0.87 ± 0,05 n=9, see figure 6.3 C).

Altered Firing Properties of Stimulated Neurons

For electrophysiological slice recordings, a fluorescent dye (Alexa^{488}) was routinely added to the internal solution in order to determine the spatial position of each neuron recorded from within the MNTB of control and acoustically stimulated mice (figure 6.4 A). No change in passive membrane properties (resting membrane potential, input resistance or cell capacitance) was observed for MNTB neurons from sound stimulated animals compared to control animals. Previous studies examining firing properties of MNTB principal neurons have revealed a difference in action potential firing between medial and lateral neurons (Brew & Forsythe, 2005; Leao *et al.*, 2006b). MNTB medial cells (MC), responding to high-frequency sound input, normally exhibit a larger high-threshold voltage-dependent potassium current than lateral cells (LC) (Brew & Forsythe, 2005), which contributes to rapid repolarisations and shorter action potential duration, giving the MNTB neurons the ability to respond to high frequency firing. In control conditions, medial MNTB neurons displayed a shorter delay than lateral MNTB neurons (control: MC 3.07±0.27 ms, LC 5.24±0.76 ms, p=0.007), and medial cells showed smaller action potential amplitudes than lateral neurons although this difference was not significant (control: MC 66.17±2.75 mV, LC 73.39±3.23 mV, p=0.06) in accordance with previous work (Leao *et al.*, 2006b) (figure 6.4 B). AP delay differences were significantly shorter comparing stimulated lateral neurons with non-stimulated medial neurons (figure 6.4 B). The average AP delay for stimulated lateral cells was decreased to 3.97±0.24 ms and significantly different from control lateral cells (p=0.05). There was no difference in AP amplitude between controls and stimulated lateral cells. Amplitudes of the post-AP after-hyperpolarization were significantly more

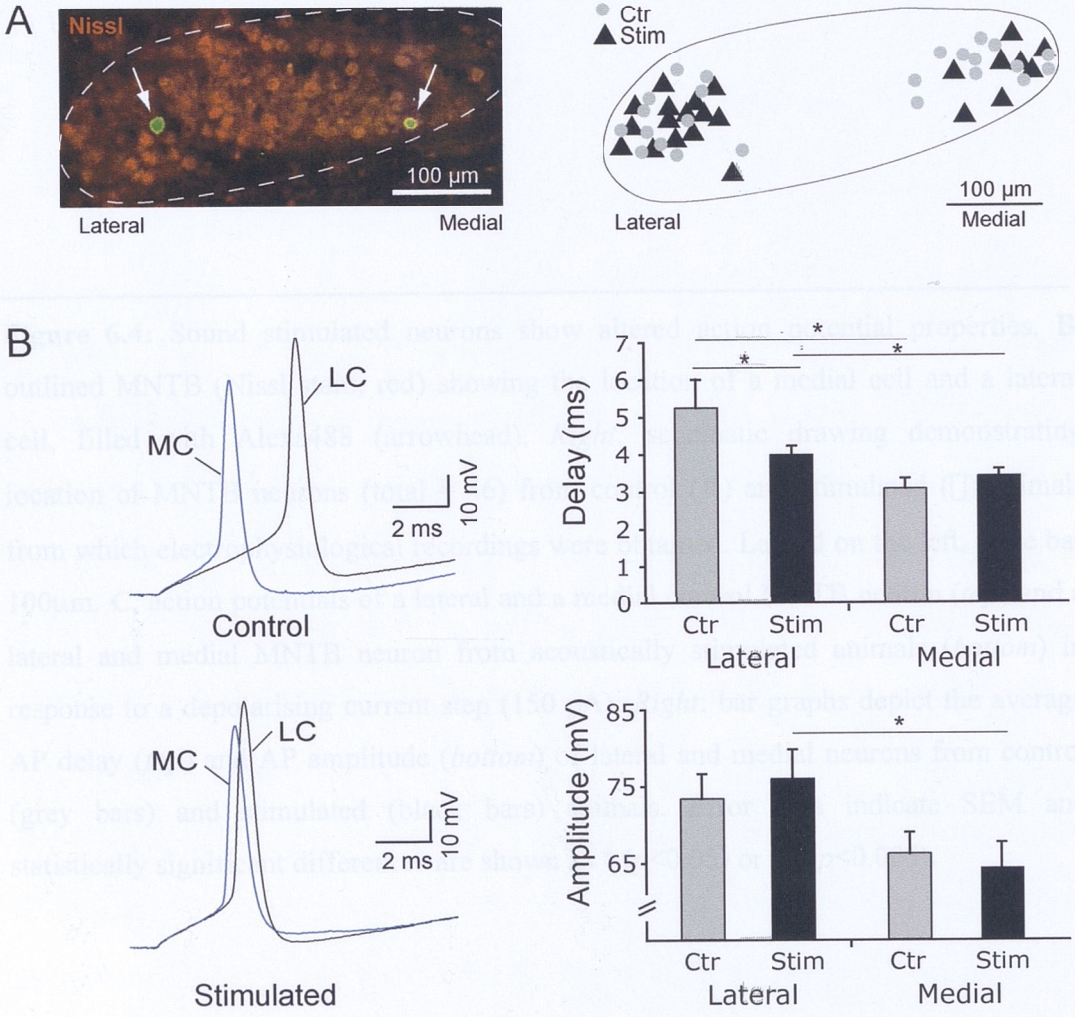
A
Nissl
100 µm
Lateral
Medial
Ctr
Stim
100 µm
Lateral
Medial
B
LC
MC
2 ms
10 mV
Control
LC
MC
2 ms
10 mV
Stimulated
Delay (ms)
0
1
2
3
4
5
6
7
Ctr
Stim
Ctr
Stim
Lateral
Medial
Amplitude (mV)
65
75
85
Ctr
Stim
Ctr
Stim
Lateral
Medial

Figure 6.4: Sound stimulated neurons show altered action potential properties. **B**, outlined MNTB (Nissl stain, red) showing the location of a medial cell and a lateral cell, filled with Alexa488 (arrowhead). *Right:* schematic drawing demonstrating location of MNTB neurons (total = 46) from control (●) and stimulated (□) animals from which electrophysiological recordings were obtained. Lateral on the left, scale bar 100μm. **C**, action potentials of a lateral and a medial control MNTB neuron (*top*) and a lateral and medial MNTB neuron from acoustically stimulated animals (*bottom*) in response to a depolarising current step (150 pA). *Right*: bar graphs depict the average AP delay (*top*) and AP amplitude (*bottom*) of lateral and medial neurons from control (grey bars) and stimulated (black bars) animals. Error bars indicate SEM and statistically significant differences are shown as * ($p<0.05$) or ** ($p<0.005$).

negative in stimulated lateral cells (~6 mV, p=0.01) when compared to lateral cells of non-stimulated animals. There was no difference in AP properties between medial cells from acoustically stimulated animals and medial cells from control animals (data not shown).

Acoustic Stimulation Affects Outward K^+ Currents

No difference was found in hyperpolarization-activated current between chirp stimulated (4 -12 kHz) and control animals. However, lateral cells from stimulated animals (n=14) exhibited significantly larger outward potassium current at voltages more positive than –22 mV when compared to control lateral neurons (n=12) (figure 6.5 A). At +44 mV, whole-cell currents were equal to 5.95 ± 0.22 nA in LC of stimulated animals and 4.42 ± 0.40 nA (p<0.001) in LC of non-stimulated mice, suggesting an increase in the high-threshold potassium current. Medial MNTB neurons from stimulated (n=8) and medial cells (n=12) from control animals showed no difference in current amplitude (figure 6.5 B).

The low-threshold potassium current of lateral control and stimulated neurons was determined, by applying the specific low-threshold potassium channel blocker dendrotoxin-I (DTX-I) to brain slices (Leao *et al.*, 2004a). Stimulated LC (n=5) displayed a significantly smaller DTX-I sensitive current compared to control cells (n=5) in response to a +2 mV voltage step (Stim: 0.20 ± 0.03 nA, Control: 0.50 ± 0.10 nA, p=0.01). Stimulated MNTB neurons also showed a more negative half-activation voltage ($V_{1/2}$) of the DTX-I sensitive current after fitting normalized currents with a Boltzmann equation (I/Imax = 1/(1+e((V-$V_{1/2}$)/k)) (Stim: -30.4 ± 1.4 mV, Control: -25.4 ± 2.2 mV, p<0.05).

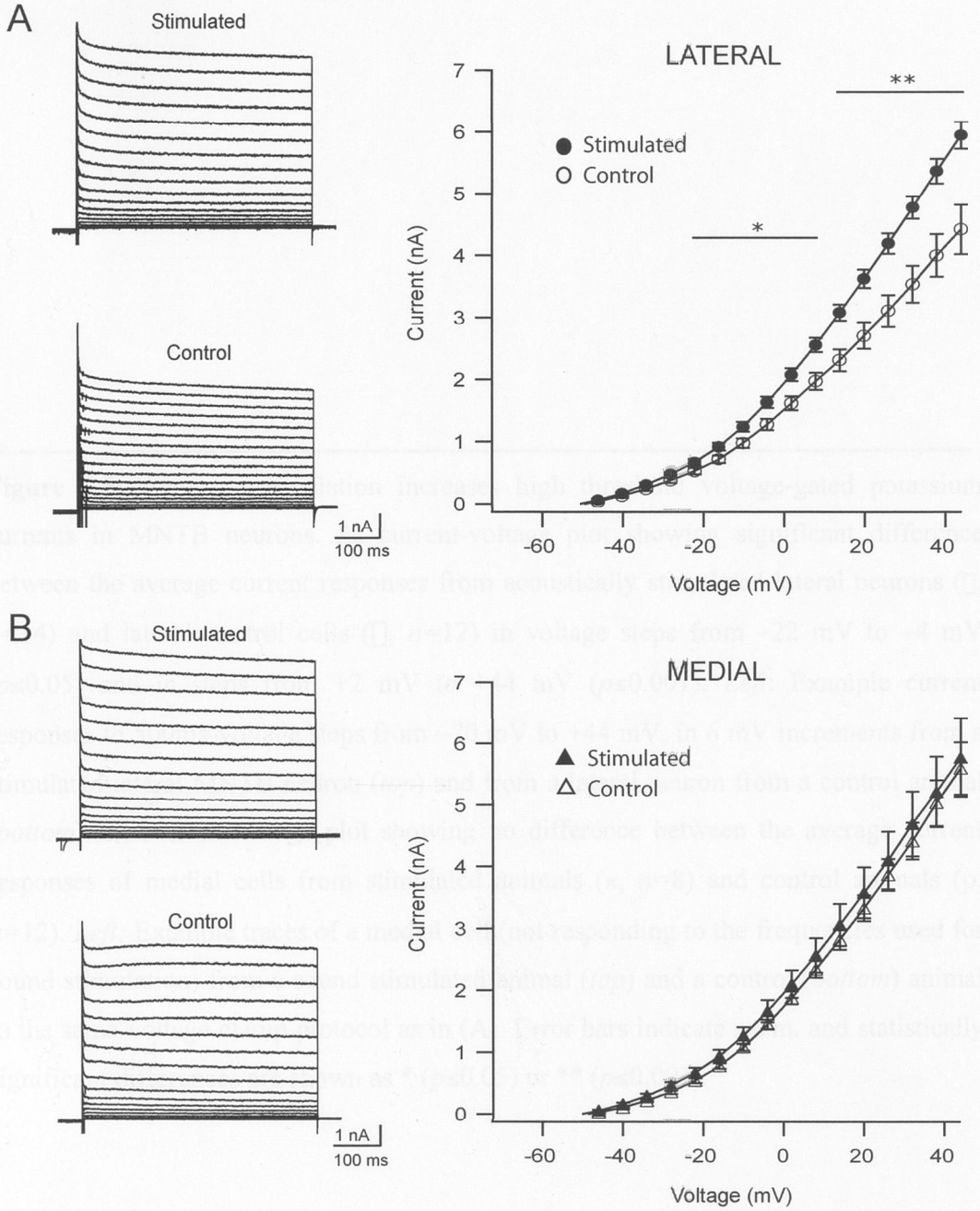
A
Stimulated
Control
1 nA
100 ms
LATERAL
Stimulated
Control
**
*
Current (nA)
Voltage (mV)
B
Stimulated
Control
1 nA
100 ms
MEDIAL
Stimulated
Control
Current (nA)
Voltage (mV)

Figure 6.5: Acoustic stimulation increases high threshold voltage-gated potassium currents in MNTB neurons. **A**, current-voltage plot showing significant difference between the average current responses from acoustically stimulated lateral neurons (□, n=14) and lateral control cells (□, n=12) in voltage steps from –22 mV to –4 mV ($p \leq 0.05$) and in steps from +2 mV to +44 mV ($p \leq 0.001$). *Left*: Example current responses to 500ms-voltage steps from –70 mV to +44 mV, in 6 mV increments from a stimulated lateral MNTB neuron (*top*) and from a lateral neuron from a control animal (*bottom*). **B**, current-voltage plot showing no difference between the average current responses of medial cells from stimulated animals (π, n=8) and control animals (ρ, n=12). *Left:* Example traces of a medial cell (not responding to the frequencies used for sound stimulation) from a sound stimulated animal (*top*) and a control (*bottom*) animal to the same voltage clamp protocol as in (A). Error bars indicate s.e.m. and statistically significant differences are shown as * ($p \leq 0.05$) or ** ($p \leq 0.001$).

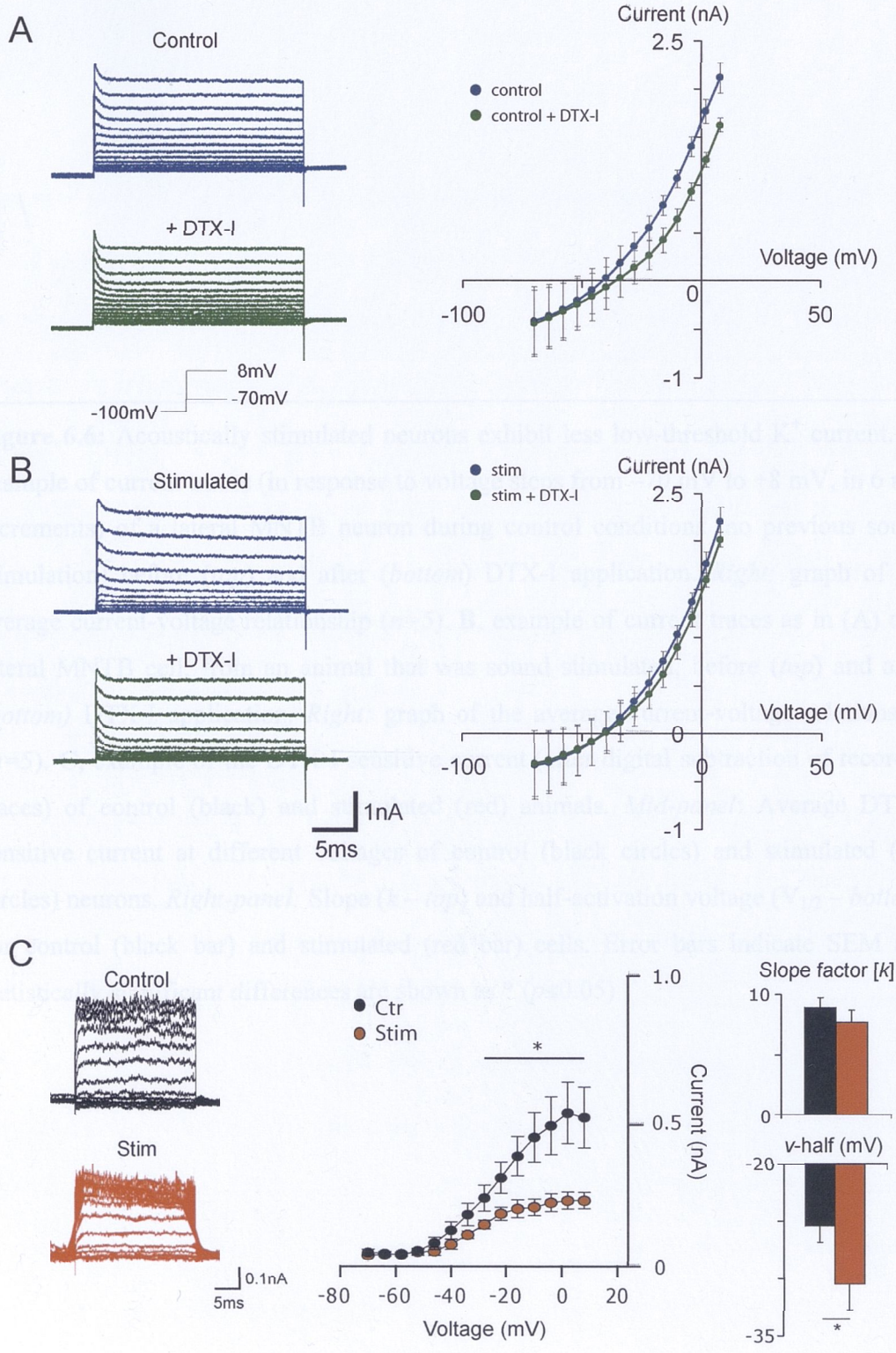
A
Control
+ DTX-I
8mV
-70mV
-100mV
Current (nA)
2.5
control
control + DTX-I
Voltage (mV)
-100
0
50
-1
B
Stimulated
+ DTX-I
1nA
5ms
stim
stim + DTX-I
Current (nA)
2.5
Voltage (mV)
-100
0
50
-1
C
Control
Stim
0.1nA
5ms
Ctr
Stim
1.0
0.5
0
Current (nA)
*
-80
-60
-40
-20
0
20
Voltage (mV)
Slope factor [k]
10
0
v-half (mV)
-20
-35
*

Figure 6.6: Acoustically stimulated neurons exhibit less low-threshold K^+ current. **A**, example of current traces (in response to voltage steps from –70 mV to +8 mV, in 6 mV increments) of a lateral MNTB neuron during control conditions (no previous sound stimulation) before (*top*) and after (*bottom*) DTX-I application. *Right:* graph of the average current-voltage relationship (n=5). **B**, example of current traces as in (A) of a lateral MNTB cell, from an animal that was sound stimulated, before (*top*) and after (*bottom)* DTX-I application. *Right:* graph of the average current-voltage relationship (n=5). **C**, example of the DTX-I sensitive current (after digital subtraction of recorded traces) of control (black) and stimulated (red) animals. *Mid-panel*: Average DTX-I sensitive current at different voltages of control (black circles) and stimulated (red circles) neurons. *Right-panel:* Slope (k – *top*) and half-activation voltage ($V_{1/2}$ – *bottom*) for control (black bar) and stimulated (red bar) cells. Error bars indicate SEM and statistically significant differences are shown as * ($p \leq 0.05$)

Discussion

Increased neuronal activity has been demonstrated using immunohistochemical labeling of the protein c-Fos, which is encoded by the gene *c-fos*, a transcription regulator (see Friauf, 1992). Previous studies have shown that sound levels of 35-55 dB do not increase the expression of c-Fos protein significantly (Brown and Liu, 1995). Sound pressure levels causing damage to the auditory system, and potentially tinnitus like symptoms, have been demonstrated after sound stimulation levels between 97-125 dB (Basta & Ernest 2004, Basta et al., 2005, Ma et al., 2006, Willott, 2001). In this study, a non-harmful sound pressure level of 75 dB was found to produce clear c-Fos staining in the appropriate area of auditory nuclei.

These results provide direct evidence that acoustic stimulation can lead to modifications in the membrane properties of central auditory neurons. A shortening of AP delay and increased amplitude of AP afterhyperpolarization in MNTB neurons was observed in sound stimulated mice. These alterations can be attributed to changes in expression of Kv3.1 or Kv1 channels. Previous experiments have shown that blocking I_{LT} causes MNTB neurons to fire multiple APs (Wang *et al.*, 1998; Leao *et al.*, 2004a) as well as shortening the delay of AP generation (Guan *et al.*, 2007). In the presence of tetraethylammonium (TEA), which in small concentrations can block the high-threshold potassium current (from Kv3.1 channels), AP afterhyperpolarization is decreased (Ishikawa *et al.*, 2003). In this study a shorter delay was observed to the firing of action potentials and an increase in afterhyperpolarization magnitude for the stimulated neurons. In addition, stimulation led to a rapid increase (around 1/2 to 1 hr) in the expression level of Kv3.1b potassium channels, and an increase of the magnitude of I_{HT}.

Brew and Forsythe (2005) have reported a gradient expression of a K^+ current with an intermediate voltage-threshold in the rat MNTB, with lateral neurons expressing stronger intermediate current than medial neurons (Brew & Forsythe, 2005). This current may also be affected by sound stimulation, if present in the mouse MNTB, and may contribute to the significant increase in outward potassium current seen at potentials below –10 mV (where the high-threshold potassium current begins to activate). The increase in outward K^+ current could also be due to a shift in voltage-dependency of I_{HT}.

Other studies have reported a rapid decrease of Kv1.1 and Kv3.1 subunits protein in the chick nucleus magnocellularis after unilateral removal of the cochlear (Lu *et al.*, 2004) and a lack of Kv3.1 topographic gradient in the MNTB of hearing impaired mice (von Hehn *et al.*, 2004). Leao *et al.*, also found a lack of topographic Kv1 and Kv3.1 channel distribution in the MNTB of deaf mice (Leao *et al.*, 2006b). Song and others described rapid (minutes) changes in phosphorylation state of Kv3.1 channels (stimulation) that can increase the amplitude of the high-threshold voltage-gated K^+ current (Song *et al.*, 2005). The present study contributes to these finding by demonstrating that sound stimulation can cause an increase in high-threshold voltage-gated potassium current by increasing the expression of the Kv3.1b channel protein, as a whole (not only related to rapid dephosphorylation). Kv3.1 gene expression is known to be long-term regulated by elevate levels of cyclic AMP (cAMP) or calcium, due to changes in intrinsic excitability of neurons (Liu & Kaczmarek, 1998; Kaczmarek *et al.*, 2005). The Kv3.1 promotor can be regulated by a CRE (cAMP/calcium Response Element) that binds CREB (CRE-binding protein) (Kaczmarek *et al.*, 2005). Channel trafficking, regulation by beta subunits or changes in protein transcription or translation may also contribute to the observed reversal of Kv3.1b protein gradient, and an increase in the high-threshold

potassium current, in sound stimulated MNTB neurons (Martens *et al.*, 1999; Misonou & Trimmer, 2004; Heusser & Schwappach, 2005).

No significant difference was observed in Kv1.1 or Kv1.2 immunoreactivity, although the Kv1.1 gradient (lateral to medial) was slightly intensified after stimulating the lateral neurons. It has previously been suggested that the Kv1.1 and Kv3.1 channels might be controlled by common transcription factors, shared promotor regions or parallel signaling pathways that are affected by afferent activity (Bortone *et al.*, 2006). The Kv1.2 immunoreactivity gradient (lateral to medial) was, instead, weakened after sound stimulation. Both Kv1.1 and Kv1.2 protein expression was strongly present in the cytosol, and therefore cannot be easily related to the amount of functional ion channels at the cell membrane. The observed decrease in low-threshold voltage-gated potassium current (generated through both Kv1.1 and Kv1.2 channels) could explain the differences in AP delay. The more negative half-activation potential of the low-threshold current of the stimulated neurons may suggest an increased expression of Kv1.1 channels (known to have a more negative $V_{1/2}$ than Kv1.2 channels (Coetzee *et al.*, 1999). Kv1 channels can exist as both homo- and heteromeres (Dodson *et al.*, 2002), and the reduction in any of the two subtypes might still lead to a reduction of the total amount of functional Kv1 channels. The cell surface expression of Kv1.1 and Kv1.2 channels has recently been shown to be modulated by the glycosylation state of channels, which can affect protein folding, stability and trafficking to the cell surface (Watanabe *et al.*, 2007).

Most of the previous insights in activity-dependent changes at the cellular level have come from isolated neuronal culture systems. These results in a brainstem auditory nucleus provide a valuable and direct example of such adaptations in the intact nervous system.

Chapter 7. General Discussion

This thesis focuses on the role of cochlear activity in generating, preserving and modifying membrane properties of brainstem auditory neurons. Firstly, it emphasizes the variety of specific ion channels which auditory neurons express in order to perform different input/output functions, in particularly, it investigates the relationship between the hyperpolarization-activated cation current (I_h) and properties of brainstem auditory neurons of the anteroventral cochlear nucleus (AVCN), the medial nucleus of the trapezoid body (MNTB) and the lateral superior olive (LSO).

The role of afferent activity in regulating brainstem auditory neurons was assessed using two different approaches. In order to study the effect of lack of activity, on the firing properties of AVCN bushy cells, congenitally deaf mice were compared to normal mice. Conversely, the effects of increased cochlear activity were studied in normal hearing mice following ear canal opening and the onset of hearing. In these studies, changes in ion channel expression in auditory neurons were assessed in response to brief sound stimulation. The work presented in this thesis provides several insights on the role of activity in regulating the membrane properties of auditory neurons: it explores intrinsic activity, lack of cochlear activity during development, and brief increased sensory activity at a fixed time point in development.

The intrinsic activity of neurons is defined by the mixture of ion channels operating near the resting potential of cells. I have investigated one such significant ion channel, the hyperpolarization-activated cyclic nucleotide-gated (HCN) channel, generating I_h, which helps set the resting membrane potential and modulates neuronal excitability

(Pape, 1996). Specifically, the expression of HCN1 and HCN4 subunits were investigated in neurons of the AVCN, MNTB and LSO. Primary neurons showed individual expression of isoforms with specific subcellular labelling of the examined HCN channels. In summary, the LSO displayed strong HCN1 expression, the AVCN displayed both HCN1 and HCN4 labelling while the MNTB primarily showed HCN4 labelling.

In auditory neurons, I_h improves the temporal precision of input processing by lowering input resistance, shortening time constants and reducing temporal summation (Oertel, 1999). By altering membrane time constants, temporal integration in neurons can be dynamically regulated by ion channels opening or closing at rest. In LSO neurons, especially, I_h appears to contribute considerably to the resting membrane potential. Another current that activates around, or at resting potential, in auditory neurons is the low-threshold K^+ current, I_{LT}, that acts contrary to I_h (I_{LT} activates during membrane depolarizations and I_h activates during hyperpolarizations). I_{LT} generates outward K^+ currents that impede the invasion of more than one AP during a single event (Dodson *et al.*, 2002) and activates much faster than I_h (several milliseconds compared to tens/hundreds of milliseconds). The activation kinetics of I_h can be accelerated by cyclic nucleotides (Ludwig *et al.*, 1999), while I_{LT} activation is primarily modulated by membrane potential. AVCN bushy cells and MNTB principal cells exhibited slowly activating I_h and showed strong expression of HCN4 channel subunits, known to be modulated by cyclic nucleotides that inhibit HCN channel gating (Wainger *et al.*, 2001), permitting the channels to open more rapidly and completely after repolarization of action potentials (Pape, 1996). As I_h displays slow kinetic, compared to voltage-gated Na^+ or K^+ currents, these currents would act at rest as leak currents during a small number of PSPs. Banks *et al.*, (1993) suggested that the modulation of I_h, via noradrenaline and cAMP, is the mechanism for changing the resting membrane

potential of MNTB neurons to more depolarised potentials, leading to activation of I_{LT} that can decrease the duration of EPSPs (Banks *et al.*, 1993). However, after prolonged depolarizations I_h deactivates, causing the membrane time constant to rise and therefore potentiate temporal integration, while prolonged hyperpolarization (or inhibition) would cause the opposite effect. In conclusion I_h is an essential contributor to the resting membrane potential and can modulate cell excitability in bushy cells of the AVCN, and principal cells of the MNTB and the LSO.

The relationship between I_h function and HCN channel expression has been investigated by examining gradients of HCN channel expression within auditory nuclei (displaying different frequency bands containing neurons of different characteristic frequencies). For example, I_h regulates coincidence detection in the nucleus laminaris of the chick (equivalent of the mammal medial superior olive), which displays a gradient in the expression of HCN1 channels with the highest expression in low-characteristic frequency neurons, while HCN2 is evenly distributed across the nucleus (Yamada *et al.*, 2005). In mice, a gradient of HCN4 expression has been observed in the MNTB, with the medial, high-frequency input region, expressing stronger HCN4-immunoreactivity than lateral MNTB cells, contributing to the specific firing properties of these neurons (Leao *et al.*, 2006b). The presence of HCN1 channels in low-frequency input neurons shows the value of a short membrane time constant when detecting coinciding small inputs (e.g. MSO neurons integrate excitatory input when comparing ITD of low-frequency sound), while slow activating HCN4 channels of MNTB neurons could potentially modulate high-frequency input through shortening the delay of AP generation or by modulating resting membrane potential through cyclic nucleotide binding. HCN channels can also be unevenly distributed along different cell compartments. For example, in dendrites of cortical pyramidal neurons, I_h shows a gradient of expression, with the highest densities of HCN channels in the distal dendrite

(Berger *et al.*, 2003; Kole *et al.*, 2006) creating variation of input-output properties along the somatodendritic axis of pyramidal neurons (Oviedo & Reyes, 2005).

In addition, more physiological roles of I_h in the central nervous system have been studied in HCN1-knock-out mice, showing that HCN1 channels are important for motor learning and memory (Nolan *et al.*, 2003). HCN2-knock-out mice have been shown to exhibit spontaneous absence seizures, due to a near-complete loss of I_h in thalamocortical relay neurons (Ludwig *et al.*, 2003). Recently, Carr *et al.*, (2007) demonstrated that inhibition of HCN channels, by α2-noradrenalin receptor simulation, enhanced excitability and synaptic integration of prefrontal cortex pyramidal neurons. This inhibition of HCN channels was suggested to generate enhanced signal to noise ratio, leading to the suppression of isolated excitatory inputs while enhancement of the response to bursts of synaptic activity in the prefrontal cortex (Carr *et al.*, 2007). HCN channels in the auditory system may be of significance for increasing the temporal acuity of the auditory pathway during a heightened state of arousal, through the modulation of I_h by neurotransmitters and cyclic nucleotides, such as noradrenaline and cAMP (Banks *et al.*, 1993). I_h, as a slow conductance, may also contribute to the ability of neurons to respond to duration of sound stimuli (Hooper *et al.*, 2002). For example, if a sound generate inhibitory input to a cell, slowly activating I_h, the duration of the inhibitory input would create a temporal frame within which excitation can occur. Upon the termination of the stimuli, I_h could generate a rebound depolarisation, which itself may be insufficient to produce a spike, but if coincident with a delayed excitatory synaptic inputs an AP can be produce. Sound duration coding neurons have been found in the inferior colliculus, the MNTB and the superior paraolivary nucleus (Casseday *et al.*, 1994; Pollak *et al.*, 2002; Kadner *et al.*, 2006), of which the inferior colliculus and the MNTB are known to express HCN channels significantly (Koch *et al.*, 2004; Leao *et al.*, 2006b).

Neural activity is important for the development and regulation of synaptic and membrane properties of individual auditory neurons. However, studies involving disruption of cochlear activity have shown that neurons of different nuclei are differentially affected by changes in sensory input (Walmsley *et al.*, 2006). In the auditory system, neuronal activity appears to support cell survival, affect dendritic and axonal growth, and influence fine tuning of maps (Friauf & Lohmann, 1999). Crude tonotopic maps formation is controlled by genetic expression of molecular markers, while topographic distribution of ion channels has been shown to be dependent on spontaneous and sound evoked cochlear activity (von Hehn *et al.*, 2004; Leao *et al.*, 2006b). Another aspect regarding the effects of activity on the regulation of firing properties investigated in this thesis was the effect of congenital deafness on the development of AVCN bushy cells. These results highlights that a lack of spontaneous activity during development does not seem to affect post-synaptic bushy neurons in the same manner as MNTB principal neurons (Leao *et al.*, 2005). Whether these diverse neural properties of auditory neurons are maintained at more mature ages in the *dn/dn* mouse, or if properties eventually lead to specific compensations due to the lack of input to the auditory system, remains to be investigated. The understanding of neuronal changes following deafness is extremely important for cochlear implantations. Measurements of cortical auditory evoked potentials in congenitally deaf children with cochlear implants have shown that central auditory pathways are maximally plastic for a period of about 3.5 years (Sharma & Dorman, 2006). The functional maturation of the auditory cortex of congenitally deaf cats, fitted with cochlear implants at the age of 3-4 months, occurred between the third and eight month of life (Klinke *et al.*, 1999). A recovery of normal morphology of auditory nerve synaptic endings, following three months of sound stimulation, has also been demonstrated in congenitally deaf cats fitted with cochlear implants (Ryugo *et al.*, 2005). In addition to cochlear implants, auditory

brainstem implants are being developed to help patients of whom the auditory nerve is abnormal or has been removed (e.g. due to tumours) (Colletti, 2007). In a brainstem implant, a microelectrode array stimulates the surface or penetrates the ventral cochlear nucleus directly (Rauschecker & Shannon, 2002). The placement of the implant along the VCN is crucial for preservation of tonotopic map, which is important for speech understanding (Rauschecker & Shannon, 2002). In cochlear implants, the frequency organization of the cochlea allows the electrode to be appropriately placed along the tonotopic axis of the cochlea, producing better clinical results than auditory brainstem implants, nevertheless cochlear implant users show poor understanding of speech in noisy backgrounds and poor spatial hearing (Middlebrooks & Snyder, 2007). The poor performance of implants may be caused by the changes observed in the auditory system following deafness and optimal implants would account for the neuronal alterations. A novel approach to improve auditory prostheses is to implant the multielectrode array directly into the auditory nerve (as the conventional cochlear implant suffer limitations due to the remote location of the stimulating electrode; the scala tympani of the cochlea lies in a bony compartment filled with electrically conductive fluid) (Middlebrooks & Snyder, 2007). Understanding the plasticity of neurons in the auditory pathways remains important for further improvement of hearing aids. The results of the studies of congenitally deaf mice, in this thesis, showed that there is no significant changes in firing properties of AVCN bushy cells, however, previous studies have demonstrated presynaptic changes in the AVCN of *dn/dn* mice (Oleskevich & Walmsley, 2002) that may help preserve normal firing properties of AVCN bushy cells. Patients receiving auditory brainstem implants have had the auditory nerve removed, which may affect the properties of VCN neurons, and thus affect the functional outcome of the implant. In patients with a damaged cochlea, auditory nerve implants may be beneficial, although auditory brainstem neurons may have undergone plastic alterations of membrane

properties due to cochlear dysfunction, as seen in the MNTB of congenitally deaf mice (Leao *et al.*, 2004a).

A major finding of this thesis was that sound stimulation can drastically affect potassium channel expression in MNTB principal neurons of normal hearing mice. A significant increase in expression of Kv3.1b channels was observed in the region of the MNTB that contains neurons that normally respond to the frequencies of the applied sound stimuli. In the MNTB, electrophysiological recordings exhibited an increase in high-threshold K^+ currents, and a decrease in low-threshold K^+ currents following one hour of frequency specific sound stimulation. A rapid (minutes) increase in outward potassium currents amplitude has been reported after dephosphorylation of the Kv3.1b channel following brief high-frequency acoustic stimulation of rats (Song *et al.*, 2005). Similar activity-dependent regulation of potassium channels has been seen in the avian auditory system: unilateral removal of the cochlea leads to a rapid (hours) reduction in the expression of both Kv1.1 and Kv3.1 immunoreactivity, which is followed by a restoration of expression back to base line levels (Lu *et al.*, 2004). Neuronal activity can also affect the proportion of Kv3.1b channel (the adult splice variant of the Kv3.1 channel) expression compared to the immature Kv3.1a channel expression in the chick (Feng & Morest, 2006). In this study, one hour of sound stimulation was sufficient to dramatically increase the expression of Kv3.1 channels and increase in high-threshold potassium current. Also, a shortening of AP delay and increased amplitude of AP afterhyperpolarization in MNTB neurons was observed in sound stimulated mice. This may be due to the decrease in I_{LT} and increase in I_{HT}, respectively. Modeling of MNTB neurons has shown that large Kv3.1-mediated currents decrease the timing accuracy of action potentials but enable neurons to follow high-frequency stimuli (Song *et al.*, 2005). Further experiments using different sound stimulation parameters (e.g. higher

frequencies), also in other areas of the auditory brainstem, will provide additional understanding of how sound stimulation can modify the output functions of auditory neurons.

The examined Kv1.1 and Kv1.2 immunoreactivity was predominantly intracellular, hindering a direct correlation between channel expression and the low-threshold potassium current. The presence of a gradient distribution may still imply a functional relevance of the quantity of channels expressed, whether it being homomeric and/or heteromeric Kv1 channel expression. A gradient of Kv1.1 channel expression has been reported in the rat MNTB (Brew & Forsythe, 2005) although with the opposite expression gradient found in the mouse MNTB (Leao *et al.*, 2006b). A study in the rat LSO have shown stronger Kv1.1 channel expression in the lateral, low-frequency input region (Barnes-Davies *et al.*, 2004) similar to the Kv1.1 and Kv1.2 immunoreactivity observed in this thesis in MNTB cells. In the LSO, the Kv1.1 channel gradient reflects the distribution of I_{LT}, giving LSO principal neurons their typical single or multiple AP firing properties (Barnes-Davies *et al.*, 2004). I_{LT} has been shown to enhance the signal-to-noise ratio and phase locking to low-amplitude inputs in the MSO of gerbils, when neurons were presented with small signals in a noisy background (Svirskis *et al.*, 2002). Interestingly, a 'non-noisy' acoustic environment (4-12 kHz chirps in a sound shielded chamber) produced a reduction in I_{LT} of MNTB principal neurons. Less I_{LT} could cause increased excitability in MNTB cells (Leao *et al.*, 2004a), however, the more negative half-activation potential of the I_{LT} of sound stimulated MNTB neurons could potentially compensate for the reduced current magnitude, by allowing more current to be active at resting potential.

Experiments using mice chronically exposed to a click stimulus, at non-harmful sound pressure levels, demonstrated that neurons of the inferior colliculus developed broader than normal tuning curves, suggesting that frequency tuning requires patterned, or

random, activity (Sanes & Constantine-Paton, 1985). Humans might be able to consciously block or ignore repetitive, 'uninteresting' stimuli at higher brain regions. Auditory neurons would most likely still transmit information on the repetitive signal, although it is not possible to determine whether the dynamic regulation of potassium channels seen in these experiments would facilitate or impede the interpretation of the sound. In experiments with rats exposed to 5 kHz tone pips, from P9-P30, sensory experience of a sound was shown to result in expanded cortical representations of that sound, however the perceptual discrimination between the over-represented sound was impaired (Han *et al.*, 2007). Interestingly, the animals instead appeared more sensitive to the neighboring under-represented frequencies (Han *et al.*, 2007). Additional studies subjecting mice to broadband sound at a daily basis (e.g. one hour sound stimulation per day for a week) can potentially further investigate the long-term plasticity of auditory brainstem neurons.

An intriguing question related to the studies of mice exposed to brief sound stimulation is whether there is a physiological advantage of rapid up-regulation of Kv3.1b channels or if it is an 'artifact' of repetitively increasing the levels of Ca^{2+} and/or cAMP, leading to increased gene transcription. Activity-dependent changes in gene expression have been studied in cultured rat cortical neurons, focusing on genes, selectively responding to particular routes of Ca^{2+} entry, such as vesicle trafficking proteins, ion channels and neurotransmitter systems (Xiang *et al.*, 2007). That work found 248 genes to be activity-dependent, where the majority were induced (233 genes) and the minority (15 genes) suppressed by enhanced activity (Xiang *et al.*, 2007). This indicates that neuronal activity-dependent gene transcription may be a key feature of brain development and function.

The relationship between neuronal activity and potassium channel modulation have been documented for Kv2.1 channels, where continuous seizures in rats lead to less

clustering of Kv2.1 channel protein (Misonou *et al.*, 2004). The same group showed that glutamate stimulation of cultured rat hippocampal pyramidal neurons causes dephosphorylation of Kv2.1 protein, translocation of Kv2.1 channels from clusters to a more uniform localization, and a shift in the voltage-dependent activation of Kv2.1 mediated potassium current (Misonou *et al.*, 2004). In addition, activity-dependent trafficking of Kv4.2 potassium channel subunits has been observed in dendrites of cultured hippocampal neurons, where Kv4.2 channels were internalized into spines and dendrites upon glutamate receptor stimulation (Kim *et al.*, 2007). This Kv4.2 redistribution was also found upon evoked long-term potentiation (LTP) in neurons of hippocampal slice cultures, potentially allowing subthreshold Na^+ channel activation to enhance EPSPs (Kim *et al.*, 2007). Neuronal cultures can provide valuable information on activity-dependent neuronal plasticity, however, studies in the intact central nervous system are critical for a better understanding of the regulation of these mechanisms. In this thesis, increased neuronal activity was studied in the intact auditory system, displaying activity-dependent modulation of Kv channel expression. Together with the studies of congenitally deaf mice, the results in this thesis provide important insights to the role of sensory (and spontaneous) activity in regulating the membrane properties of auditory neurons.

Bibliography

Accili EA, Proenza C, Baruscotti M & DiFrancesco D. (2002). From funny current to HCN channels: 20 years of excitation. *News Physiol Sci* **17,** 32-37.

Altomare C, Terragni B, Brioschi C, Milanesi R, Pagliuca C, Viscomi C, Moroni A, Baruscotti M & DiFrancesco D. (2003). Heteromeric HCN1-HCN4 channels: a comparison with native pacemaker channels from the rabbit sinoatrial node. *J Physiol* **549,** 347-359.

Bal R & Oertel D. (2000). Hyperpolarization-activated, mixed-cation current (I(h)) in octopus cells of the mammalian cochlear nucleus. *J Neurophysiol* **84,** 806-817.

Ball KK, Gandhi GK, Thrash J, Cruz NF & Dienel GA. (2007). Astrocytic connexin distributions and rapid, extensive dye transfer via gap junctions in the inferior colliculus: Implications for [(14)C]glucose metabolite trafficking. *J Neurosci Res.*

Banks MI, Pearce RA & Smith PH. (1993). Hyperpolarization-activated cation current (Ih) in neurons of the medial nucleus of the trapezoid body: voltage-clamp analysis and enhancement by norepinephrine and cAMP suggest a modulatory mechanism in the auditory brain stem. *J Neurophysiol* **70,** 1420-1432.

Barnes-Davies M, Barker MC, Osmani F & Forsythe ID. (2004). Kv1 currents mediate a gradient of principal neuron excitability across the tonotopic axis in the rat lateral superior olive. *Eur J Neurosci* **19,** 325-333.

Baruscotti M, Bucchi A & Difrancesco D. (2005). Physiology and pharmacology of the cardiac pacemaker ("funny") current. *Pharmacol Ther* **107,** 59-79.

Basta D & Ernest A. (2004). Noise-induced changes of neuronal spontaneous activity in mice inferior colliculus brain slices. *Neurosci Lett* **368,** 297-302.

Batra R, Kuwada S & Fitzpatrick DC. (1997). Sensitivity to interaural temporal disparities of low- and high-frequency neurons in the superior olivary complex. I. Heterogeneity of responses. *J Neurophysiol* **78,** 1222-1236.

Berger T, Senn W & Luscher HR. (2003). Hyperpolarization-activated current Ih disconnects somatic and dendritic spike initiation zones in layer V pyramidal neurons. *J Neurophysiol* **90,** 2428-2437.

Beutner D & Moser T. (2001). The presynaptic function of mouse cochlear inner hair cells during development of hearing. *J Neurosci* **21,** 4593-4599.

Bock GR, Frank MP & Steel KP. (1982). Preservation of central auditory function in the deafness mouse. *Brain research* **239,** 608-612.

Bortone DS, Mitchell K & Manis PB. (2006). Developmental time course of potassium channel expression in the rat cochlear nucleus. *Hear Res* **211,** 114-125.

Brew HM & Forsythe ID. (1995). Two voltage-dependent K+ conductances with complementary functions in postsynaptic integration at a central auditory synapse. *J Neurosci* **15,** 8011-8022.

Brew HM & Forsythe ID. (2005). Systematic variation of potassium current amplitudes across the tonotopic axis of the rat medial nucleus of the trapezoid body. *Hear Res* **206,** 116-132.

Brown MC & Liu TS. (1995). Fos-like immunoreactivity in central auditory neurons of the mouse. *J Comp Neurol* **357,** 85-97.

Burrone J, O'Byrne M & Murthy VN. (2002). Multiple forms of synaptic plasticity triggered by selective suppression of activity in individual neurons. *Nature* **420,** 414-418.

Carr DB, Andrews GD, Glen WB & Lavin A. (2007). Alpha-2 Noradrenergic Receptor Activation Enhances Excitability and Synaptic Integration in Prefrontal Cortex Pyramidal Neurons via Inhibition of HCN Currents. *J Physiol.*

Casseday JH, Ehrlich D & Covey E. (1994). Neural tuning for sound duration: role of inhibitory mechanisms in the inferior colliculus. *Science* **264,** 847-850.

Chen C. (1997). Hyperpolarization-activated current (Ih) in primary auditory neurons. *Hear Res* **110,** 179-190.

Coetzee WA, Amarillo Y, Chiu J, Chow A, Lau D, McCormack T, Moreno H, Nadal MS, Ozaita A, Pountney D, Saganich M, Vega-Saenz de Miera E & Rudy B. (1999). Molecular diversity of K+ channels. *Annals of the New York Academy of Sciences* **868,** 233-285.

Colletti L. (2007). Beneficial auditory and cognitive effects of auditory brainstem implantation in children. *Acta Otolaryngol* **127,** 943-946.

Cuttle MF, Rusznak Z, Wong AY, Owens S & Forsythe ID. (2001). Modulation of a presynaptic hyperpolarization-activated cationic current (I(h)) at an excitatory synaptic terminal in the rat auditory brainstem. *J Physiol* **534,** 733-744.

Davis RL. (2003). Gradients of neurotrophins, ion channels, and tuning in the cochlea. *Neuroscientist* **9,** 311-316.

Desai NS, Rutherford LC & Turrigiano GG. (1999). Plasticity in the intrinsic excitability of cortical pyramidal neurons. *Nat Neurosci* **2,** 515-520.

Dodson PD, Barker MC & Forsythe ID. (2002). Two heteromeric Kv1 potassium channels differentially regulate action potential firing. *J Neurosci* **22,** 6953-6961.

Eggermont JJ. (2005). Tinnitus: neurobiological substrates. *Drug Discov Today* **10,** 1283-1290.

Feng JJ & Morest DK. (2006). Development of synapses and expression of a voltage-gated potassium channel in chick embryonic auditory nuclei. *Hear Res* **216-217,** 116-126.

Francis HW & Manis PB. (2000). Effects of deafferentation on the electrophysiology of ventral cochlear nucleus neurons. *Hear Res* **149,** 91-105.

Friauf E. (1992). Tonotopic Order in the Adult and Developing Auditory System of the Rat as Shown by c-fos Immunocytochemistry. *Eur J Neurosci* **4,** 798-812.

Friauf E, Hammerschmidt B & Kirsch J. (1997). Development of adult-type inhibitory glycine receptors in the central auditory system of rats. *J Comp Neurol* **385,** 117-134.

Friauf E & Lohmann C. (1999). Development of auditory brainstem circuitry. Activity-dependent and activity-independent processes. *Cell and tissue research* **297,** 187-195.

Fuchs PA, Glowatzki E & Moser T. (2003). The afferent synapse of cochlear hair cells. *Curr Opin Neurobiol* **13,** 452-458.

Grigg JJ, Brew HM & Tempel BL. (2000). Differential expression of voltage-gated potassium channel genes in auditory nuclei of the mouse brainstem. *Hear Res* **140,** 77-90.

Grothe B. (2003). New roles for synaptic inhibition in sound localization. *Nature reviews* **4,** 540-550.

Guan D, Lee JC, Higgs MH, Spain WJ & Foehring RC. (2007). Functional roles of Kv1 channels in neocortical pyramidal neurons. *Journal of neurophysiology* **97,** 1931-1940.

Han YK, Kover H, Insanally MN, Semerdjian JH & Bao S. (2007). Early experience impairs perceptual discrimination. *Nat Neurosci.*

Hermann J, Pecka M, von Gersdorff H, Grothe B & Klug A. (2007). Synaptic transmission at the calyx of held under in vivo like activity levels. *J Neurophysiol* **98,** 807-820.

Heusser K & Schwappach B. (2005). Trafficking of potassium channels. *Curr Opin Neurobiol* **15,** 364-369.

Hille B. (2001). *Ion channels of excitable membranes.* Sinauer, Sunderland, Mass.

Hooper SL, Buchman E & Hobbs KH. (2002). A computational role for slow conductances: single-neuron models that measure duration. *Nat Neurosci* **5,** 552-556.

Illing RB, Kraus KS & Michler SA. (2000). Plasticity of the superior olivary complex. *Microsc Res Tech* **51,** 364-381.

Imig TJ & Durham D. (2005). Effect of unilateral noise exposure on the tonotopic distribution of spontaneous activity in the cochlear nucleus and inferior colliculus in the cortically intact and decorticate rat. *The Journal of comparative neurology* **490,** 391-413.

Ishikawa T, Nakamura Y, Saitoh N, Li WB, Iwasaki S & Takahashi T. (2003). Distinct roles of Kv1 and Kv3 potassium channels at the calyx of Held presynaptic terminal. *J Neurosci* **23,** 10445-10453.

Jentsch TJ, Stein V, Weinreich F & Zdebik AA. (2002). Molecular structure and physiological function of chloride channels. *Physiological reviews* **82,** 503-568.

Kaczmarek LK, Bhattacharjee A, Desai R, Gan L, Song P, von Hehn CA, Whim MD & Yang B. (2005). Regulation of the timing of MNTB neurons by short-term and long-term modulation of potassium channels. *Hear Res* **206,** 133-145.

Kadner A, Kulesza RJ, Jr. & Berrebi AS. (2006). Neurons in the medial nucleus of the trapezoid body and superior paraolivary nucleus of the rat may play a role in sound duration coding. *J Neurophysiol* **95,** 1499-1508.

Kaltenbach JA, Zhang J & Finlayson P. (2005). Tinnitus as a plastic phenomenon and its possible neural underpinnings in the dorsal cochlear nucleus. *Hear Res* **206,** 200-226.

Keats BJ, Nouri N, Huang JM, Money M, Webster DB & Berlin CI. (1995). The deafness locus (dn) maps to mouse chromosome 19. *Mamm Genome* **6,** 8-10.

Kim G & Kandler K. (2003). Elimination and strengthening of glycinergic/GABAergic connections during tonotopic map formation. *Nature neuroscience* **6,** 282-290.

Kim J, Jung SC, Clemens AM, Petralia RS & Hoffman DA. (2007). Regulation of dendritic excitability by activity-dependent trafficking of the A-type K+ channel subunit Kv4.2 in hippocampal neurons. *Neuron* **54,** 933-947.

Kim JJ, Gross J, Potashner SJ & Morest DK. (2004). Fine structure of degeneration in the cochlear nucleus of the chinchilla after acoustic overstimulation. *J Neurosci Res* **77,** 798-816.

Klein B, Kuschinsky W, Schrock H & Vetterlein F. (1986). Interdependency of local capillary density, blood flow, and metabolism in rat brains. *The American journal of physiology* **251,** H1333-1340.

Klinke R, Kral A, Heid S, Tillein J & Hartmann R. (1999). Recruitment of the auditory cortex in congenitally deaf cats by long-term cochlear electrostimulation. *Science* **285,** 1729-1733.

Klug A & Trussell LO. (2006). Activation and deactivation of voltage-dependent K+ channels during synaptically driven action potentials in the MNTB. *Journal of neurophysiology* **96,** 1547-1555.

Koch U, Braun M, Kapfer C & Grothe B. (2004). Distribution of HCN1 and HCN2 in rat auditory brainstem nuclei. *Eur J Neurosci* **20,** 79-91.

Koch U & Grothe B. (2003). Hyperpolarization-activated current (Ih) in the inferior colliculus: distribution and contribution to temporal processing. *J Neurophysiol* **90,** 3679-3687.

Kole MH, Hallermann S & Stuart GJ. (2006). Single Ih channels in pyramidal neuron dendrites: properties, distribution, and impact on action potential output. *J Neurosci* **26,** 1677-1687.

Kopp-Scheinpflug C, Lippe WR, Dorrscheidt GJ & Rubsamen R. (2003). The medial nucleus of the trapezoid body in the gerbil is more than a relay: comparison of pre- and postsynaptic activity. *J Assoc Res Otolaryngol* **4,** 1-23.

Kotak VC, Fujisawa S, Lee FA, Karthikeyan O, Aoki C & Sanes DH. (2005). Hearing loss raises excitability in the auditory cortex. *J Neurosci* **25,** 3908-3918.

Kurima K, Yang Y, Sorber K & Griffith AJ. (2003). Characterization of the transmembrane channel-like (TMC) gene family: functional clues from hearing loss and epidermodysplasia verruciformis. *Genomics* **82,** 300-308.

Kuwabara N & Zook JM. (1991). Classification of the principal cells of the medial nucleus of the trapezoid body. *J Comp Neurol* **314,** 707-720.

Leao RN, Berntson A, Forsythe ID & Walmsley B. (2004a). Reduced low-voltage activated K+ conductances and enhanced central excitability in a congenitally deaf (dn/dn) mouse. *J Physiol* **559,** 25-33.

Leao RN, Naves MM, Leao KE & Walmsley B. (2006a). Altered sodium currents in auditory neurons of congenitally deaf mice. *Eur J Neurosci* **24,** 1137-1146.

Leao RN, Oleskevich S, Sun H, Bautista M, Fyffe RE & Walmsley B. (2004b). Differences in glycinergic mIPSCs in the auditory brain stem of normal and congenitally deaf neonatal mice. *J Neurophysiol* **91,** 1006-1012.

Leao RN, Sun H, Svahn K, Berntson A, Youssoufian M, Paolini AG, Fyffe RE & Walmsley B. (2006b). Topographic organization in the auditory brainstem of juvenile mice is disrupted in congenital deafness. *J Physiol* **571,** 563-578.

Leao RN, Svahn K, Berntson A & Walmsley B. (2005). Hyperpolarization-activated (I) currents in auditory brainstem neurons of normal and congenitally deaf mice. *Eur J Neurosci* **22,** 147-157.

Lee DJ, Cahill HB & Ryugo DK. (2003). Effects of congenital deafness in the cochlear nuclei of Shaker-2 mice: an ultrastructural analysis of synapse morphology in the endbulbs of Held. *Journal of neurocytology* **32,** 229-243.

Li W, Kaczmarek LK & Perney TM. (2001). Localization of two high-threshold potassium channel subunits in the rat central auditory system. *The Journal of comparative neurology* **437,** 196-218.

Liu SQ & Kaczmarek LK. (1998). Depolarization selectively increases the expression of the Kv3.1 potassium channel in developing inferior colliculus neurons. *J Neurosci* **18,** 8758-8769.

Lu Y, Monsivais P, Tempel BL & Rubel EW. (2004). Activity-dependent regulation of the potassium channel subunits Kv1.1 and Kv3.1. *The Journal of comparative neurology* **470,** 93-106.

Ludwig A, Budde T, Stieber J, Moosmang S, Wahl C, Holthoff K, Langebartels A, Wotjak C, Munsch T, Zong X, Feil S, Feil R, Lancel M, Chien KR, Konnerth A, Pape HC, Biel M & Hofmann F. (2003). Absence epilepsy and sinus dysrhythmia in mice lacking the pacemaker channel HCN2. *The EMBO journal* **22,** 216-224.

Ludwig A, Zong X, Hofmann F & Biel M. (1999). Structure and function of cardiac pacemaker channels. *Cell Physiol Biochem* **9,** 179-186.

Ludwig A, Zong X, Jeglitsch M, Hofmann F & Biel M. (1998). A family of hyperpolarization-activated mammalian cation channels. *Nature* **393,** 587-591.

Ma WL, Hidaka H & May BJ. (2006). Spontaneous activity in the inferior colliculus of CBA/J mice after manipulations that induce tinnitus. *Hear Res* **212,** 9-21.

Ma YP, Cui J, Hu HJ & Pan ZH. (2003). Mammalian retinal bipolar cells express inwardly rectifying K+ currents (IKir) with a different distribution than that of Ih. *J Neurophysiol* **90,** 3479-3489.

Mahlke C & Wallhausser-Franke E. (2004). Evidence for tinnitus-related plasticity in the auditory and limbic system, demonstrated by arg3.1 and c-fos immunocytochemistry. *Hear Res* **195,** 17-34.

Manis PB & Marx SO. (1991). Outward currents in isolated ventral cochlear nucleus neurons. *J Neurosci* **11,** 2865-2880.

Marcotti W, Erven A, Johnson SL, Steel KP & Kros CJ. (2006). Tmc1 is necessary for normal functional maturation and survival of inner and outer hair cells in the mouse cochlea. *J Physiol* **574,** 677-698.

Martens JR, Kwak YG & Tamkun MM. (1999). Modulation of Kv channel alpha/beta subunit interactions. *Trends in cardiovascular medicine* **9,** 253-258.

Marx T, Gisselmann G, Stortkuhl KF, Hovemann BT & Hatt H. (1999). Molecular cloning of a putative voltage- and cyclic nucleotide-gated ion channel present in the antennae and eyes of Drosophila melanogaster. *Invert Neurosci* **4,** 55-63.

Middlebrooks JC & Snyder RL. (2007). Auditory prosthesis with a penetrating nerve array. *J Assoc Res Otolaryngol* **8,** 258-279.

Misonou H, Mohapatra DP, Park EW, Leung V, Zhen D, Misonou K, Anderson AE & Trimmer JS. (2004). Regulation of ion channel localization and phosphorylation by neuronal activity. *Nat Neurosci* **7,** 711-718.

Misonou H & Trimmer JS. (2004). Determinants of voltage-gated potassium channel surface expression and localization in Mammalian neurons. *Crit Rev Biochem Mol Biol* **39,** 125-145.

Moosmang S, Biel M, Hofmann F & Ludwig A. (1999). Differential distribution of four hyperpolarization-activated cation channels in mouse brain. *Biol Chem* **380,** 975-980.

Mostafapour SP, Cochran SL, Del Puerto NM & Rubel EW. (2000). Patterns of cell death in mouse anteroventral cochlear nucleus neurons after unilateral cochlea removal. *J Comp Neurol* **426,** 561-571.

Much B, Wahl-Schott C, Zong X, Schneider A, Baumann L, Moosmang S, Ludwig A & Biel M. (2003). Role of subunit heteromerization and N-linked glycosylation in the formation of functional hyperpolarization-activated cyclic nucleotide-gated channels. *J Biol Chem* **278,** 43781-43786.

Nayagam DA, Clarey JC & Paolini AG. (2005). Powerful, onset inhibition in the ventral nucleus of the lateral lemniscus. *J Neurophysiol* **94,** 1651-1654.

Nolan MF, Malleret G, Dudman JT, Buhl DL, Santoro B, Gibbs E, Vronskaya S, Buzsaki G, Siegelbaum SA, Kandel ER & Morozov A. (2004). A behavioral role for dendritic integration: HCN1 channels constrain spatial memory and plasticity at inputs to distal dendrites of CA1 pyramidal neurons. *Cell* **119,** 719-732.

Nolan MF, Malleret G, Lee KH, Gibbs E, Dudman JT, Santoro B, Yin D, Thompson RF, Siegelbaum SA, Kandel ER & Morozov A. (2003). The hyperpolarization-activated HCN1 channel is important for motor learning and neuronal integration by cerebellar Purkinje cells. *Cell* **115,** 551-564.

Oertel D. (1999). The role of timing in the brain stem auditory nuclei of vertebrates. *Annu Rev Physiol* **61,** 497-519.

Oleskevich S & Walmsley B. (2002). Synaptic transmission in the auditory brainstem of normal and congenitally deaf mice. *J Physiol* **540,** 447-455.

Oleskevich S, Youssoufian M & Walmsley B. (2004). Presynaptic plasticity at two giant auditory synapses in normal and deaf mice. *J Physiol* **560,** 709-719.

Oviedo H & Reyes AD. (2005). Variation of input-output properties along the somatodendritic axis of pyramidal neurons. *J Neurosci* **25,** 4985-4995.

Pal B, Por A, Pocsai K, Szucs G & Rusznak Z. (2005). Voltage-gated and background K+ channel subunits expressed by the bushy cells of the rat cochlear nucleus. *Hear Res* **199,** 57-70.

Pape HC. (1996). Queer current and pacemaker: the hyperpolarization-activated cation current in neurons. *Annu Rev Physiol* **58,** 299-327.

Perney TM & Kaczmarek LK. (1997). Localization of a high threshold potassium channel in the rat cochlear nucleus. *J Comp Neurol* **386,** 178-202.

Pollak GD, Burger RM, Park TJ, Klug A & Bauer EE. (2002). Roles of inhibition for transforming binaural properties in the brainstem auditory system. *Hear Res* **168,** 60-78.

Poolos NP, Migliore M & Johnston D. (2002). Pharmacological upregulation of h-channels reduces the excitability of pyramidal neuron dendrites. *Nat Neurosci* **5,** 767-774.

Popper AN & Fay RR. (1992). *The Mammalian auditory pathway : neurophysiology.* Springer-Verlag, New York.

Popper AN, Fay RR & Oertel D. (2002). *Integrative functions in the mammalian auditory pathway.* Springer, New York ; London.

Proenza C & Yellen G. (2006). Distinct populations of HCN pacemaker channels produce voltage-dependent and voltage-independent currents. *J Gen Physiol* **127,** 183-190.

Raphael Y & Altschuler RA. (2003). Structure and innervation of the cochlea. *Brain Res Bull* **60,** 397-422.

Rauschecker JP & Shannon RV. (2002). Sending sound to the brain. *Science* **295,** 1025-1029.

Roberts RC & Ribak CE. (1987). GABAergic neurons and axon terminals in the brainstem auditory nuclei of the gerbil. *J Comp Neurol* **258,** 267-280.

Rothman JS & Manis PB. (2003). The roles potassium currents play in regulating the electrical activity of ventral cochlear nucleus neurons. *J Neurophysiol* **89,** 3097-3113.

Rudy B & McBain CJ. (2001). Kv3 channels: voltage-gated K+ channels designed for high-frequency repetitive firing. *Trends Neurosci* **24,** 517-526.

Ryugo DK, Kretzmer EA & Niparko JK. (2005). Restoration of auditory nerve synapses in cats by cochlear implants. *Science* **310,** 1490-1492.

Ryugo DK, Pongstaporn T, Huchton DM & Niparko JK. (1997). Ultrastructural analysis of primary endings in deaf white cats: morphologic alterations in endbulbs of Held. *The Journal of comparative neurology* **385,** 230-244.

Salvi RJ, Hamernik RP & Henderson D. (1978). Discharge patterns in the cochlear nucleus of the chinchilla following noise induced asymptotic threshold shift. *Exp Brain Res* **32,** 301-320.

Sanes DH & Constantine-Paton M. (1985). The sharpening of frequency tuning curves requires patterned activity during development in the mouse, Mus musculus. *J Neurosci* **5,** 1152-1166.

Santoro B & Baram TZ. (2003). The multiple personalities of h-channels. *Trends Neurosci* **26,** 550-554.

Santoro B, Chen S, Luthi A, Pavlidis P, Shumyatsky GP, Tibbs GR & Siegelbaum SA. (2000). Molecular and functional heterogeneity of hyperpolarization-activated pacemaker channels in the mouse CNS. *J Neurosci* **20,** 5264-5275.

Santoro B, Grant SG, Bartsch D & Kandel ER. (1997). Interactive cloning with the SH3 domain of N-src identifies a new brain specific ion channel protein, with homology to eag and cyclic nucleotide-gated channels. *Proc Natl Acad Sci U S A* **94,** 14815-14820.

Shaikh AG & Finlayson PG. (2003). Hyperpolarization-activated (I(h)) conductances affect brainstem auditory neuron excitability. *Hear Res* **183,** 126-136.

Shaikh AG & Finlayson PG. (2005). Excitability of auditory brainstem neurons, in vivo, is increased by cyclic-AMP. *Hear Res* **201,** 70-80.

Sharma A & Dorman MF. (2006). Central auditory development in children with cochlear implants: clinical implications. *Advances in oto-rhino-laryngology* **64,** 66-88.

Sharp AA, O'Neil MB, Abbott LF & Marder E. (1993). Dynamic clamp: computer-generated conductances in real neurons. *J Neurophysiol* **69,** 992-995.

Sheng M & Greenberg ME. (1990). The regulation and function of c-fos and other immediate early genes in the nervous system. *Neuron* **4,** 477-485.

Shepherd GM. (1994). *Neurobiology*. Oxford University Press, New York.

Sie KC & Rubel EW. (1992). Rapid changes in protein synthesis and cell size in the cochlear nucleus following eighth nerve activity blockade or cochlea ablation. *J Comp Neurol* **320,** 501-508.

Sokolowski B, Harvey M, Venkataramu C & Duzhyy D. (2005). Protein-protein interactions of a Kvbeta subunit in the cochlea. *J Neurosci Res* **79,** 459-467.

Soler-Llavina GJ, Chang TH & Swartz KJ. (2006). Functional interactions at the interface between voltage-sensing and pore domains in the Shaker K(v) channel. *Neuron* **52,** 623-634.

Song P, Yang Y, Barnes-Davies M, Bhattacharjee A, Hamann M, Forsythe ID, Oliver DL & Kaczmarek LK. (2005). Acoustic environment determines phosphorylation state of the Kv3.1 potassium channel in auditory neurons. *Nature neuroscience* **8,** 1335-1342.

Spangler KM, Warr WB & Henkel CK. (1985). The projections of principal cells of the medial nucleus of the trapezoid body in the cat. *The Journal of comparative neurology* **238,** 249-262.

Steel KP & Bock GR. (1984). Electrically-evoked responses in animals with progressive spiral ganglion degeneration. *Hear Res* **15,** 59-67.

Sterling P & Matthews G. (2005). Structure and function of ribbon synapses. *Trends Neurosci* **28,** 20-29.

Svirskis G, Kotak V, Sanes DH & Rinzel J. (2002). Enhancement of signal-to-noise ratio and phase locking for small inputs by a low-threshold outward current in auditory neurons. *J Neurosci* **22,** 11019-11025.

Wainger BJ, DeGennaro M, Santoro B, Siegelbaum SA & Tibbs GR. (2001). Molecular mechanism of cAMP modulation of HCN pacemaker channels. *Nature* **411,** 805-810.

Walmsley B, Berntson A, Leao RN & Fyffe RE. (2006). Activity-dependent regulation of synaptic strength and neuronal excitability in central auditory pathways. *J Physiol* **572,** 313-321.

Wang LY, Gan L, Forsythe ID & Kaczmarek LK. (1998). Contribution of the Kv3.1 potassium channel to high-frequency firing in mouse auditory neurones. *J Physiol* **509 (Pt 1),** 183-194.

Wang Y & Manis PB. (2005). Synaptic transmission at the cochlear nucleus endbulb synapse during age-related hearing loss in mice. *J Neurophysiol* **94,** 1814-1824.

Watanabe I, Zhu J, Sutachan JJ, Gottschalk A, Recio-Pinto E & Thornhill WB. (2007). The glycosylation state of Kv1.2 potassium channels affects trafficking, gating, and simulated action potentials. *Brain research* **1144,** 1-18.

Willott JF. (2001). *Handbook of mouse auditory research : from behavior to molecular biology*. CRC Press, Boca Raton, FL.

von Gersdorff H & Borst JG. (2002). Short-term plasticity at the calyx of held. *Nature reviews* **3,** 53-64.

von Hehn CA, Bhattacharjee A & Kaczmarek LK. (2004). Loss of Kv3.1 tonotopicity and alterations in cAMP response element-binding protein signaling in central auditory neurons of hearing impaired mice. *J Neurosci* **24,** 1936-1940.

Xiang G, Pan L, Xing W, Zhang L, Huang L, Yu J, Zhang R, Wu J, Cheng J & Zhou Y. (2007). Identification of activity-dependent gene expression profiles reveals specific subsets of genes induced by different routes of Ca(2+) entry in cultured rat cortical neurons. *Journal of cellular physiology* **212,** 126-136.

Yamada R, Kuba H, Ishii TM & Ohmori H. (2005). Hyperpolarization-activated cyclic nucleotide-gated cation channels regulate auditory coincidence detection in nucleus laminaris of the chick. *J Neurosci* **25,** 8867-8877.

Yin TCT. (2002). Neural Mechanisms of Encoding Binaural Localization Cues in the Auditory Brainstem. In *Integrative Functions in the Mammalian Auditory Pathway*, pp. 99-159. Fay R. R.,Oertle D. and Popper A. N.